ROMTECH

RTR 218-01, Vol. I

(NASA-CR-192455) BASE HEATING METHODOLOGY IMPROVEMENTS, VOLUME 1 Final Report, Sep. 1989 - Nov. 1992 (Romtech) 112 p

N93-22350

Unclas

G3/20 0157552

# FOREWORD

The need for improvements in launch vehicle base heating prediction methodology was recognized by the ALS Program in 1989 and implemented through Advanced Development Plan #4202. This plan was contracted to REMTECH by NASA/MSFC through Contract NAS8–38141. REMTECH was supported in this effort by SECA, Inc., of Huntsville, AL, and PST, Inc., of Princeton, NJ. The period of performance was from September 1989 through November 1992.

The important output from this effort is a new Design Base Heating Code which incorporates the improvements and provides quick-look capability to assess base heating from a variety of launch vehicle concepts. The analyses leading to the methodology improvements are reported in this document. A companion user's guide document is also provided to assist potential users with the code.

The NASA/MSFC Contract Officer's Technical Representative for this contract was Mr. Peter Sulyma, of the Induced Environments Branch, Aerophysics Division of the Structures and Dynamics Laboratory, ED33. Overall coordination of ADP #4202 was provided by Mr. Robert Nixon from the Space Transportation and Exploration Office, PT31.

# Contents

FOREWORD . . . . . i
List of Figures . . . . . iv
List of Tables . . . . . vi
1 INTRODUCTION . . . . . 1
1.1 ALS/NLS Program Chronology . . . . . 1
1.2 ADP 4202 Objectives . . . . . 4
1.3 ADP 4202 Limitations and Constraints . . . . . 6
1.4 Design Code Development Plan . . . . . 6
1.5 Goals for the Design Code . . . . . 7
2 HISTORICAL REVIEW — BASE HEATING METHODOLOGY . . . . . 9
2.1 Components of Base Heating . . . . . 9
2.1.1 Convection Environments . . . . . 9
2.1.2 Radiation Environments . . . . . 16
2.2 Difficulties and Errors . . . . . 20
2.2.1 Convection . . . . . 21
2.2.2 Radiation . . . . . 21
3 HISTORICAL REVIEW — MODEL AND FLIGHT BASE HEATING DATA . . . . 22
4 CODE CAPABILITY SELECTION CRITERIA . . . . . 28
4.1 ALS/NLS Concepts . . . . . 28
4.2 Criteria for Limiting Code Capability . . . . . 34
5 GENERAL CODE DESCRIPTION . . . . . 41
5.1 Code Architecture . . . . . 41
5.2 Input . . . . . 43
5.3 Convective Subprogram . . . . . 44
5.4 Radiation Subprogram . . . . . 49
5.5 Output . . . . . 56
6 CODE METHODOLOGY DEVELOPMENT . . . . . 59
6.1 Plume Radiation . . . . . 59
6.1.1 Configuration Approximations . . . . . 60
6.1.2 $RP/O_2$ Plumes . . . . . 60
6.1.3 SRM Plumes . . . . . 61
6.1.4 $H_2O_2$ Plumes . . . . . 67
6.1.5 Output Format . . . . . 73

6.2 Convection . . . . . 73
6.2.1 Utilization of the Flight and Model Databases . . . . . 74
6.2.2 Initial Recirculation Altitude . . . . . 75
6.2.3 Convective Environment at Choking Conditions . . . . . 80
6.2.4 Convective Heating Adjustments for Altitude and Geometry Distributions . . . . . 86
6.2.5 Convection During Early Flight (Aspirating Flow) . . . . . 88
6.2.6 Wall Temperature Effects . . . . . 89
7 SUBCONTRACT OUTPUTS . . . . . 90
7.1 Forebody Flowfield Module (PST, Inc.) . . . . . 90
7.2 ALS/NLS Plume Descriptions (SECA, Inc.) . . . . . 95
8 RECOMMENDED IMPROVEMENTS . . . . . 103
9 REFERENCES . . . . . 104
Appendix I ALS BASE HEATING TECHNICAL NOTES . . . . . I-1
Appendix II TURBINE EXHAUST DISPOSAL REPORTS . . . . . II-1
Appendix III NLS CYCLE 1 AND NLS 2 BASE HEATING TECHNICAL NOTES III-1
Appendix IV SUBCONTRACTOR FINAL REPORTS . . . . . IV-1

# List of Figures

1 Typical ALS Vehicle Configurations — Circa 1988 . . . . . 2
2 Typical NLS Vehicle Concepts — February 1992 . . . . . 3
3 Early Heavy-Lift Launch Vehicle — October 1992 . . . . . 5
4 Flowchart for Convective Heat Rate Determination . . . . . 10
5 L/D Determination . . . . . 11
6 Generic Curves for $Alt_1$ and $Alt_2$ Determination . . . . . 11
7 Generic Base Pressure Plot . . . . . 12
8 Integrated Average Temperature Mass Flow in Nozzle Boundary Layer at Any Point from the Wall to the Edge of the Boundary Layer . . . . . 13
9 Determination of Total Possible Boundary Layer Flow into Base Region . . . . . 13
10 Determination of the Recovery Temperature at $Alt_2$ Based on the Amount of Nozzle Boundary Layer Flow Turned into the Base Region . . . . . 14
11 Determination of Recovery Temperature at All Altitudes . . . . . 14
12 Determination of Convective Heating . . . . . 15
13 Flow Chart for Radiative Heat Rate Determination . . . . . 17
14 Scaling Factors Used to Adjust Radiative Heating from Sea Level Plumes to Altitude . . . . . 18
15 Solid Shape Representation of Plume . . . . . 19
16 Monte Carlo Derived Solid Shape Representation of Plume . . . . . 20
17 STAS Candidate Launch Vehicle Concepts . . . . . 30
18 ALS Reference Launch Vehicle Concepts . . . . . 31
19 Parallel and Series Burn Launch Vehicle Concepts . . . . . 31
20 ALS System Study Results . . . . . 33
21 ALS Family of Launch Vehicles . . . . . 35
22 Launch Vehicle Evolution in 1991 . . . . . 36
23 NLS Architecture Options . . . . . 37
24 NLS Evolution to SEI . . . . . 38
25 Early Heavy Lift Launch Vehicle Concept — Fall 1992 . . . . . 39
26 Design Code Architecture . . . . . 42
27 Main Input Menu . . . . . 44
28 Typical Configuration Menu Selection and Graphical Displays . . . . . 45
29 Typical Body Point Menu Selections and Graphical Displays . . . . . 46
30 Computational Flow Processes for the Convective Subprogram . . . . . 47
31 Subroutine Map for the Convective Subprogram . . . . . 49
32 Typical Convective Subprogram Output . . . . . 50
33 $O_2/H_2$ Plumes in Band Model Module . . . . . 53
34 Plume Structure for $O_2/H_2$ Engines . . . . . 54
35 Typical Format for Radiation Heating Output . . . . . 56
36 Typical Design Code Graphical Output . . . . . 58
37 $RP1/O_2$ Sea-Level Plume Radiation Model . . . . . 62
38 Altitude Adjustment Functions for $RP1/O_2$ Plume Radiation . . . . . 63
39 SRM Sea-Level Plume Model Geometry . . . . . 65

40 SRM Sea-Level Emissive Power as a Function of Plume Position and Aluminum Fraction . . . . . 66
41 SRM Altitude and Shutdown-Spike Adjustments . . . . . 68
42 Heat Shield Convective Heating As a Function of Altitude . . . . . 76
43 Heat Shield Convective Heating As a Function of Chamber Pressure . . . . . 77
44 Heat Shield Convective Heating As a Function of Nozzle Vent Area . . . . . 78
45 Altitude of Initial Recirculation . . . . . 81
46 Choked Base Flow Experimental Data . . . . . 83
47 Afterbody Code Methodology . . . . . 91
48 Spherical Nose Initialization . . . . . 91
49 Definition of Body Geometry . . . . . 92
50 SPLITP Mapped Grid . . . . . 93
51 Run Summary . . . . . 94
52 Exterior Base Calculation . . . . . 95
53 Mach Number Contours for 30:1 Engine Plume at 20,000 Feet . . . . . 97
54 Inviscid Plume Boundaries for 60:1 Engine Including Free-Stream Effects . . . . 98
55 Temperature Contours for STME Plume (75 Percent Thrust) at 10,000 Feet . . . 99
56 Heating Rate vs. Time for Body Point 7 on MLT . . . . . 100
57 Upper STME Sustainer Engine (No Gimbal) Plume Impingement Forces and Moments on the Propulsion Module as a Function of Distance from the Separation Plane . . . . . 101
58 STME Plume Impingement Forces and Moments vs. Time from Separation on the HLLV ASRBs . . . . . 102

# Section 1
# INTRODUCTION

This document is the final report for NASA MSFC Contract NAS8–38141. The contracted effort had the broad objective of improving launch vehicle ascent base heating methodology to improve and simplify the determination of that environment for Advanced Launch System (ALS) concepts. It was pursued as an Advanced Development Plan (ADP) for the Joint DoD/NASA ALS program office with project management assigned to NASA/MSFC. The original study was to be completed in 26 months beginning September 1989. Because of several program changes and emphasis on evolving launch vehicle concepts, the period of performance was extended to the current completion date of November 1992.

A computer code incorporating the methodology improvements into a quick prediction tool has been developed and is operational for basic configuration and propulsion concepts. The code and its users guide are also provided as part of the contract documentation. Background information describing the specific objectives, limitations, and goals of the contract is summarized in the following sections. A brief chronology of the ALS/NLS program history is also presented to provide the reader with an overview of the many variables influencing the development of the code over the past three years.

## 1.1 ALS/NLS Program Chronology

Advanced launch systems studies began in1987. They were initially directed at launch systems to deliver large payloads (both in weight and size) to low earth orbit. Various concepts were studied for the Air Force by a variety of major contractor or contractor teams through 1988. The program was reevaluated and reduced in scope to continuation of small studies in the 1988 — 1989 period. Some typical ALS configurations under initial considerations are shown in Fig. 1.

A coordinated DoD/NASA program emerged in 1989 to develop focused technology for the ALS program. These advanced development programs were varied and included specific objectives in propulsion, structures, and recovery systems. Launch vehicle base heating was identified as an area where focused technology would help improve the vehicle design process. The contract with REMTECH to improve base heating prediction methods was initiated September 8, 1989, and designated ADP #4202.

The National Launch System, or NLS, was the name assigned to the Joint Defense Department/NASA program for the proposed family of new launchers which was reborn in spring 1991. It promised to develop efficient, new launch vehicles for military, scientific, and commercial payloads. The NLS program was structured to develop two launch vehicles which had common elements in the core stage. These vehicles would provide needed replacements for aging, expendable launchers and give the country a heavy-lift booster to support construction and operations of the NASA/International space station. Typical NLS concepts are shown in Fig. 2.

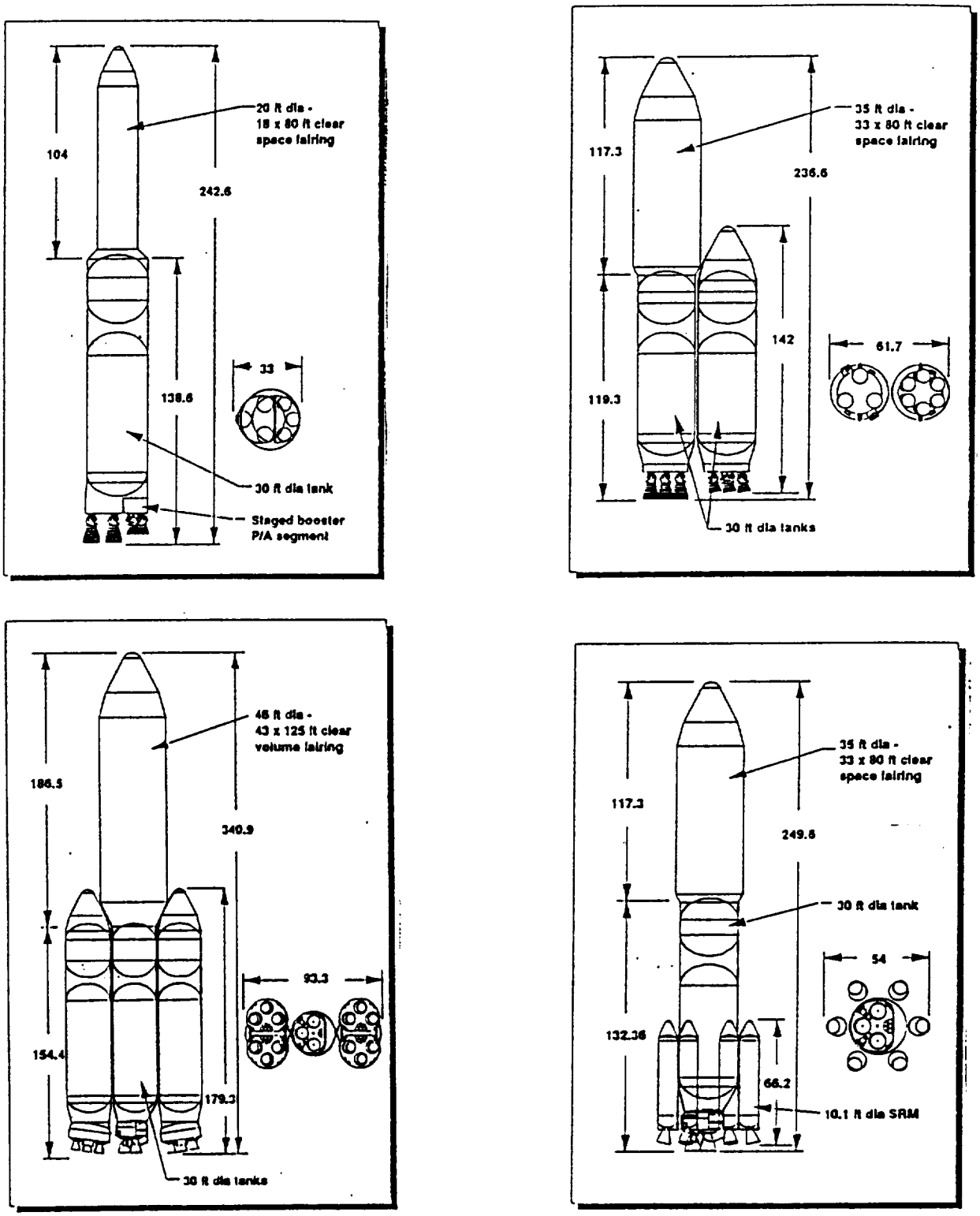


Figure 1: Typical ALS Vehicle Configurations — Circa 1988

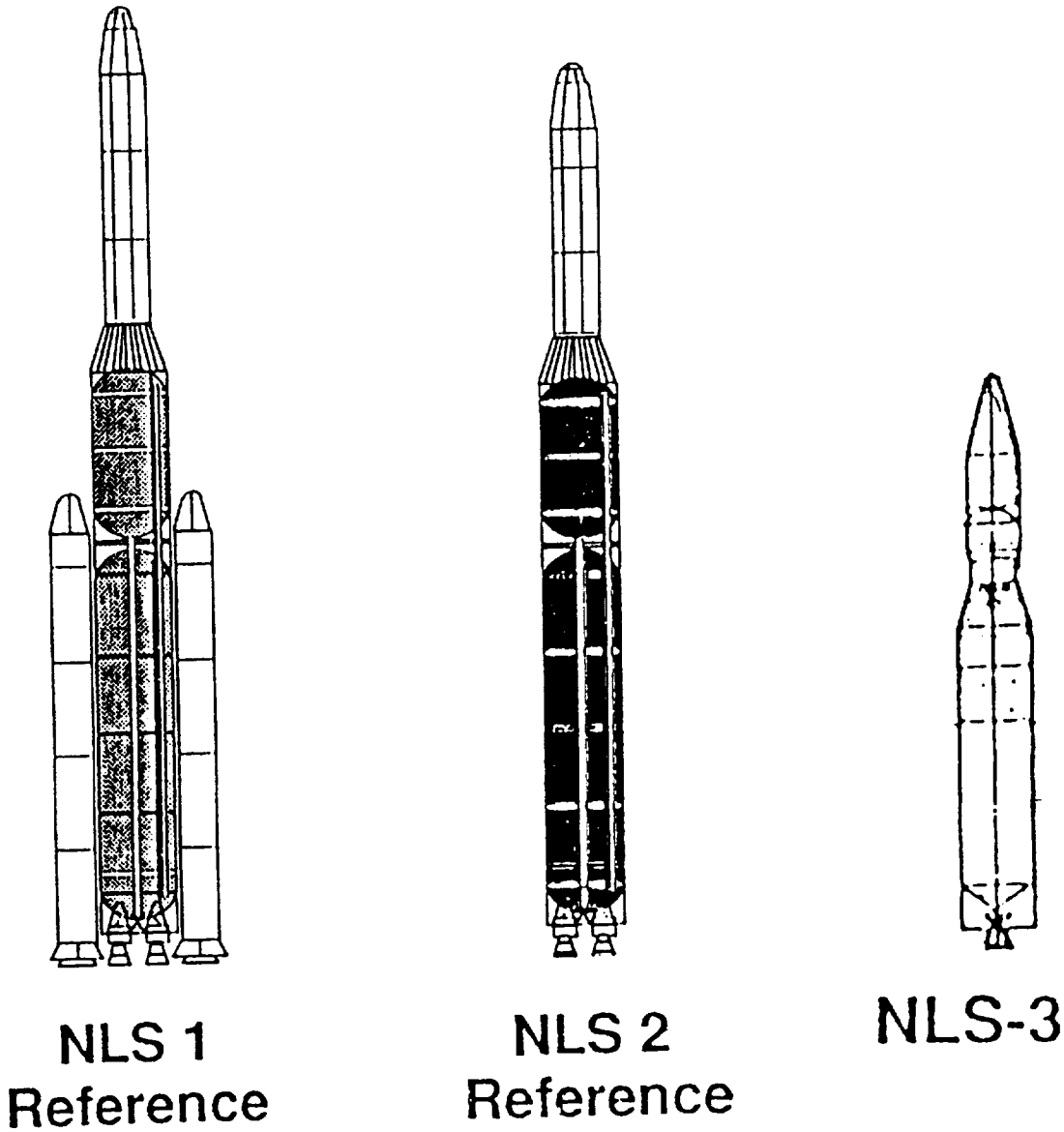


Figure 2: Typical NLS Vehicle Concepts — February 1992

Several changes occurred in the NLS program during the 1991–1992 time period. The HLLV vehicle which utilized two STS SRBs was not pursued and the focus was redirected toward development of a 1.5 stage vehicle which had a propulsion module with multiple $LOX/LH_2$ engines. Recently, the U. S. Congress (in early October 1992) ordered termination of the National Launch System; however, NASA is continuing studies of heavy-lift launchers for near-term support of the deployment of the space station. The most recent study is directed toward defining a heavy-lift vehicle designated EHLLV or Early HLLV which uses many elements from the existing Space Shuttle national space transportation system. The EHLLV vehicle is shown schematically in Fig. 3.

The variations and different program directions experienced during the past three years have had a dramatic effect on the base heating technology development program. Code development has been targeted at a generic launch vehicle which also contains many features considered in both the ALS and NLS studies. Effort was also diverted from the code development at various times to support specific base heating studies for vehicles of interest. The overall development effort and its relationship to the ALS/NLS programs is depicted below.

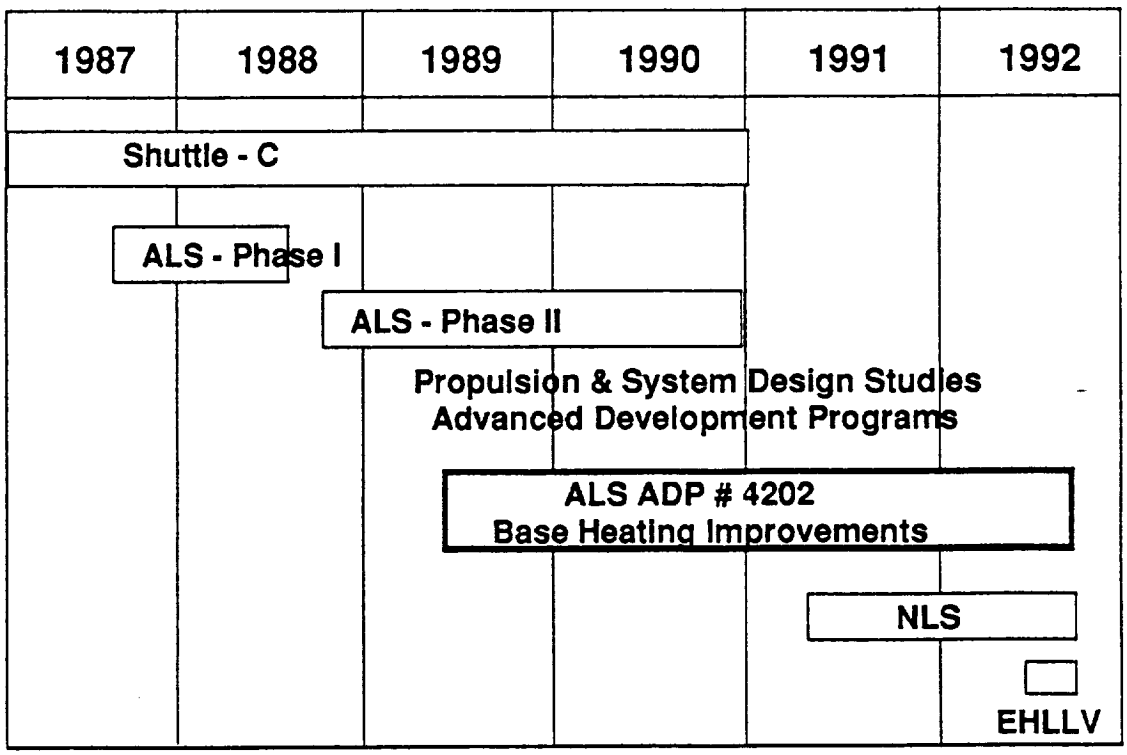


## 1.2 ADP 4202 Objectives

The overall objective [1] was to develop an improved base heating prediction methodology for ALS class vehicles. The improved methodology was targeted at incorporating existing base heating models and flight test data trends with new or improved plume flowfield and radiation models and CFD analysis of base flowfields into a comprehensive

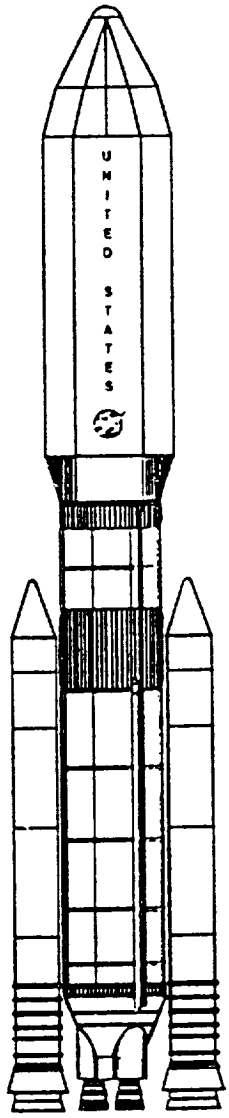


Figure 3: Early Heavy-Lift Launch Vehicle — October 1992

design tool which could be used for fast and accurate design environment predictions. A secondary objective was to maintain cognizance of the launch vehicle evolution through the ALS/NLS programs and provide base heating assessments and design recommendations as required.

## 1.3 ADP 4202 Limitations and Constraints

The design tool or base heating prediction code was originally intended to be fully comprehensive with the capability to treat all conceivable (or practical) launch vehicle configurations and propulsion systems. As the analysis progressed it became evident that certain limitations in the code would be required to meet the contract schedule as well as the "fast and accurate" criteria. Therefore, the code as presently configured addresses only the macro problem with these limitations.

- Simple base configuration and engine arrangement
- Propulsion systems of interest
- Simple forebody shapes
- Simple operational requirements (such as throttling and staging)
- Environments at limited number of locations

The code does not model

- Gimbaling
- Mass addition in base
- Complex base configuration with shrouds, etc.
- Unusual separation sequence
- Surface reflection and emission
- TPS ablation or outgassing
- Direct plume impingement

In general, the code was developed to meet the normal base heating prediction accuracy of ± 20 percent for both radiation and convection.

## 1.4 Design Code Development Plan

To accomplish the code development, several tasks were pursued simultaneously early in the contract. The results or output were then assembled and integrated into the code. These tasks are summarized below:

TASK A — PLUME MODELING

- Develop new plume modeling techniques which incorporate
  - Approach flow/base flow
  - Nozzle boundary layer with variable wall temperature
  - Improve shear layer/afterburning model
  - Improved plume radiation and base flow models

TASK B — FLOWFIELD MODELING

- Develop a flow model of the interior base region bounded by the base heat shield, nozzles and plume boundaries
- Add a heat transfer calculation scheme utilizing base flowfield properties determined by the flow model

TASK C — DATABASE EVALUATION

- Develop a flight and model database plus scaling methodology
- Supplement analytical computations developed in Tasks A & B

TASK D — DESIGN CODE DEVELOPMENT

- Develop a design tool which can quickly estimate base environments for specified base locations of typical large launch vehicle designs

## 1.5 Goals for the Design Code

As the analyses tasks were completed and the code development began, a set of goals for the code was formulated by REMTECH and received concurrence from the COTR. The goals were:

- Usable with generic ALS/NLS configurations
  - Main stage using $0_2/H_2$ propellants
  - Parallel booster stages using $O_2/H_2$, $O_2$/RP1, or AP/A1 (solid)
- Sufficient accuracy to provide meaningful trade-off results
- User friendly window environment interfaces
  - Easy input of configuration variables
  - Default or user selected body point locations
- Graphic and printed output
  - Graphic display of cold wall convection and radiation
  - Tabulated output files for detail analysis:
    - Convective cold wall rates
    - Convective heat transfer coefficient and recovery temperature
    - Booster radiation contribution
    - Main engine radiation contribution
    - Total radiation

In general, the code in its current status (November 1992) meets the goals described above. ALS/NLS concepts which are sufficiently generic to be handled by the code will be discussed in the section of this document devoted to code capability selection criteria. Details of the code methodology development are also described along with the subcontractors inputs to the overall study. A general code description is included, and finally, a summary of current code capability is provided. Many detailed reports have been prepared which address specific launch vehicle base heating scenarios. These reports are included in Appendices I through IV.

# Section 2
# HISTORICAL REVIEW — BASE HEATING METHODOLOGY

The base heating code undertaken in this project was a response to the need to simplify and speed the base heating design methodology in current use. This methodology is difficult to apply correctly because it is highly empirical and requires vast experience with databases from previous space boosters and detailed familiarity with scaling procedures. Even with this knowledge only persons with extensive experience in previous programs had the judgment to evaluate and couple the convection phenomena and plume radiation models necessary to predict the heating with any accuracy. This code removes these severe restrictions by computerizing trends from the databases and establishing algorithms to accomplish the difficult scaling and judgmental procedures needed. This was possible only because of the wealth of experience and data now available so that procedures and trends could be seen from various theoretical analyses, experiments, and flight measurements.

To understand the code developed it will first be necessary to review the methods currently used. These methods provided the basis for the development of the code's structure and dictated the inputs and outputs. This section reviews and briefly discusses the significant features of the methodology used before the code.

## 2.1 Components of Base Heating

Base heating is due to convection and radiation from a number of plume phenomena. For the most complicated case of multiple engines in a cluster with solid rocket boosters, convection heating occurs when the plume boundaries intersect and cause the nozzle boundary layers to turn back between the nozzles. This condition is worsened when fuel-rich turbo-exhaust gases are dumped or aspirated into the base and burn. Radiation comes from the solid and liquid rocket plumes and the Mach discs of low altitude liquid rocket plumes. Typically the convection and radiation are handled separately and combined into a total environment in the last step of the analysis. The analyses take two forms: 1) determining the design thermal environment for vehicles that have not flown and 2) determining the design thermal environment for new points on vehicles that have flown and have flight data.

### 2.1.1 Convection Environments

The determination of design thermal convection environments for points on a new vehicle is a complex process. It relies on theoretical calculations and semi- and empirical correlations derived from databases generated for similar vehicles and previous analyses. A flow chart of the methodology is shown in Fig. 4. The steps show how $T_r$ (recovery temperature), $\dot{q}_c$ (the convective rate), and $h_c$ (convective film coefficient) are determined.

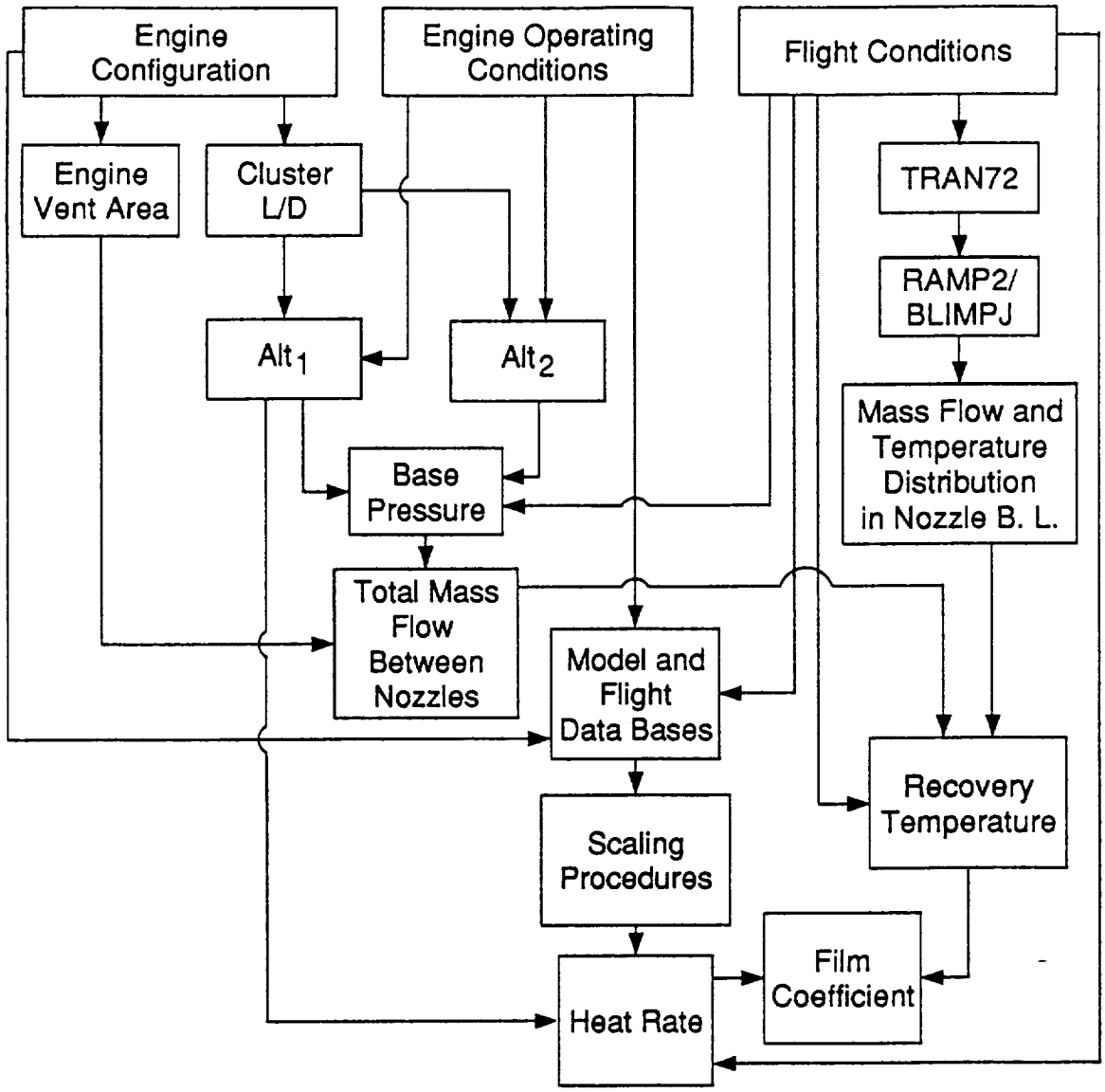


Figure 4: Flowchart for Convective Heat Rate Determination

The analyst must have the following information to use this methodology:

1. Engine — nozzle exit area, area ratio ($A_e$, $A_e/A^*$), and shape; chamber pressure and temperature ($P_c$, $T_c$); fuel, oxidizer, and O/F.
2. Configuration - engine arrangement, heat shield position, shroud position, turbo-exhaust scheme.
3. Flight Conditions — trajectory, gimballing.

The first step in the analysis is to determine the altitude ($Alt_1$) at which the plumes first intersect and nozzle boundary layer gases begin to be turned into the heat shield. The second step is to determine the altitude ($Alt_2$) at which the volume between the nozzles is completely filled with these gases and they are venting through the area between

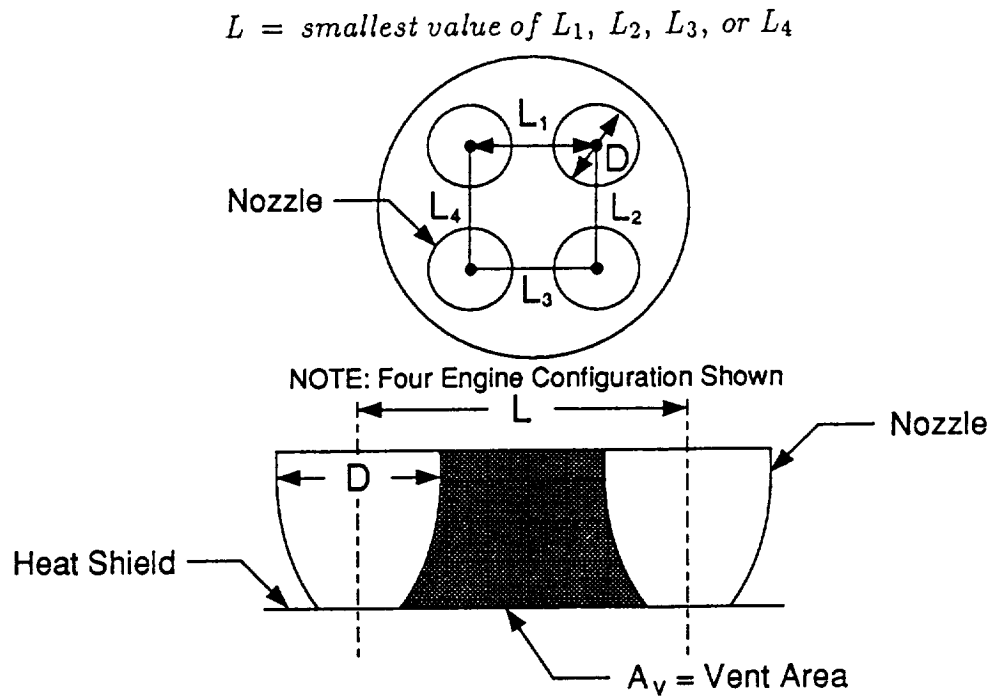


Figure 5: L/D Determination

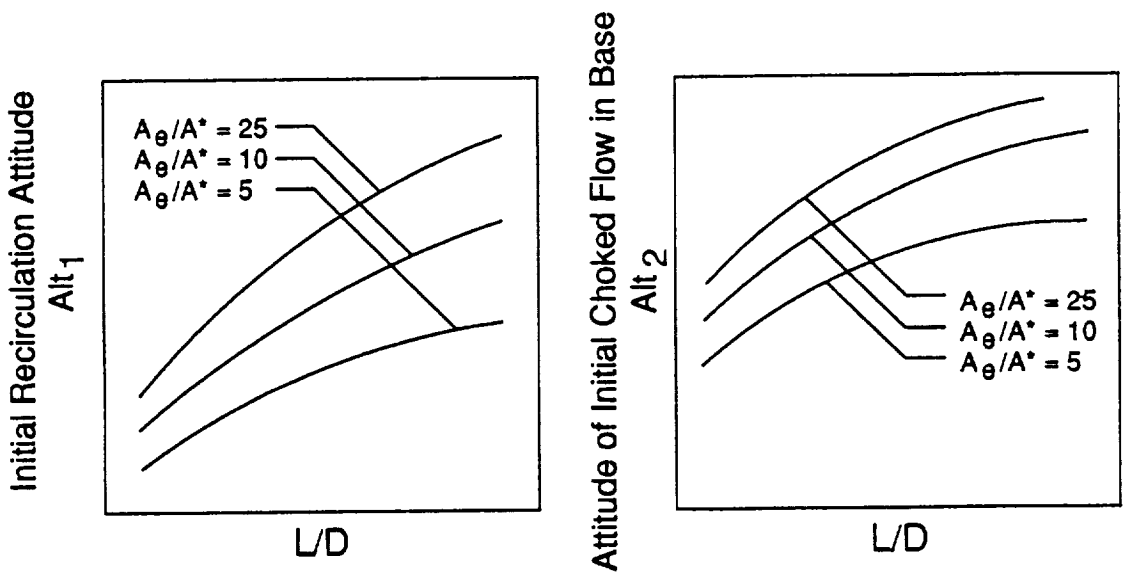


Figure 6: Generic Curves for $Alt_1$ and $Alt_2$ Determination

the nozzles ($A_v$) at choked conditions. These steps are accomplished by computing the L/D (see Fig. 5) of the engine cluster and applying the curves shown generically in Fig. 6. These curves were derived using databases and scaling techniques developed over many years for different liquid fuels and oxidizers.

The next step is to determine the amount of mass being vented between the nozzles. To do this a base pressure ($P_b$) plot is constructed (Fig. 7). Initially the ambient pressure ($P_a$) is plotted for a reference atmosphere and lines denoting $Alt_1$ and $Alt_2$ are shown.

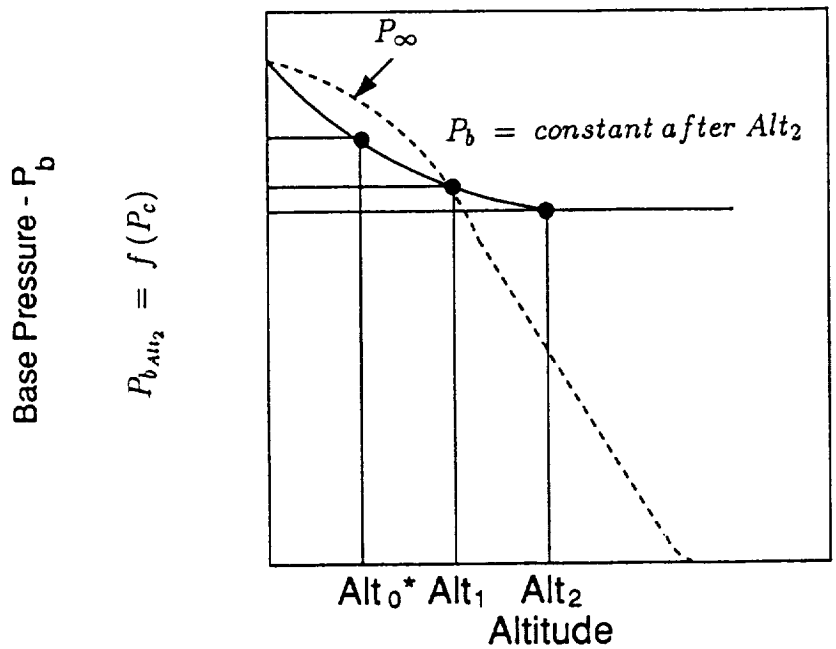


*NOTE: $Alt_o$ = Altitude where $P_{exit} = P_\infty$ (Maximum Aspiration)

Figure 7: Generic Base Pressure Plot

Careful study of the databases has shown that at the point where the nozzle boundary layer gases begin to be turned toward the heat shield ($Alt_1$) $P_b$ is equal to $P_\infty$. It has also been seen that although base pressure is a weak function of L/D, it is a strong function of $P_c$ at choked conditions. Using an empirical relation established over the years, the choked $P_b$ is calculated from $P_c$. These two points are now established on the $P_b$ curve; and since the flow remains choked after $Alt_2$, $P_b$ is constant and a straight line is extended to the right. Another point is established at the altitude ($Alt_0$) where the nozzle exit pressure ($P_e$), determined by $P_c$ and $A_e/A^*$ , is equal to $P_\infty$. At this point the databases have shown that $P_b$ is approximately 1.5 psid lower than $P_b$. (This point is not critical to the analysis and this approximation is sufficient for accuracy.) Since $P_b$ equals $P_\infty$ at launch, four points now exist so that the important curve from $Alt_1$ to$Alt_2$, the time during which the volume between the nozzles is being filled with plume exhaust, is now determined.

The base temperature ($T_b$) is estimated as 0.45 $T_c$ (based on trends from the databases). Using this and $P_b$ and assuming stagnation conditions, the density is calculated from the equation of state. Concurrent to this, a nozzle boundary layer code (BLIMPJ [2]) must be run to determine the specific heat ratio. Now the flow is expanded to choked conditions and the choked velocity and density times $A_v$ determine the mass flow rate between two nozzles ($\dot{m}^*$).

The final steps in the $T_r$ determination require a good deal of judgment. First the percentage of flow in the nozzle boundary layer ($\dot{m}_{bl}$) necessary to equal $\dot{m}^*$ is determined from the nozzle boundary layer code as is the average boundary layer temperature ($T_{bl}$) versus distance from the wall (and thus increasing mass flow) (Fig. 8). This calculation is

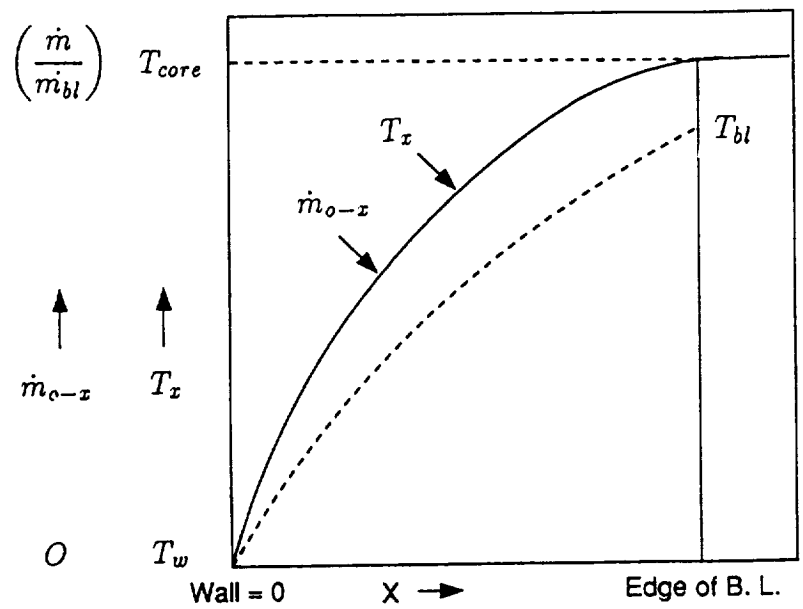


Figure 8: Integrated Average Temperature Mass Flow in Nozzle Boundary Layer at Any Point from the Wall to the Edge of the Boundary Layer

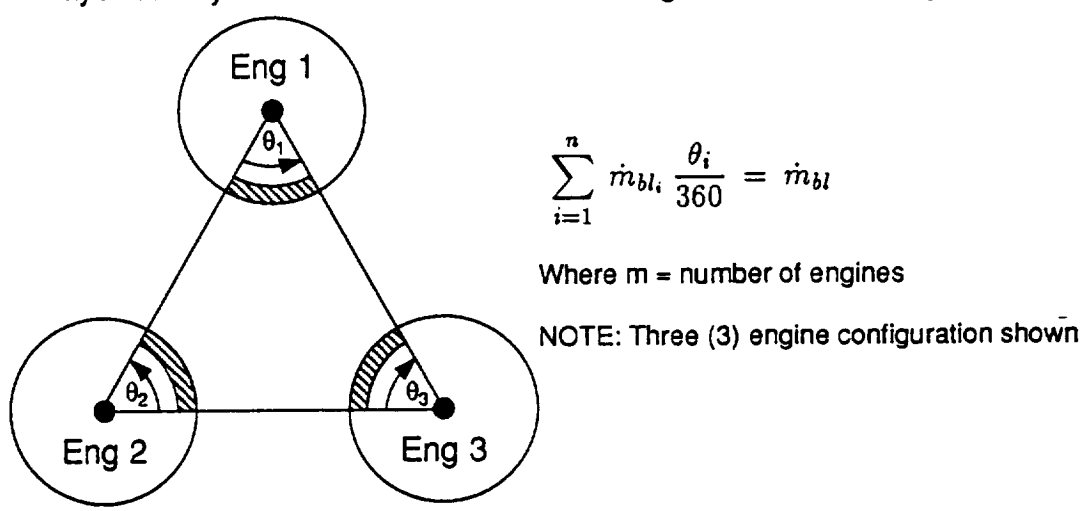


Figure 9: Determination of Total Possible Boundary Layer Flow into Base Region

based on the estimated wall temperature which is a major judgment factor. It is assumed at this stage that only a portion of $\dot{m}_{bl}$, based on lines of symmetry (Fig. 9), is available to flow through $A_v$. Next, this information is plotted and $T_{bl}$ is read (Fig. 10). At this point, $Alt_2$, $T_r$ is assumed to be $T_b$ which is assumed to equal $T_{bl}$. (This assumption is based on the databases.) Because conditions remain choked, $T_r$ remains constant and is plotted is a horizontal line on a $T_r$ versus altitude plot (Fig. 11). From 0 to $Alt_1$, $T_r$ is assumed to be the free stream total temperature value calculated from the trajectory and is also plotted. (Again, the assumption is verified by the databases.) Between $Alt_1$ and $Alt_2$, $T_r$ is assumed to be an "S-curve" based on the assumption that the amount

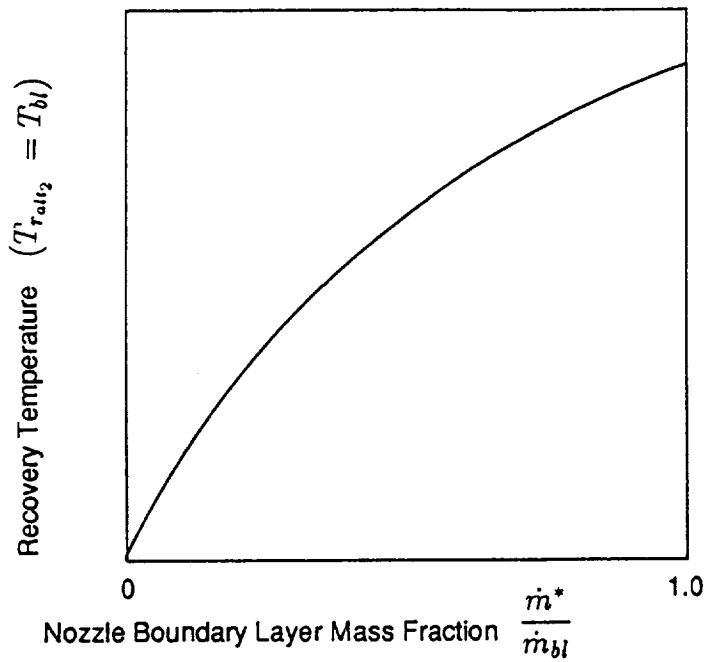


Figure 10: Determination of the Recovery Temperature at $Alt_2$ Based on the Amount of Nozzle Boundary Layer Flow Turned into the Base Region

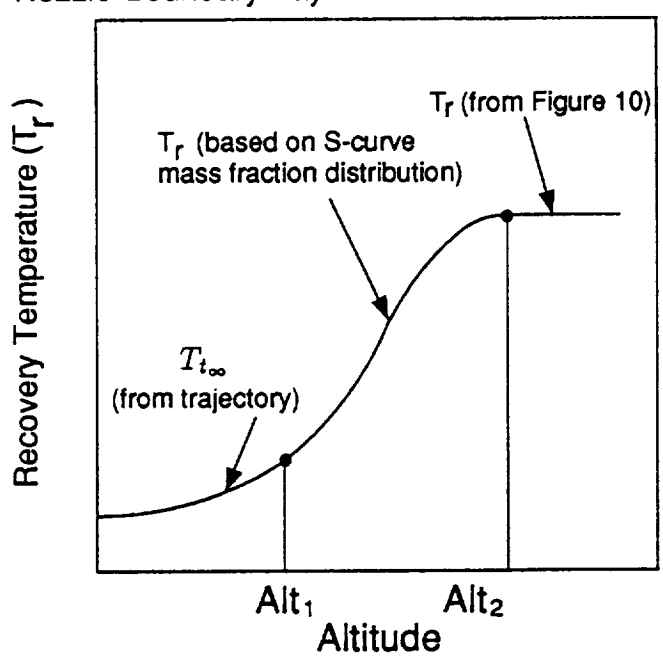


Figure 11: Determination of Recovery Temperature at All Altitudes

of plume gases in the base goes from 0 to 100% and ambient air goes from 100 to 0% along a standard distribution curve. This then completes the $T_r$ determination.

The evaluation of $\dot{q}_c$ is easier although heavily dependent on the data bases. At choked conditions, $Alt_2$, $\dot{q}_c$ has been empirically determined to be a function of $A_e/A^*$

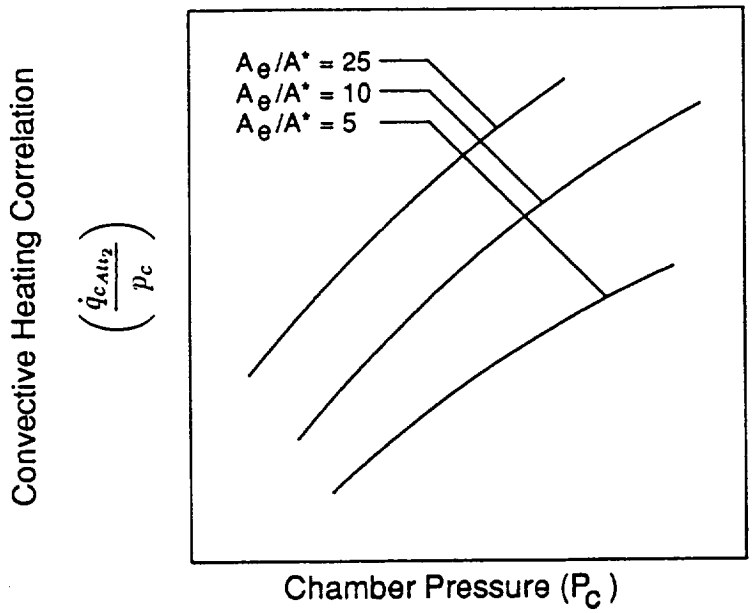


NOTE: Similar Curves Required for Each Different Propellant

(a) Convective Heating at $Alt_2$

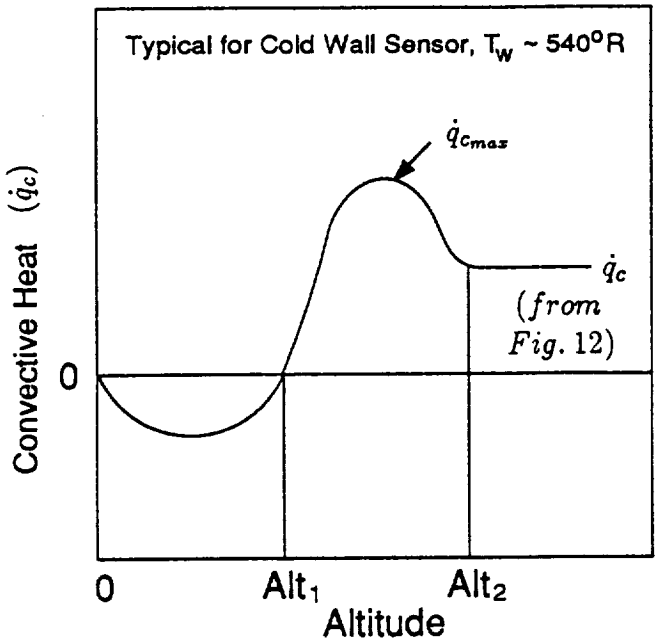


NOTE: Similar Curves Required for Each Different Propellant

(b) Convective Heating at All Altitudes

Figure 12: Determination of Convective Heating

and $P_c$ for a specific fuel, oxidizer, and O/F. Figure 12a is a generic representation of that relationship. From this, $\dot{q}_c$ versus altitude can be plotted as a horizontal line after $Alt_2$ (Fig. 12b). From launch to $Alt_1$ the base is actually cooled by the ambient air and $\dot{q}_c$ is negative. At $Alt_1$ $\dot{q}_c$ has been seen to equal 0, so this portion of the curve can be

plotted. Between $Alt_1$ and $Alt_2$ a maximum heating of approximately 1.6 times the value at $Alt_2$ has been repeatedly seen in the databases. The altitude at which this occurs is a matter of judgment and experience with the data. Now the plot can be completed by making a standard distribution approximation from $Alt_1$ to $\dot{q}_{max}$ and from $\dot{q}_{max}$ to $Alt_2$. With approximations of $T_r$ and $\dot{q}_c$, $h_c$ is calculated from $\dot{q}_c = hc(T_r - T_w)$. For cold wall, $Tw$ = 460°R and $h_c = \dot{q}_c/T_r$.

The procedure above assumes that the heat shield is at the nozzle throat and no shrouds, gimballing, or afterburning exist. If any or all of the first three conditions are different, empirical scaling factors for each condition are applied separately to modify the values determined using the steps above.

Afterburning is a much more difficult modification and not enough data exists to forecast a general trend. Each case is handled separately and the afterburning heat is added as a component like convection and radiation. Afterburning is not accounted for in the code and, therefore, is not reviewed in detail here.

For vehicles already in service, the flight data are used to construct the curves and define the trends used. Also, judicious use is made of some model and flight data from similar vehicles. Otherwise, the steps are the same.

### 2.1.2 Radiation Environments

Two types of analysis are used to determine radiation. (The methodology flow chart is shown in Fig. 13.) They depend on whether the plume is all gas or has solid particles. For the gaseous plume, the analysis starts with running a combustion code (e.g., TRAN72 [3]) and a nozzle flowfield code (e.g., RAMP2 [4]) to determine the characteristics of the plume. If the plume is overexpanded (low altitude), programs which account for the plume boundary shear layer and internal Mach discs (e.g., BLIMPJ and SPF/3 [2]) must also be run. Next, a series of GASRAD [5] runs are made with different points of interest input. GASRAD computes radiation to these points using internal spectral band models based on the plume constituents, temperatures, pressures, and view factors. By running at various altitudes, a set of scaling factors to adjust the low altitude values is determined (Fig. 14).

Because of the complexity and time involved in running GASRAD in earlier (1970's) analyses, not all points of interest were calculated in this manner. Typically, only a few points representing a surface in the base were so determined. To complete the analysis solid shapes were used to represent the plume(s) (Fig. 15). These shapes were usually cones, cylinders, and circles that were either opaque or transparent. Each was given an emissive power such that when the view factors to all the GASRAD points times the emissive powers were calculated using a modified version of RAVFAC [6] the resulting energy to these points equaled the values computed by GASRAD. This was an iterative process requiring a good deal of trial and error and relying heavily on engineering judgment. Then the radiate energy to all other points of interest was computed at low altitude with RAVFAC. These values were adjusted for altitude using the derived altitude scaling factors. For operational vehicles, the solid shape plume models were adjusted

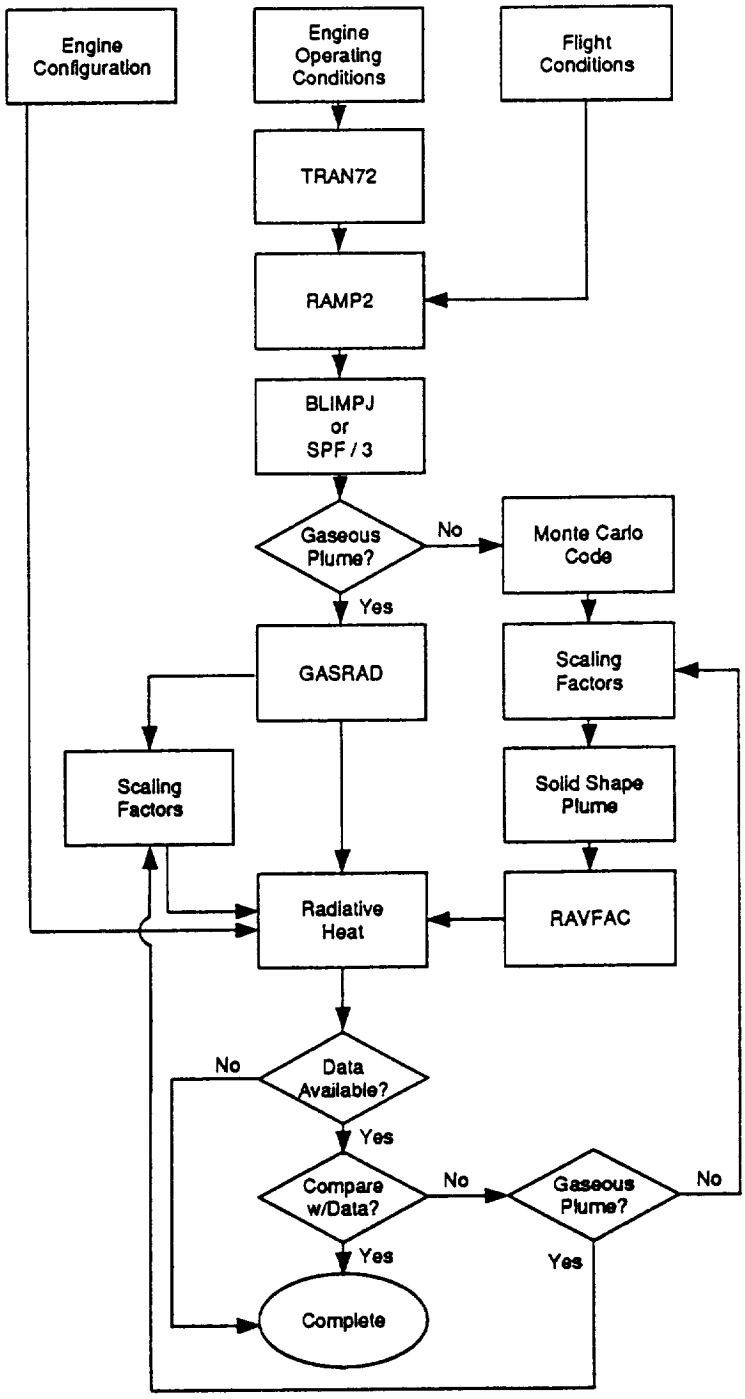


Figure 13: Flow Chart for Radiative Heat Rate Determination

to yield flight measured values. This adjusted model was then used for all subsequent design work.

Current computers are fast enough that most analyses since 1985 have used the GASRAD calculations exclusively for all points.

| ALTITUDE ADJUSTMENT for 160 kft | | | | | | | |
|---|---|---|---|---|---|---|---|
| Code Letter | K | L | M | N | O | P | Q |
| $q_{160k}/q_{SL}$ | 0.06 | 0.12 | 0.18 | 0.24 | 0.30 | - | - |
| $q_{160k}$ (Btu/ft -sec) | - | - | - | - | | 0.1 | 0.2 |

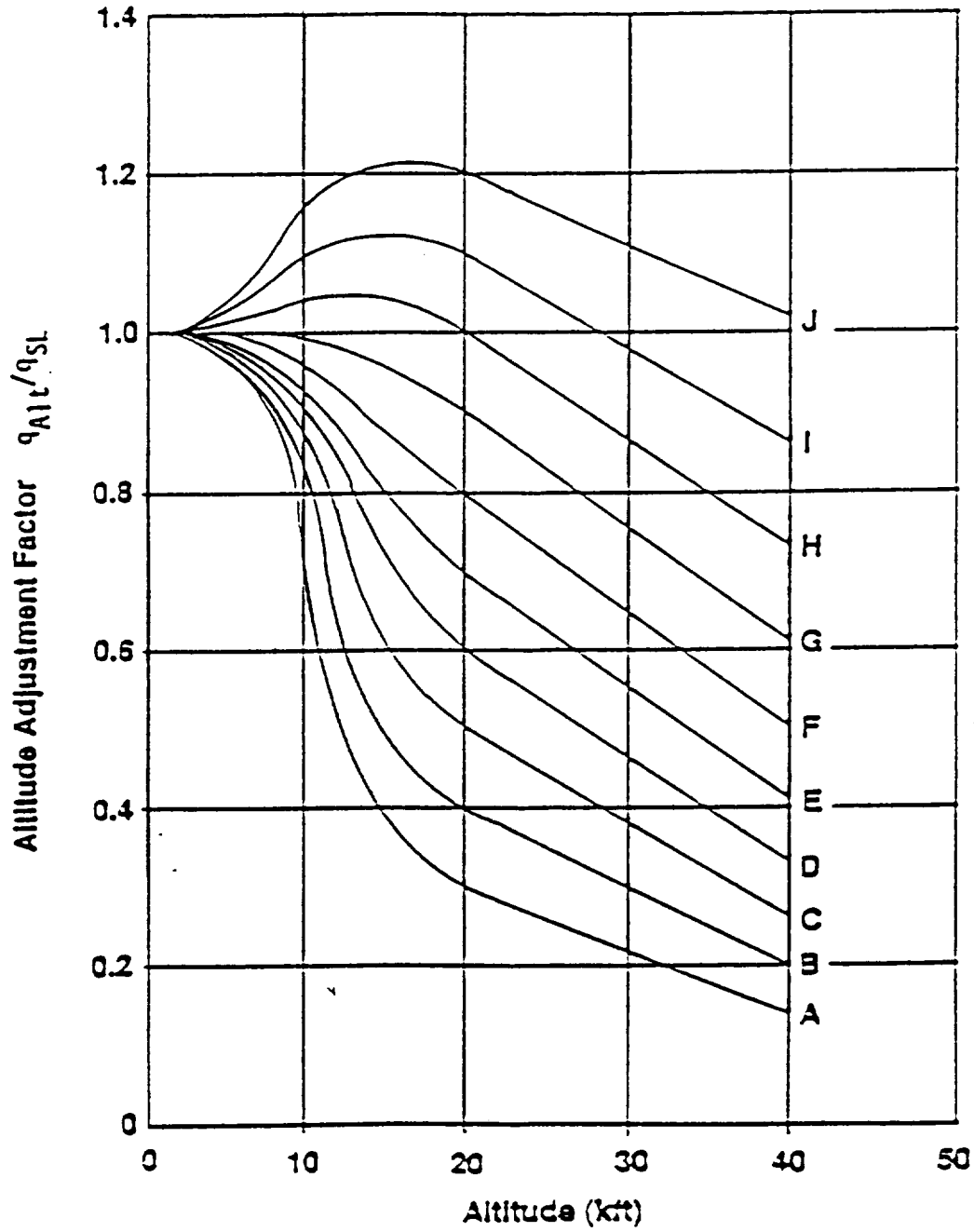


Figure 14: Scaling Factors Used to Adjust Radiative Heating from Sea Level Plumes to Altitude

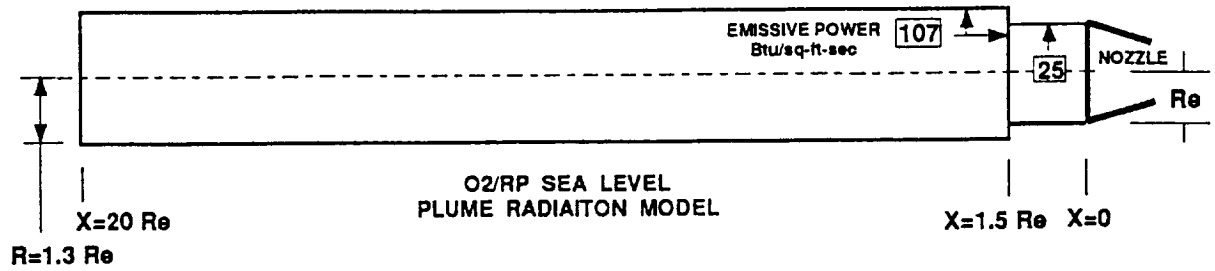


(a) Saturn S-I Plume ($RP1/LO_2$

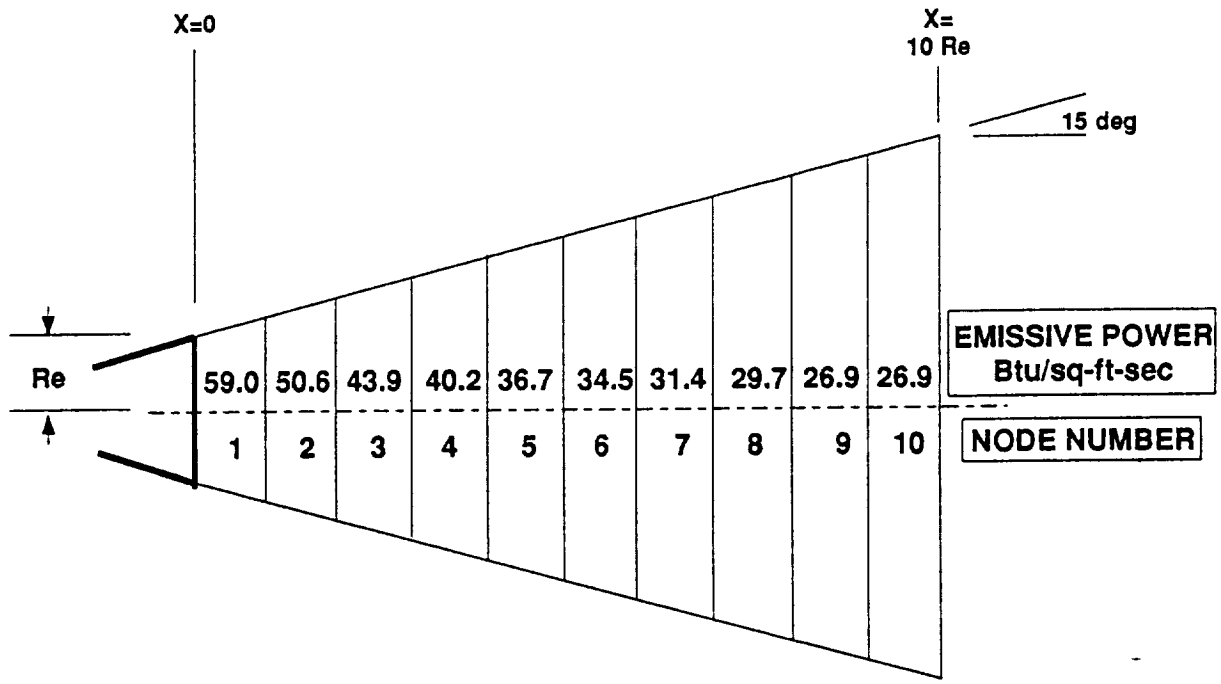


**REFERENCE SRM PLUME MODEL**
**WITH EMISSIVE POWERS FOR 16% ALUMINUM**

(b) STS SRB Plume (SRM)

Figure 15: Solid Shape Representation of Plume

Plumes with particles in them such as carbon from $RP1/LO_2$ and $Al_2O_3$ from solid rocket fuel present such a great theoretical challenge that most of the analyses rely on semi- and empirical methods. Accordingly, solid shape plume models are generated for the analyses necessary. The initial model is developed by running a two-phase nozzle and plume flowfield code at low altitude similar to the gaseous plume methodology. Current procedure is to use a combination of RAMP2 and SPF/3 which yields the gas and particle parameters necessary for input to a reverse Monte Carlo code [7]. This latter code then calculates the thermal radiance at the edge of the plume. Unfortunately, the SPF/3 code overpredicts particle parameters when used for this purpose, and the

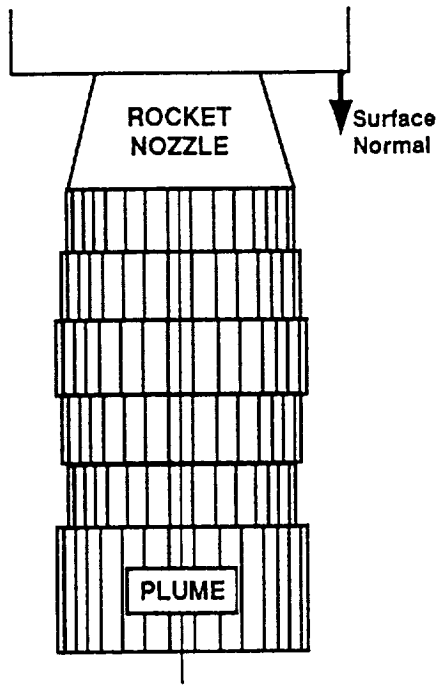


Figure 16: Monte Carlo Derived Solid Shape Representation of Plume

analyst typically must lower the heat transfer coefficient between the gas and the particle to produce a higher particle temperature. This has the effect of increasing the emissive power predicted by the reverse Monte Carlo code. Next, the solid shapes are broken into nodes which are assigned the predicted emissive powers (Fig. 16), and the view factors to all points of interest are calculated and multiplied by the emissive powers (using the modified RAVFAC) to obtain the incident radiant energy. If model data are (or become) available, the plume model is adjusted. This is also true when flight data become available.

By running a series of selected points at various altitudes, altitude corrections are generated similar to the gaseous plumes. Again, flight data are used to adjust these when they become available.

## 2.2 Difficulties and Errors

Several sources of error are inherent in the methodology:

1. Imprecise scaling.
2. Limits in database applicability — new vehicles must look and behave like previous ones.
3. Simultaneous effects - errors may compound.
4. Difficulty in $T_r$ determination.
5. Lack of complete flowfield definition.
6. Plume interaction regions not fully simulated — source of radiation.

This section discusses some of these problems as they apply to the convection and radiation environment determinations.

### 2.2.1 Convection

In computing the convection heating a number of generalities were accepted. Although it has been observed that the altitude at which the plume gases begin to enter the base region ($Alt_1$) and the altitude at which the plume gases fill the base region ($Alt_2$) can be correlated by L/D and $A_e/A^*$, the real situation is far more complex. CFD techniques would have to be used to model the complete flowfield and even then, only very simple situations could be handled. Also a tremendous amount of computer time would be needed for even a simple case. Thus the use of the semi-empirical curves in the standard methodology is the only practical solution but the potential for errors must be recognized.

The use of $P_a$ and $P_c$ to determine $P_b$ used in calculating $\dot{m}$ causes some error. The databases have shown this to be a good approximation in the past, but $P_b$ is more of a direct function of the post bow shock pressure and the vehicle boundary layer being turned into the base instead of $P_a$ initially. Also $P_c$ does affect the plume gases from the nozzle boundary layer turned into the base region, but it is certainly not the only effect. Future vehicles may well need a complete vehicle and nozzle boundary layer analysis for accuracy.

The final determination of $T_r$ has several database correlations which could cause errors. The mass flow distribution between $Alt_1$ and $Alt_2$ has not been critical to past analyses; nevertheless, the assumption that it is a standard distribution could have significant consequences for future vehicles. Also, in the past only a small portion of the nozzle boundary layer mass flow was needed to fill the base region and $T_r$ was equal to the average temperature of that portion of the boundary layer. It is possible that a vehicle could be designed such that all the boundary layer and possibly some of the core flow could enter which could alter the calculation of $T_r$.

The determination of $\dot{q}_c$ is heavily dependent on empiricism. Different O/F ratios are not accounted for in $\dot{q}_c/P_c$ curves since the O/F for each fuel and oxidizer combination in the databases has always been the same. If other ratios were used a new set of curves or an entirely new correlation would have to be determined. Finally, the $\dot{q}_c$ versus altitude curve has only four points on it which, except for altitude equal zero, are completely dependent on previous data.

### 2.2.2 Radiation

Radiant heating analysis errors come from the use of solid shapes to represent the plumes. It takes judgment to determine the angles and diameters of the cones, cylinder, and circles used. It is also difficult to correctly determine the emissive power that should be assigned to each node. There is no closed form method of doing this so that even when predictions match theoretical calculations or data there is still reason to question predictions for other points on the vehicle.

# Section 3
# HISTORICAL REVIEW — MODEL AND FLIGHT BASE HEATING DATA

As previously discussed, the determination of the convective and radiative environments is heavily dependent on databases gathered over the years. The model and flight base heating database for large launch vehicles is quite extensive, with unclassified information available from most NASA and Air Force programs since the late 1950's. The convective database contains environments measured on models and flight vehicles utilizing a variety of propulsion systems. The model data are primarily from subscale model tests performed before 1978. Subscale model tests usually provide considerable detail about convective heating trends, but are subject to scaling uncertainty. Scaling data from the database to a new configuration and propulsion system is relatively simple provided both gamma of the exhaust products and chamber temperature are approximately the same for both the new configuration and the data source. Flight data and other radiometer data from subscale motor firings have also been utilized to generate plume radiation prediction models. Plumes containing soot or alumina have been based historically upon the empirically generated models.

Table 1 summarizes the databases that are available and have been used in creating the current methodology. As shown, there have been a number of different vehicles, Mach numbers, fuels, O/F ratios, nozzle configurations, heat shield locations, gimbal angles, and altitudes used. The data gathered have been static, pitot, and total pressure in the chamber, nozzle, base, and plume from cold flow and hot firing tests as well as flight instrumentation. Thermal data have consisted of direct and indirect base surface and gas temperatures and radiant, convection, and total heating measurements from model tests and flight instrumentation as well.

The databases also include information about a number of special cases. Such unusual factors as boattails, shrouds, base bleed, turbine exhaust burning, and engine-out effects are documented and have been used in various design efforts.

A number of papers and reports have been used to develop the current methodology. Many of these documents used the same databases referenced here. Table 2 catalogs them and it may be seen that they are the foundation for every aspect of the methodology outlined in the previous Section.

Table 1: Databases Used for Base Heating Determination

| Base | Flight or Model | Traj/ Alt | Fuel/ Oxidizer | Mach | Data* | Purpose | Ref |
|---|---|---|---|---|---|---|---|
| Titan II w/2 SRM | 5.5% Mod | Ascent | 15%AlSRM | 0.6-3 | P,T,Qc, Qt | Only SRM Fired; No Liquid Motor Sim | [8] |

Table 1: (Continued) Databases Used for Base Heating Determination

| Base | Flight or Model | Traj/ Alt | Fuel/ Oxidizer | Mach | Data* | Purpose | Ref |
|---|---|---|---|---|---|---|---|
| Titan II | Flight | Flt | N2O2/ Aerozine | Flt | Qt | Qt Data | [9] |
| Titan IIIC | Flight | Flt | N2O2/ Aerozine SRM | Flt | Qc,Qr | Q Data | [9] |
| Thor | Flight | Flt | JP4/LO2 SRM | 1.2-4 | | Effect of Turbo Exh | [10] |
| Thor DSV-2A | Flight | Flt | RJ1/LO2 | Flt | P,Qt | Compare to Design | [9] |
| Thor DSV-2A | 10.7% Mod | | RJ1/LO2 | 0 | Qt | Qtbase Data | [9] |
| Thor DSV-2C | Flight | Flt | RJ1/LO2 SRM | Flt | P,Qr,Qt | Compare to Design w/3 SRM | [9] |
| Thor DSV-2C | 10.7% Mod | | RJ1/LO2 SRM | 0 | Qt | Qt Data for 3 SRM | [9] |
| Thor DSV-2L | Flight | Flt | RJ1/LO2 SRM | Flt | Qc,Qr,Qt | Q Data for Long Flt | [9] |
| Thor DSV-3L | Flight | Flt | RJ1/LO2 SRM | Flt | Qc,Qr,Qt | Q Data for 6 SRM | [9] |
| S-I | Flight | Ascent | RP1/LO2 | 0-4 | P,Qc,Qr, Qt | Compare to Design | [9] |
| S-I | 1/33 Mod 8 Eng | SL | Cold Air | 0.1-2 | P | Pbase Data;Effect of Base Bleed,Heat Shld | [11] |
| S-IC | Flight | Ascent | LH2/LO2 | ? | P,Qr,Qt | Compare to Design | [9] |
| S-II | Flight | Ascent | LH2/LO2 | ? | P,Qc,Qt | Compare to Design | [9] |
| S-II | 1/25 Mod of Base Region | 240K-300Kft | GH2/GO2 | 0 | P,Tg,Qt | P,Qtbase,Tg Data | [12] |
| S-II | Flight | Ascent | LH2/LO2 | 0-4 | P,T,Tg, Qr,Qt | Compare to Design | [12] |
| S-IV | 1/10 Mod | | GH2/GO2 | 0 | P,Qt | P&Qt Data, 4&6 Eng | [13] |

Table 1: (Continued) Databases Used for Base Heating Determination

| Base | Flight or Model | Traj/ Alt | Fuel/ Oxidizer | Mach | Data* | Purpose | Ref |
|---|---|---|---|---|---|---|---|
| S-IV | 1/27 Mod | | Cold Air | 0 | P | Pbase Data, 4 Eng | [14] |
| S-IV | 1/27 Mod | 100K-194Kft | Cold Air | 0 | P | Alt2, Heat Shield Location, Gimbal, Eng Out, Pc, Tc, Turbo Exh | [15] |
| S-IV | Mod w/4 Eng | 120K-200Kft | GH2/GO2, Hot GN2 | 0 | P,Qt | Pplume, Effect of Heat Shield Off | [16] |
| J-2 | 1/25 Mod w/ 3 Eng | 30K-80Kft | GH2/GO2 | 0 | P,Qt | P & Qbase Data | [17] |
| STS-1 | Flight | Ascent | LH2/LO2 | Flt | P,Tg,Qr, Qt | Compare to Design | [18] |
| STS-2 | Flight | Ascent | LH2/LO2 | Flt | P,Tg,Qr, Qt | Compare to Design | [19] |
| STS-3 | Flight | Ascent | LH2/LO2 | Flt | P,Tg,Qr, Qt | Compare to Design | [20] |
| STS-4 | Flight | Ascent | LH2/LO2 | Flt | P,Tg,Qr, Qt | Compare to Design | [21] |
| STS-5 | Flight | Ascent | LH2/LO2 | Flt | P,Tg,Qr, Qt | Compare to Design | [22] |
| Generic | Plug Noz Model | SL | Cold Air | 0 | P | Pbase Data; Effect Base Bleed | [23] |
| Generic | 500 lb Thrust Mod | SL | MMH/N2O4 | 0.3-3 | Qr | Qr Data; Effect of Qr | [24] |
| Generic | Mod w/Skirt 1-6 Eng | SL | Cold Air | 2.3-4.7 | P | Pbase; Effect of Multi-Eng, Shroud Conf | [25] |
| Generic | 500 lb Thrust Mod | SL | JP4/LO2 | 2-3.5 | P,Tg,Qt | Effect of Gimbal, Eng Conf, Pc, Base Bleed | [26] |
| Generic | 1000 lb Thrust Mod | SL | JP4/LO2 | 0.8-2 | P,Tg | Effect of Afterbody Conf, O/F | [27] |
| Generic | 1000 lb Thrust Mod | SL | JP4/LO2 | 0.8-2 | P,Tg | Effect of Boattail | [28] |

Table 1: (Continued) Databases Used for Base Heating Determination

| Base | Flight or Model | Traj/ Alt | Fuel/ Oxidizer | Mach | Data* | Purpose | Ref |
|---|---|---|---|---|---|---|---|
| Generic | Mod w/1 Eng | SL | Cold Air H2O2 | 1.6-2 | P,T,Tg | P&Tbase;Effect of A/A*,Base Bleed Data | [29] |
| Generic | 4000 lb Thrust Mod | 72Kft | SP4/LO2 | 3 | T,Tg,Qc, Qt | Effect of 1 Eng,O/F | [30] |
| Generic | Mod w/3 Eng | 180K-320Kft | SRM | 0 | P,Tg,Qc | Effect of Widely Spaced Nozzles | [31] |
| Generic | Mod w/4 Eng | Vacuum | Hot&Cold Air | 0 | P,T | Effect of Vacuum | [32] |
| Generic | Mod w/4 & 5 Eng | 60K-200Kft | Cold Air | 0 | P | Effect of Noz Conf, Gimbal,Heat Shield | [33] |
| Generic | Mod w/4 Eng | 61K-100Kft | Hot&Cold Air | 0 | P,Qt | Effect of Eng Out, Shroud | [34] |
| Generic | Mod w/1 Eng | SL | Cold Air He,CF-14 | 0.9-2.5 | P | Effect of Boattail | [35]* |

*P=Base pressure, T= Base temperature, Tg=Gas temperature, Qc=Convective heating, Qr=Radiative heating, Qt=Total heating

Table 2: Documents Pertaining to Base Heating Methodology


1. Navickas, J., "Shuttle Booster and Orbiter Base Heating During Ascent," McDonnell Douglas Design Note No. I-WEST-THERMO-4, Sep. 14, 1970.
2. Capenter, P. W. and Tabakoff, W., "Survey and Evaluation of Supersonic Base Flow Theories," NASA Contractor's Report CR 97129, Oct. 1968.
3. Schuller, C. F., "Interactions between the External Flow and Rocket Exhaust Nozzle," IAS Paper No. 59-133, Oct. 1959.
4. Rosner, D. E., "Scale Effects and Correlations in Nonequilibrium Convective Heat Transfer," *AIAA J.*, Vol. 1, No. 7, July 1963, p. 1550.
5. Page, R. H., "Base Heating on a Multiple Propulsion Nozzle Missile," AIAA Paper No. 63-179, June 1963.
6. Baum, E., "Initial Development of the Laminar Boundary Layer Separated Shear Layer," *AIAA J.*, Vol. 2, No. 1, Jan. 1964, p. 128.
7. Hama, F. R., "Estimation of the Strength of Lip Shock," *AIAA J.*, Vol. 4, No. 1, Jan. 1966, p. 166.

Table 2: (Continued) Documents Pertaining to Base Heating Methodology

8. Sergeant, R. J., "Base Heating Scaling Criteria for a Four-Engine Rocket Cluster Operating at High Altitude," AIAA Paper No. 65–826, Dec. 1965.
9. Weinbaum, S., "Rapid Expansion of a Supersonic Boundary Layer and Its Application to the Near Wake," *AIAA J.*, Vol. 4, No. 2, Feb. 1966, p. 217.
10. Weiss, R. F. and Weinbaum, S., "Hypersonic Boundary-Layer Separation and the Base Flow Problem," *AIAA J.*,Vol. 4, No. 8, Aug. 1966, p. 1321.
11. Donaldson, I. S., "On the Separation of a Supersonic Flow at a Sharp Corner," *AIAA J.*, Vol. 5, No. 6, June 1967, p. 1086.
12. Weiss, R. F., "A New Theoretical Solution of the Laminar, Hypersonic Near Wake," *AIAA J.*, Vol. 5, No. 12, Dec. 1967, p. 2142.
13. Baum, E., "An Interaction Model of a Supersonic Laminar Boundary Layer on Sharp and Rounded Backward Facing Steps," *AIAA J.*, Vol. 6, No. 3, March 1968, p. 440.
14. Weiss, R. F. and Nelson, W., "Upstream Influence of the Base Pressure," *AIAA J*, Vol. 6, No. 3, March 1968, p. 466.
15. Kessler, T. J., "A Theory for Two-Dimensional Supersonic Turbulent Base Flows," AIAA Paper No. 69-68, Jan. 1969.
16. Smoot, D. L., Simonsen, J. M., and Hedman, P. O., "Development and Evaluation of a Flight Attenuation Model," Naval Weapons Center Technical Publication NWC TP 5048, Nov. 1971.
17. Smoot, D. L., Simonsen, J. M., and Williams, G. A., "Development and Evaluation of an Improved Aft-Plume Model," Naval Weapons Center Technical Publication NWC TP 5521, Nov. 1973.
18. Delery, J. and Lacau, R. G., "Prediction of Base-Flows," Paper in AGARD Report R-754, *Special Course on Missile Aerodynamics*, May 1987.
19. Lamb, J. P., Hood, C. G., and Johnson, M. G., "A Convective Transport Model for Supersonic Planar Base Flows," ASME Paper 70-HT/SpT-35, June 1970.
20. Mitchell, Jr., H. A., "An Approach to the Solution of the Base Heating Problem for an Axisymmetric Multi-Nozzle Configuration," Boeing Company Thermal Technology Research Memorandum Therm 4, Feb. 1966.
21. Addy, A. L., "Analysis of the Axisymmetric Base-Pressure and Base- Temperature Problem with Supersonic Interacting Freestream-Nozzle Flows Based on the Flow Model of Korst, et al., Part I: A Computer Program and Representative Results for Cylindrical Afterbodies," Army Missile Command Report No. RD-TR-69-12, July 1969.
22. Addy, A. L., "Analysis of the Axisymmetric Base-Pressure and Base- Temperature Problem with Supersonic Interacting Freestream-Nozzle Flows Based on the Flow Model of Korst, Et Al., Part II: A Comparison and Correlation with Experiment for Cylindrical Afterbodies," Army Missile Command Report No. RD-TR-69-13, Dec. 1969.
23. Addy, A. L., "Analysis of the Axisymmetric Base-Pressure and Base- Temperature Problem with Supersonic Interacting Freestream-Nozzle Flows Based on the Flow Model of Korst, Et. Al, Part III: A Computer Program and Representative Results

Table 2: (Continued) Documents Pertaining to Base Heating Methodology

for Cylindrical, Boattail, or Flared Afterbodies," Army Missile Command Report No. RD-TR-69-14, Feb. 1970.

24. Lamb, J. P., Abbud, K. A., and Lenzo, C. S., "A Theory for Base Pressures in Multi-Nozzle Rocket Configurations," University of Texas, Department of Mechanical Engineering Report, Feb. 1968.
25. Dixon, R. J. and Page, R. H., "Theoretical Analysis of Launch Vehicle Base Flow," Boeing Company Report No. D2-36605-1, May 1966.
26. Korst, H. H., "A Theory for Base Pressures in Transonic and Supersonic Flow," *J. of Applied Mechanics*, Vol. 23, No. 4, Dec. 1956, p. 593.
27. Ying, T. O., "A Review of Selected Methods of Predicting Base Flow Environment in Supersonic Flow, " Lockheed Missiles and Space Company Technical Report LMSC/HREC AO36435, H-64-008, July 1964.
28. Bauer, R. C. and Fox, J. H., "An Application of the Chapman-Korst Theory to Supersonic Nozzle-Afterbody Flows," AEDC Technical Report TR-76-158, Jan. 1977.
29. Chow, W. L. and Korst, H. H., "On the Flow Structure within a Constant Pressure Compressible Turbulent Jet Mixing Region," NASA Technical Note TN D-1894, April 1963.
30. Nourse, R. W., "A Numerical Routine for Defining Rocket Exhaust Characteristics and Impingement Effects," Army Missile Command Technical Report No. RD-ST-88-7, Sep. 1988.
31. Walker, B. J. and Addy, A. L., "Preliminary Investigation of the Effect of Afterburning on Base Pressure, Army Missile Command Technical Report No. RD-TM-71–6, Dec. 1971.
32. Grier, N. T., "Back Flow from Jet Plumes in Vacuum," NASA Technical Note TN D-4978, Jan. 1969.
33. Cooper, B. P., " Nozzle Boundary Layer Model Including the Subsonic Sublayer Usable for Determining Boundary Layer Effects on Plume Flowfields," McDonnell Douglas Paper WD2936, May 1979.
34. Chirivella, J. E., "Molecular Flux Measurements in the Back Flow Region of a Nozzle Plume," Jet Propulsion Laboratory Technical Memorandum 33-620, July 1973.
35. Rader, R. J., "Stagnation Heating Rates in Rocket Engine Exhaust Plumes Considering Equilibrium, Frozen, and Finite Rate Chemistry," Northrop Services, Inc. Technical Report TR-230-1186, Jan. 1973.
36. Jensen, D. E., Spalding, D. B., Tatchell, D. G., and Wilson, A. S., "Computation of Flames with Recirculating Flow and Radial Pressure Gradients," Propellants, Explosives, and Rocket Motor Establishment Report.

# Section 4
# CODE CAPABILITY SELECTION CRITERIA

The major objective of this contract effort was to develop a design code which could be utilized to predict base heating for a broad range of potential launch vehicles. A significant stumbling block in developing the code was the necessity of imposing some reasonable limits on the vehicle configurations which could be analyzed by the code, as well as limitations on the choice of propulsion systems. Over the past five years, 1987 through 1992, space transportation system studies conducted by DoD and NASA have considered a variety of concepts. REMTECH's requirement throughout its contract was to condense these studies into a set of likely vehicle concepts and develop the code to address, as a minimum, the baseline vehicles. The following review will demonstrate the breadth of concepts which were considered and describe the criteria used to select the range of concepts addressable by the code.

## 4.1 ALS/NLS Concepts

Most of the following summary information was presented by MSFC in January 1992 [36] to a joint NASA-DoD steering group which was conducting a review of historical and current space transportation systems and launch vehicle concepts. Space Transportation Architecture Studies (STAS) began in 1985 and eventually evolved through the ALS program, Shuttle Derived Vehicle studies, to the NLS program which was recently canceled. A historical perspective of the programs and objectives is summarized below.

STAS (1985–1987)

- DoD, NASA, and industry
- Built upon lessons learned, ELVs and Shuttle
- Explored a broad array of concepts
- Architecture analysis and technology needs

ALS (1987–1991)

- Clean sheet systems approach to space transportation
- Explored modular design over 20–300K payload range
- New facilities and infrastructure
- Very low operations cost objective

STS LRB Studies (1985–1988)

Shuttle Derived (1987–1990)

- Early heavy-lift capability (100 — 150K lbs)
- Minimize DDT&E costs, technical and schedule risks
- Constrained flight rate

NLS (1991–1992)

- Modular concept
- Payload range (20K/50K/150K); growth potential
- Evolutionary approach (blend new technology with existing)
- Facilities: utilize some existing, add for operability, replicate for resiliency

A variety of vehicles and launch concepts were considered initially by STAS as shown in Fig. 17. Large (one of a kind) vehicle concepts like Saturn V were passed over in favor of: 1) modular and flexible concepts for a family of vehicles; 2) lower operating costs; and 3) more rapid launch availability. The launch configuration eventually migrated toward parallel assembly and parallel burn and there was a national interest on refocusing propulsion system development toward a new LOX/$LH_2$ engine and a new LOX/hydrocarbon engine. Initially, all core stages or second stages were clearly focused on LOX/hydrogen propulsion systems while the boosters were focused primarily on LOX/hydrocarbon systems.

Following STAS the ALS program was initiated with seven contractor teams introducing reference vehicle concepts as shown in Fig. 18. The Phase 1 ALS studies continued in 1989 and the vehicle definition began to take focus as the following vehicle system studies were pursued.

- Series vs. Parallel burn
- Expendable vs. Partially Reusable vs. reusable
- Orbital vs. suborbital payload delivery
- Solid vs. Liquid booster
- Hydrogen vs. hydrocarbon core stage
- Hydrogen vs. hydrocarbon liquid booster stage
- Gas Generator vs. split expander vs. tap-off engine cycles
- Engine-Out vs. no engine-out capability

Typical parallel burn and series burn concepts are depicted in Fig. 19. As a result of the systems studies, $LH_2$ was baselined for the ALS core. Methane, propane, $LH_2$ and RP-1 were evaluated as candidate booster fuels for the ALS. $LH_2$ was selected because it:

- Eliminates cost of developing a second engine and tank system.
- Reduces development risk to one engine and propellent tank system.
- Provides a single fuel, thereby reducing facility and support costs.
- Reduces recurring cost of manufacture and operations.
- Use of RP-1 requires an increased thrust level of approximately 40 percent.

STAS

# Candidate Launch Vehicle Concepts

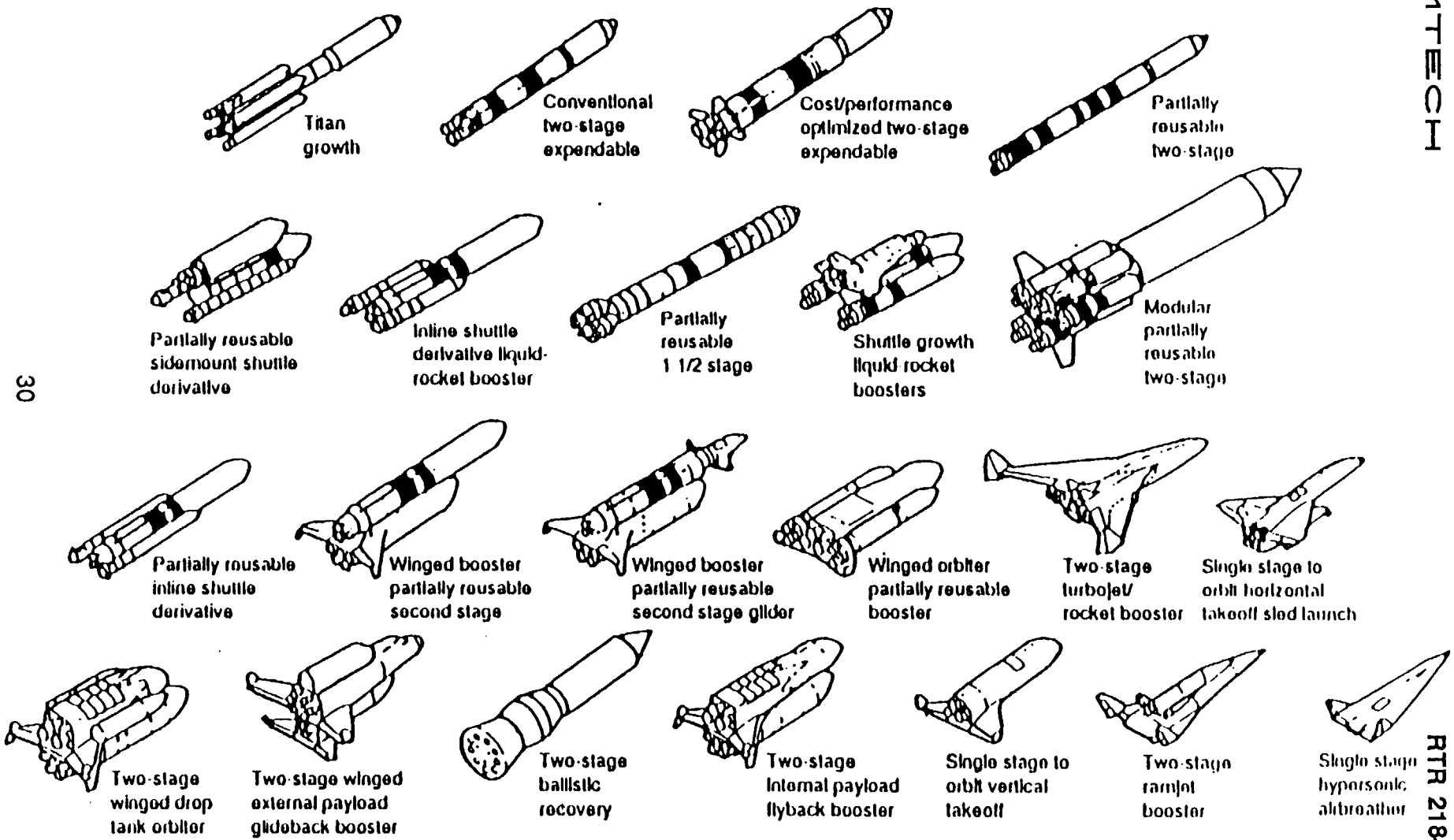


Figure 17: STAS Candidate Launch Vehicle Concepts

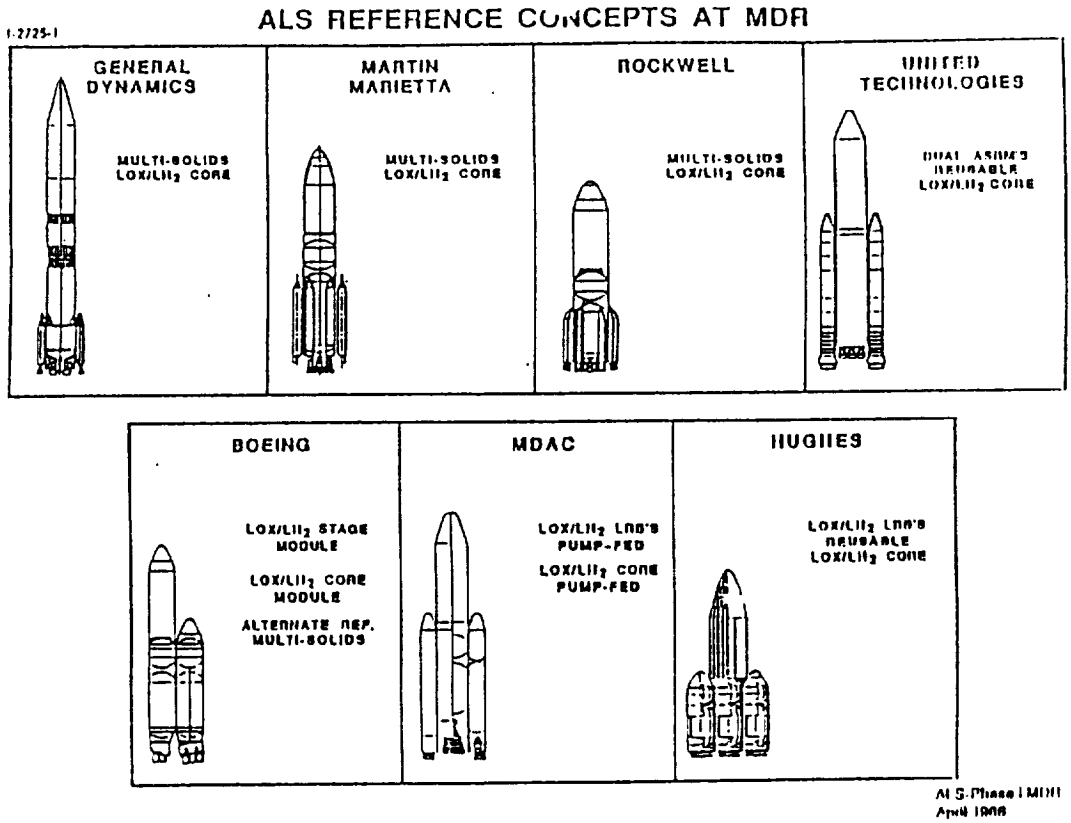


Figure 18: ALS Reference Launch Vehicle Concepts

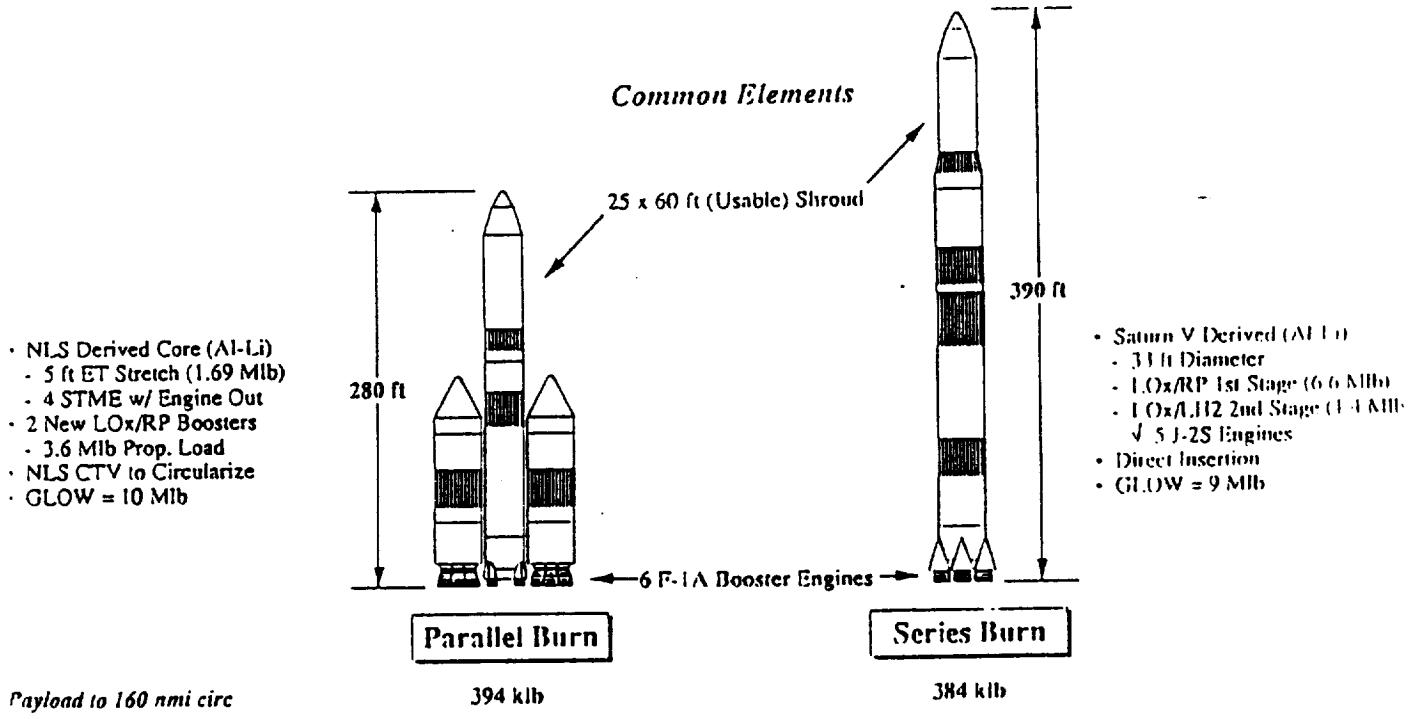


Figure 19: Parallel and Series Burn Launch Vehicle Concepts

In addition, overall system reliability and operability are improved by using a single fuel since there is only one set of engine peculiar problems to be encountered in checkout and flight. This rationale is further depicted in the schematic of Fig. 20. The final results of the systems studies are summarized below.

- All studies (STAS, ALS, NLS, in-house) (with a parallel burn strap-on booster or a second stage in a series burn) concluded that:
  - Core of second stage should be $LOX/LH_2$ to keep performance and cost reasonable/competitive
- Parallel burn was consistently recommended by STAS, ALS, in-house and NLS because:
  - Allows modular/flexible vehicles (various sizes, capable of evolving, manned/unmanned, reuse)
  - Potentially improves mission reliability
  - Less complex launch facility/access operations
- For vehicles proposed (parallel assembly/burn) $LOX/LH_2$ thrust requirement has consistently been in 500–650K range
- A low-cost, expendable or reusable/robust new engine (or engines) has been the result of trades, cost objectives, and industry capability retention

STME or Equivalent Required

- A potential option also exists to build large strap-on boosters using a common LOX/LH engine of 500–650K thrust — a potential of future cost savings via common engine

These candidate propellants were considered for liquid boosters as alternatives to solids. Study results are compared in Table 3.

At the conclusion of the ALS studies, a family of vehicles with payload capability from 40 to 300 KLBs had been identified as shown in Fig. 21. By 1991, the Air Force/DoD focus had changed from 120K to 50K vehicles, and subsequently, were directed toward 20K payloads. This initiated the transition from the ALS/Shuttle-C concepts previously studied toward a new vehicle referred to as the National Launch System (NLS). For NLS a large core vehicle was retained to support a new family of vehicles which met Air Force needs and satisfied NASA's evolution path to support the Space Exploration Initiative (SEI). A stage and on-half vehicle was preferred for the 50K payload requirement with a staging engine preferred over staging small solids. NASA goals fro NLS included an 80K+ vehicle to support the space station. Early vehicle evaluation for the NLS is depicted in Fig. 22 and architecture options are shown in Fig. 23. Progression from the NLS reference vehicles to the larger vehicles required for SEI missions is shown schematically in Fig. 24.

The most recent (Fall 1992) study initiated by NASA following cancellation of the NLS program is an early heavy lift vehicle specifically targeted at implementation of Space Station deployment. This vehicle, EHLLV, utilizes an extended Shuttle ET with a boattail to accommodate the Orbiter propulsion package of three SSMEs. Current RSRMs are

**Core Stage**

$LOX/LH_2$ vs LOX/HC → $LOX/LH_2$ Significant Advantage

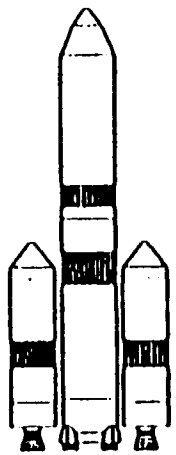

**Booster Stage**

$LOX/LH_2$ vs LOX/HC → LOX/HC Slight Advantage

**Vehicle Option 1**

$LOX/LH_2$ Core
LOX/HC Booster
→ 2 Engine Developments
2 Fuels @ KSC

**Vehicle Option 2**

$LOX/LH_2$ Core
$LOX/LH_2$ Booster
→ 1 Engine Development
1 Fuel @ KSC

Figure 20: ALS System Study Results

Table 3: Study Results of Candidate Propellants for Liquid Boosters

| | $LO_2$ /RP-1 | $LO_2$ /$CH_4$ | $LO_2$ /$LH_2$ |
|---|---|---|---|
| Environmental Impact | Some — Ignitable waste, $CO_2$ and CO in exhaust | Some — Clean burning, but $CO_2$ and CO in exhaust | Best — Benign |
| Reliability | Best — Simple, proven, but large, throttling | Lowest — 2 cryogens, new technology | Medium — Complex (two cryos), but step thrust |
| STS Compatibility | Good — Close to SRB size | Good — Next smallest | Good — large size offset by low weight/thrust |
| KSC Facility Impact | Major — Dual fuel, rebuild Saturn system | Major — All new propellant system | Some — Size impacts lower, add to existing propellant system |
| Growth Potential | Fair — Stand-alone or ALS booster, but limited reusability | Good — Stand-alone or ALS booster, better reusability | Best — Common engine with ALS, Shuttle-C, stand-alone booster and core |
| Risk | Low — Proven, but worry combustion instability | Medium — No flight experience | Low — Proven |
| Vehicle Costs | Lowest for STS LRB | High — Risky | Close to $LO_2$ /PR-1, lower with commonality |

utilized and an existing cargo carrier or payload accommodation shroud is adapted to the forward end of the ET. This concept is shown schematically in Fig. 25.

## 4.2 Criteria for Limiting Code Capability

As discussed in the previous section, almost every conceivable combination of vehicle stages and propulsion systems had been proposed. Many of the more complex vehicle arrangements proposed for heavy lift capability employ multiple boosters surrounding a core stage and also have large, complex payloads. Through the first year of its contract REMTECH studied the concepts as they were introduced to establish the initial capability goals for the design base heating code. It was obvious that some concessions to a generic vehicle had to be made. Two important questions had to be answered immediately:

1. Would the code address a complex vehicle with boosters surrounding a core?
2. Would the code have the capability to handle non-symmetric arrangements of core and booster stages?

Other questions which emerged in selecting the overall capability of the initial version of the code included:

3. How complex could the forebody configuration be?
4. Were there real limits in the types of propellants which could be considered?
5. Would engines and motors with different nozzle exit planes be considered?
6. Would engine gimbaling or engine-out be treated by the code?

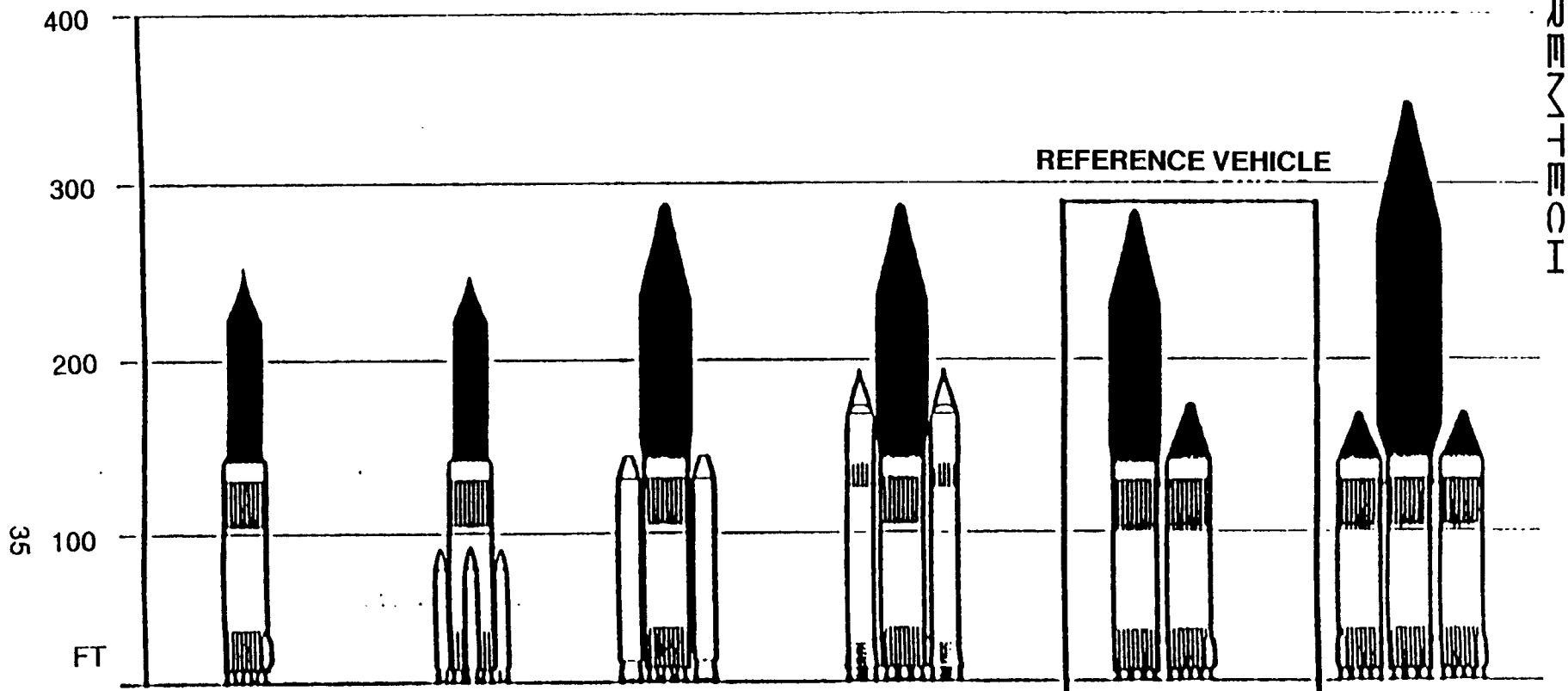


| | | | | | | |
|---|---|---|---|---|---|---|
| **RATED PAYLOAD** | 40 - 80 Klb | 40 - 80 Klb | 80 - 110 KLB | 100 - 251 Klb | 80 - 120 KLB | 120 - 300 Klb |
| **BOOSTER TYPE** | Stage and Half | ALS - SRM | SRMU | STS LRB | ALS LRB | ALS LRB |
| **BOOSTER PROP.** | L02 / LH2 | Solid | Solid | L02 / LH2 | L02 / LH2 | L02 / LH2 |
| **NO. OF BOOSTERS** | N/A | 3 - 8 | 2 - 4 | 2 - 6 | 1 | 2 - 4 |

Figure 21: ALS Family of Launch Vehicles

REMTECH

RTR 218-01

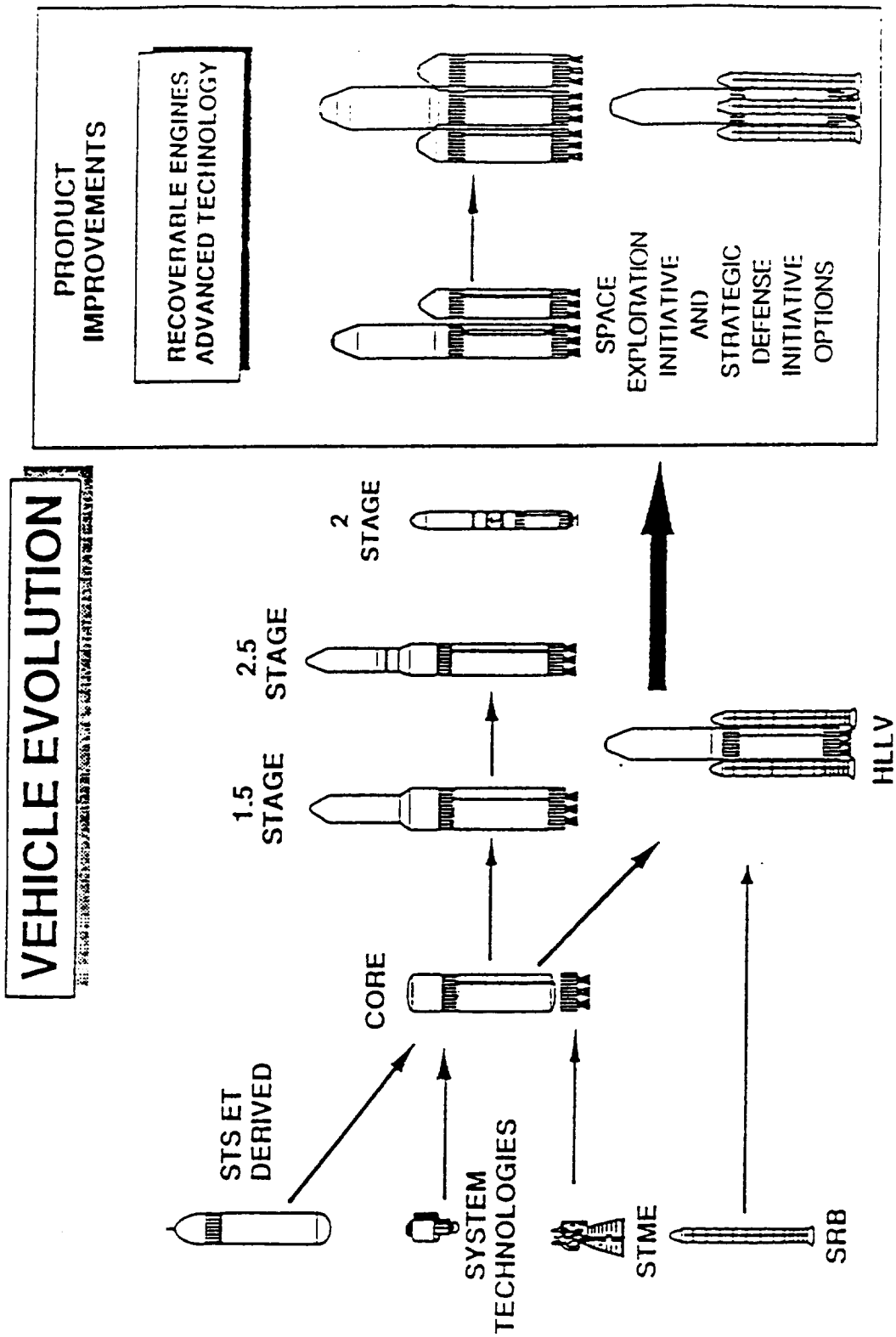


Figure 22: Launch Vehicle Evolution in 1991

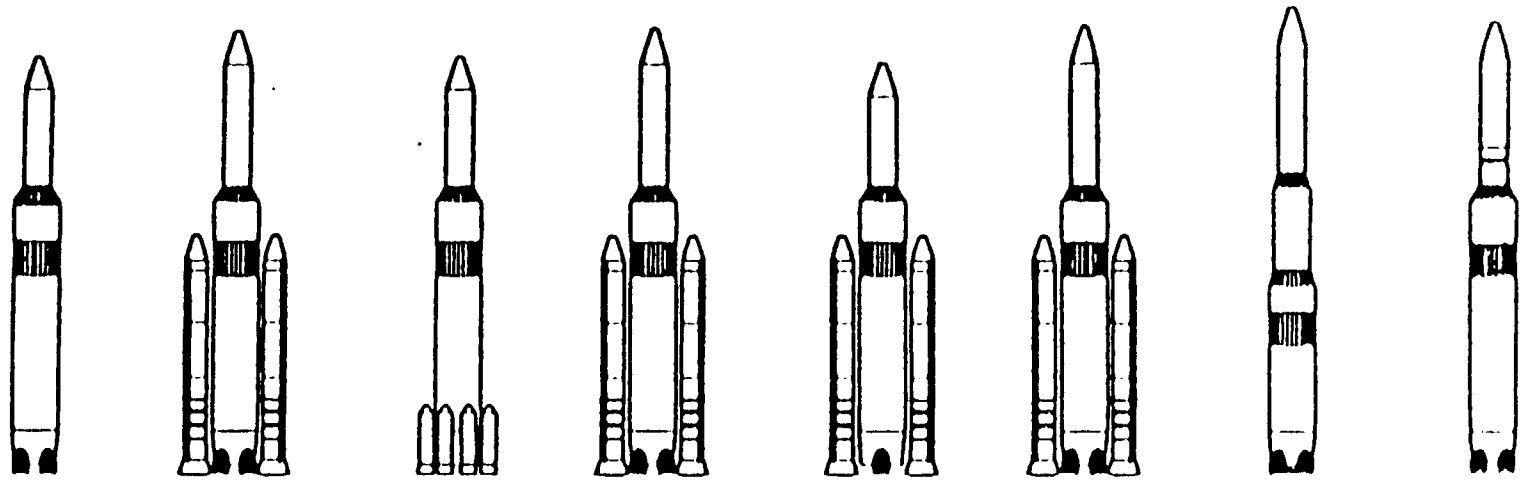

| | 1.5 Stage | HLLV | 1.5 STAGE | HLLV | HLLV | HLLV | 2.0 Stage | 2.5 Stage |
|---|---|---|---|---|---|---|---|---|
| PROPULSION | 4 STME +2 STME | 4 STME +2 ASRB | 4 STME 6 Castors | 4 STME +2 ASRB | 2 STME +2 ASRB | 4 STME +2 ASRB | 5 STME | 6 STME |
| UPPER STAGE | None | CTV | None | CTV | None | CTV | SIVB Class NUS CTV Func. | Cent. Class NUS CTV Func. |

Figure 23: NLS Architecture Options

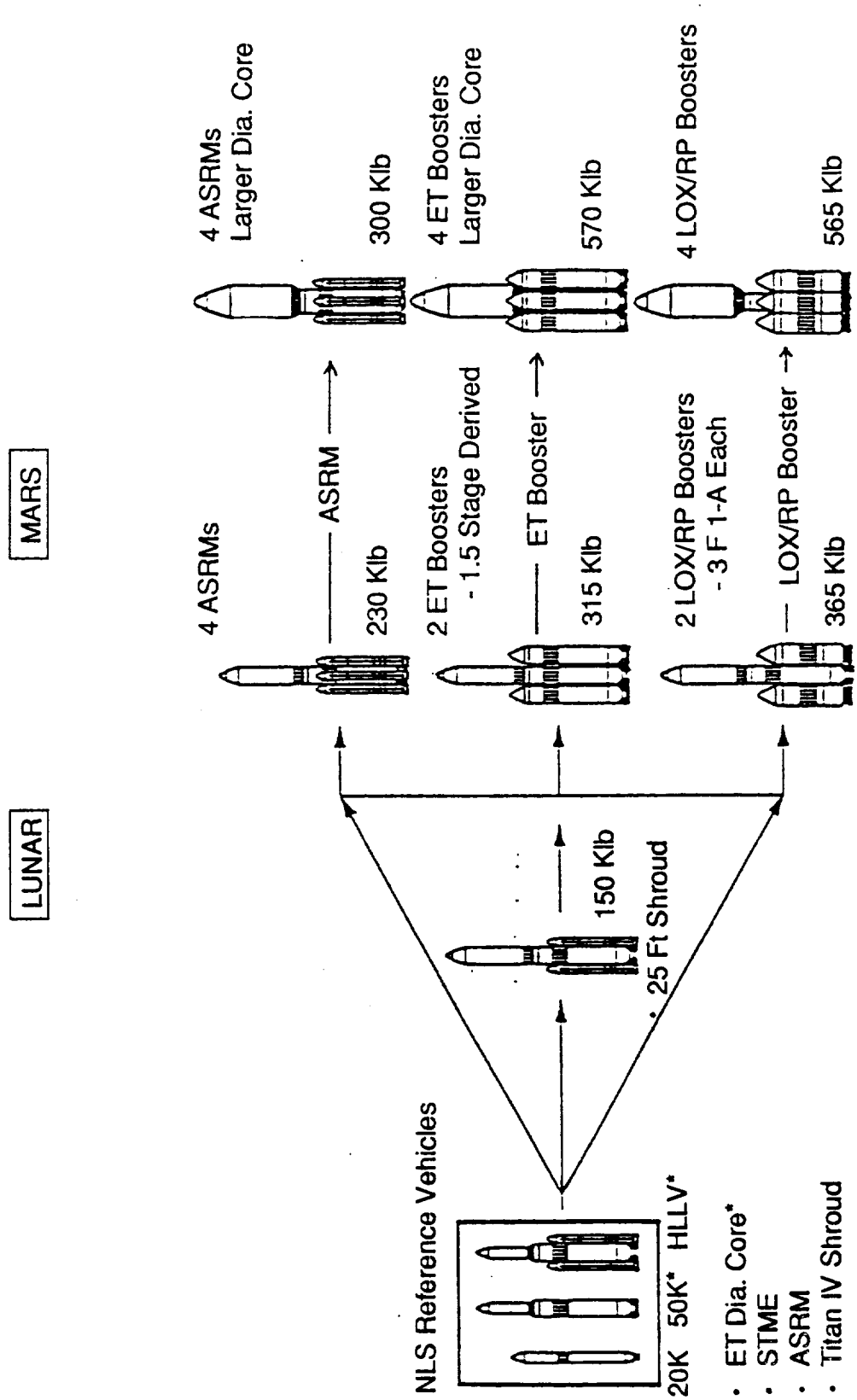


Figure 24: NLS Evolution to SEI

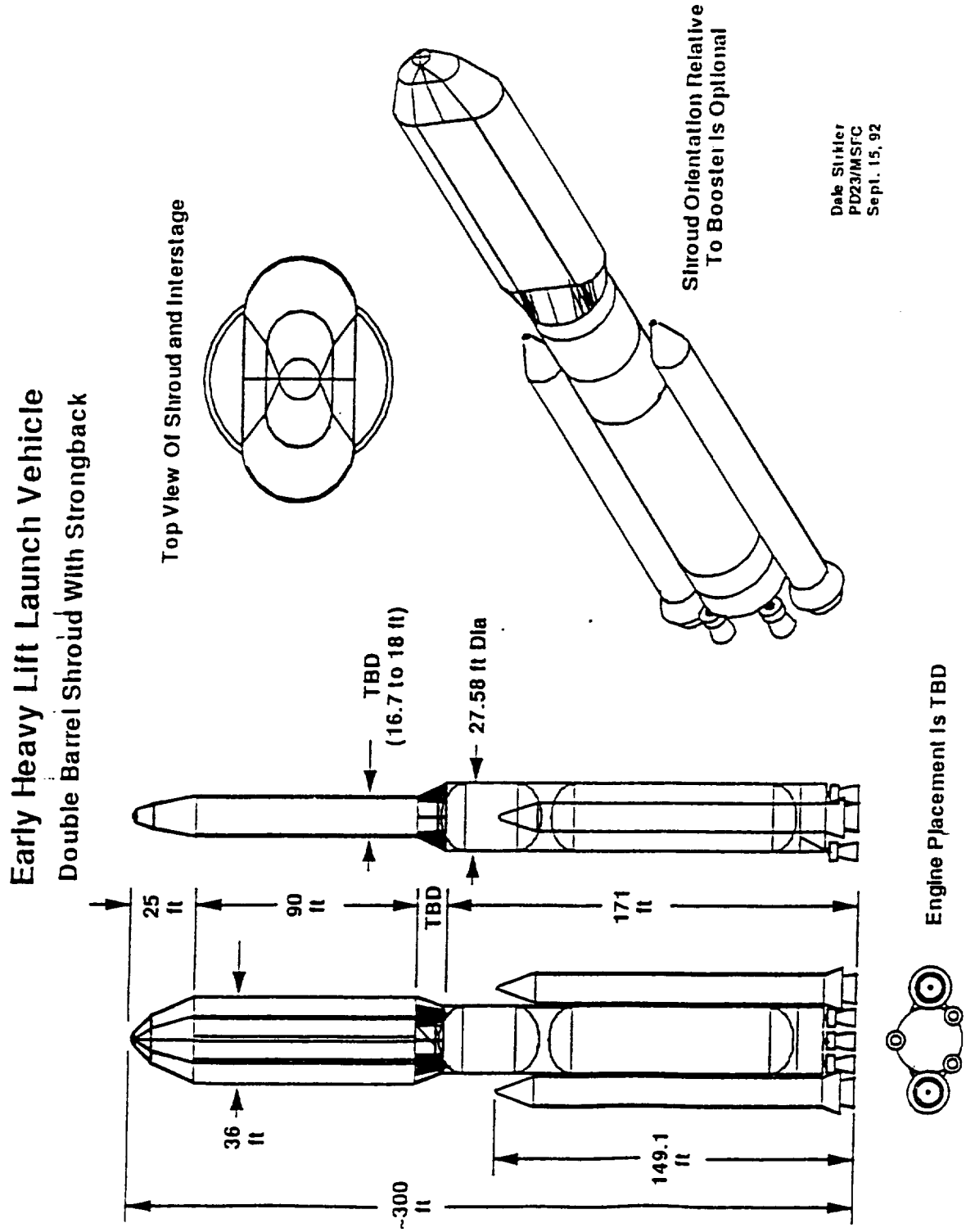


Figure 25: Early Heavy Lift Launch Vehicle Concept — Fall 1992

7. How many design body points would be investigated and where would they be positioned in the base

Since the code was essentially a developmental tool which had not been previously attempted, it was decided to limit the initial operating version as described below:

CONFIGURATION

1. Both core and parallel (opposed) booster stages can be considered.
2. Forebody must be axisymmetric and representable by cones, frustum, and cylindrical sections.
3. Aft skirt at base can be cylindrical or frustum.
4. Heat shield is a plane located normal to vehicle axis at any position forward of main engine nozzle exit.
5. Core engines can vary from one center engine up to an equally spaced arrangement of six center engines. Location of outer engines can vary to center mold line of core tankage.
6. Booster engines are centered at booster axis.
7. Nozzles will be represented by cones or truncated frustums.

PROPULSION SYSTEMS

1. Core stage on main stage restricted to $O_2/H_2$ propellants.
2. Booster stages will consider $O_2/H_2$, $O_2$/RP-1 and AP/A1 solid propellants.
3. For liquid propellants, user can select O/F, and chamber pressure.
4. For solid propellant motors, user can select aluminum loading and chamber pressure.

BODY POINTS

1. Up to nine specifically located body points on the base heat shield and engine nozzles will be automatically selected in the code.
2. Up to 11 additional body points can be specified by the user in a coordinate system compatible with the code geometry specifications.

These general program capability requirements were fixed in early 1991 and the code input procedure developed around these constraints. As will be explained in Section 5.0, the code utilizes X Windows and pop-up menus to assist the user in selecting the input parameters. A schematic of the forebody and base configuration, with the body points located on the schematic, is provided by the code to show the user the result of his input selections.

# Section 5
# GENERAL CODE DESCRIPTION

The goals of the code were stated in the introduction, Section 1, and rationale for limiting the capability were discussed in Section 4. As development of the code began, the following general guidelines governed the development processes. First, we wanted the code to produce generic environments for launch vehicle configurations similar to ALS/NLS concepts. Second, we wanted the results to have sufficient accuracy so they could be used in trade studies and other parametric comparisons. Third, and perhaps most important, we wanted the code to be easy to use and sufficiently fast so that multiple runs could be made in a relatively short time to support trade studies. Finally, we wanted the output to combine the environment components into (easy to understand and use) graphical and tabular data.

At the onset of the code development no computer preference was expressed by the users. However, many people within the NASA/DoD community wanted the code to be adaptive to their individual office equipment. In many cases, the computer of choice was a Macintosh or equivalent personal computer. After reviewing the scope of our code and delineating the various input files and computational subroutines (big and small) required, it was obvious that the code would not fit or be suitable for most PCs. Since computational speed was important, interactive graphics were desired, and a "work station" or stand-alone capability requested, it was decided to develop the code on a Sun 4 workstation with a UNIX operating system. This capability allows the user to utilize X Windows on the Sun4 for his interactive graphics through a series of pop-up menu choices. The programming language for the computational subroutines is FORTRAN 77. Much of the graphical display was programmed in C.

## 5.1 Code Architecture

The design code consists of a series of tasks which develop specific portions of the required output. Top level tasks and data stores are illustrated in Fig. 26. The radiation and convective modules are completely independent although they do utilize many of the same input data. Specific functions of input/output interfaces and computational modules are described below.

- **User input interface**
  - Prompts for user input or set defaults
  - Prepares configuration input data files
- **User provides a trajectory file**
- **Convective modules prepare files:**

  conv_hc

  altitude - time - recovery temp - heat transfer coefficients

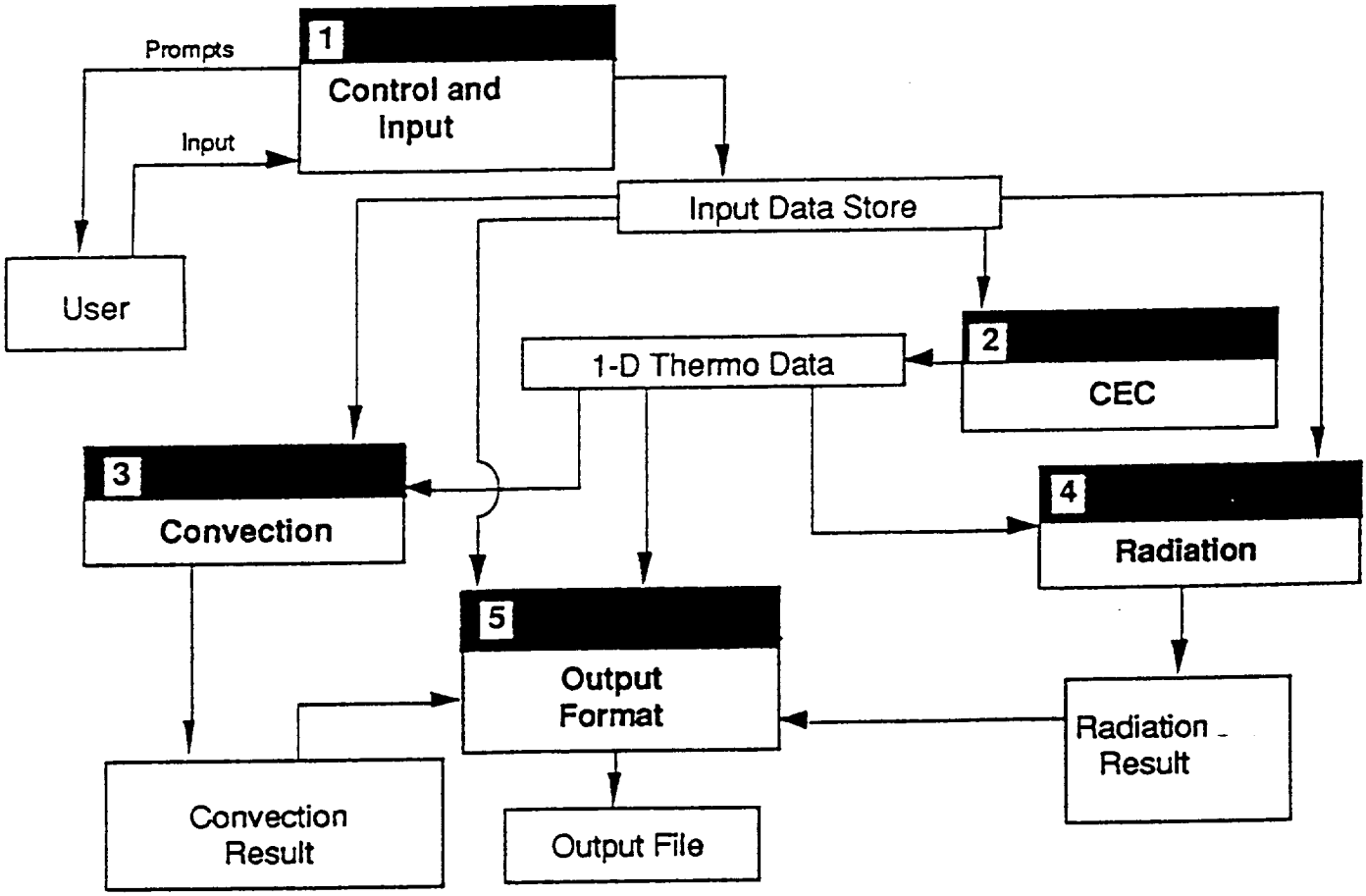


Figure 26: Design Code Architecture

- cold wall heat load

conv_hc

altitude - time - recovery temp - cold wall rates

- cold wall heat load

**— Radiation modules prepare files of:**

booster_rad

altitude - time - booster plume radiation

- integrated booster radiation heat load

main_eng_rad

altitude - time - main engine plume radiation

- integrated main engine radiation heat load

total_rad

altitude - time - total plume radiation

- integrated total radiation load

**— User output interface**

General descriptions of the various code functions are provided in the following paragraphs

## 5.2 Input

Input to the design code has been developed to offer the user maximum flexibility and immediate feedback on his choice of variables. There are four main categories of input variables which will either 1) be selected as the user progresses through the main menu, 2) assigned values by the user to fit the problem under study, or 3) read into the program as input from an existing file or data tape. These categories are:

1. Vehicle Geometry
2. Base Region Configuration
3. Engine Performance and Geometry
4. Trajectory Parameters

Within each category, each input variable has been assigned a name and a default value where applicable. The overall objective is to allow the user to perform parametric studies varying one or more of the input variables in a systematic manner without repeating all of the menu selection process. For example, if nozzle exit diameter is changed by selecting a different nozzle area ratio, the program will read only the input change to area ratio, then recompute internally all other configuration or plume parameters which are affected by the nozzle area ratio change. Since the code is a preliminary design tool, the most important objective is to keep the run time short so that parametric studies can be quickly performed.

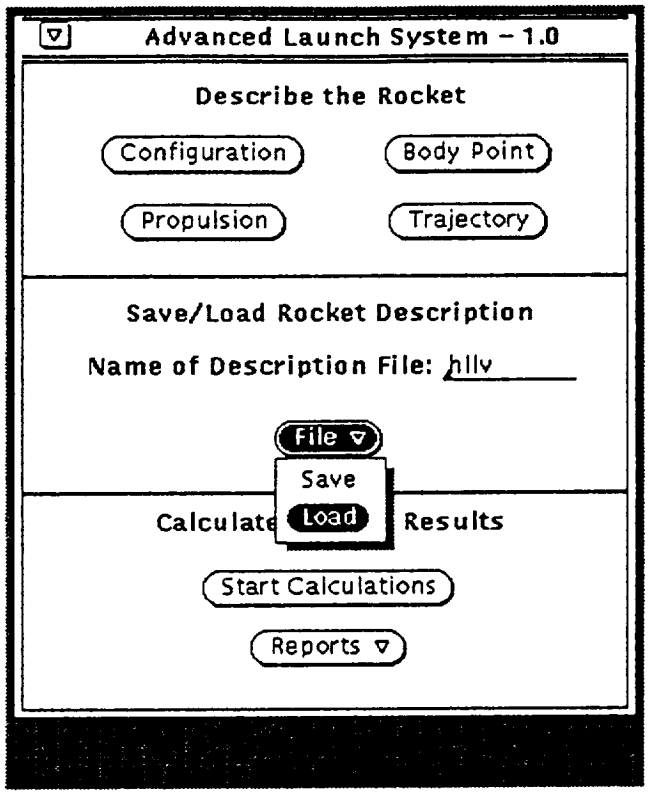


Figure 27: Main Input Menu

Individual choices available in the input menu are shown in Fig. 27. The input is being developed on a Sun 4 work station utilizing X-Windows for interactive graphics. As configuration and body point choices are made (or selected by default), the code will build a schematic of the base geometry and forebody configuration within the window. In this manner, the user can observe and correct (if necessary) his input to assure that the problem to be assessed is the one he desires. Typical configuration and body point selection menus are shown in Figs. 28 and 29, respectively.

## 5.3 Convective Subprogram

The convective subprogram utilizes input data from the user interface, to first define the base flowfields and subsequently the convective heat transfer, by the computational flow processes shown in the diagram of Fig. 30. The base flowfields are defined by a combination of empirical trends and analytical computations. Base flowfield parameters are either extracted from the empirical database or from the analytical database utilizing table or graphical look-ups which are specified for ranges of geometry and propulsion parameters. The analytical databases are developed by parametrically exercising the approach flow code, the external base flowfield code, the internal base recirculation module code, or the nozzle boundary layer code. Trajectory trends are derived from altitude effects and chamber pressure histories.

The convective heat transfer utilizes the base flowfield data with baseline heating data for each propulsion system taken from the empirical database. The heating rate

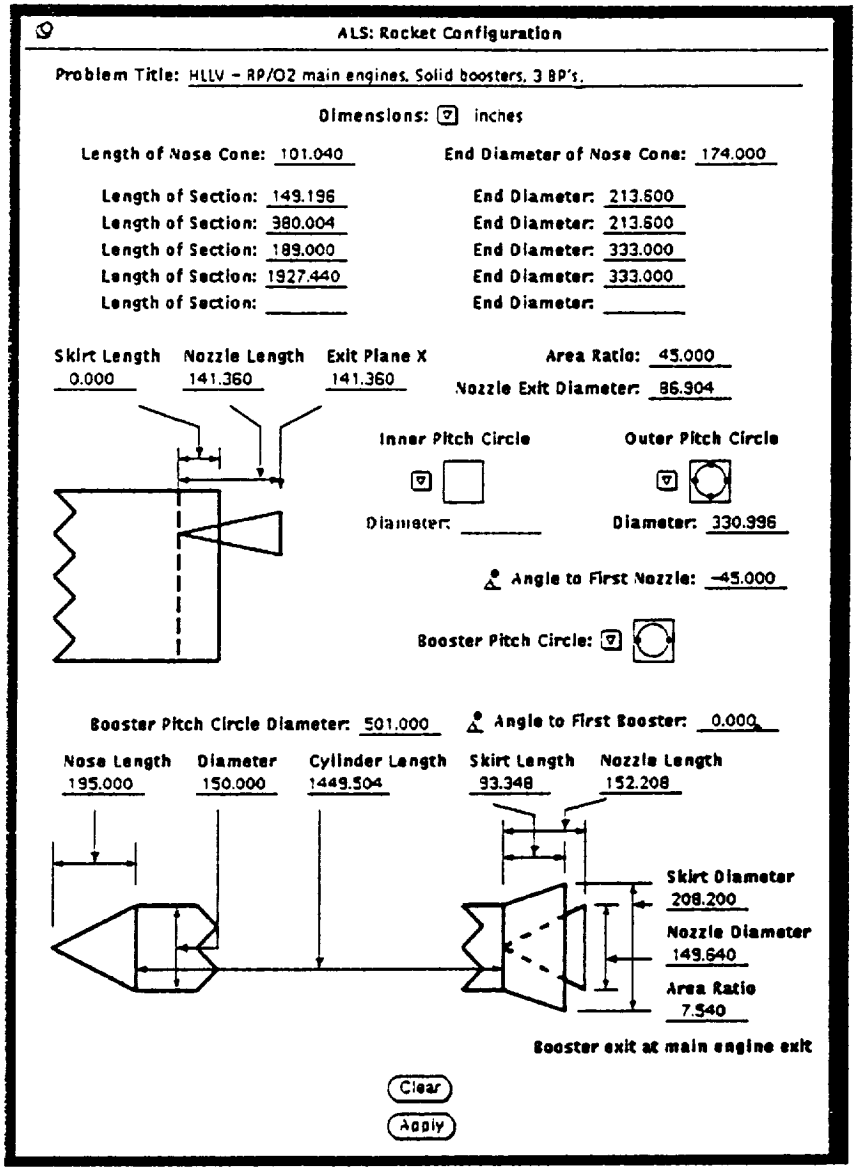


Figure 28: Typical Configuration Menu Selection and Graphical Displays

baseline is scaled to the new configuration, then reduced to heat transfer coefficient and gas temperature. Heating rates at points of interest are defined for varying wall temperatures.

The approach is summarized below.

1. **Base Flowfields**

   a. Combination of empirical trends and analytical computations
   b. Empirical database

      - Incipient recirculation
      - Choked flow altitude
      - Geometry effects/distributions

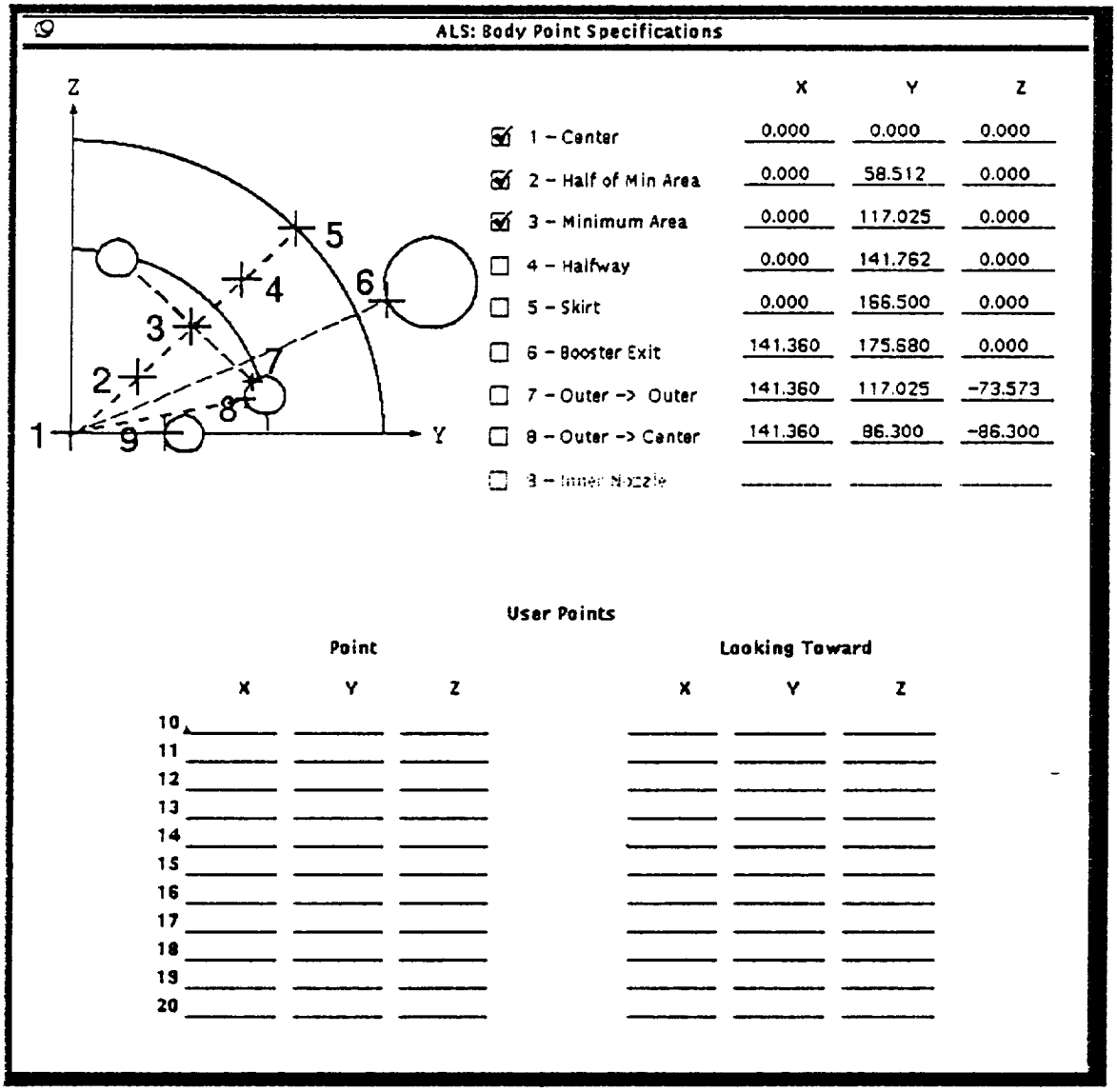


Figure 29: Typical Body Point Menu Selections and Graphical Displays

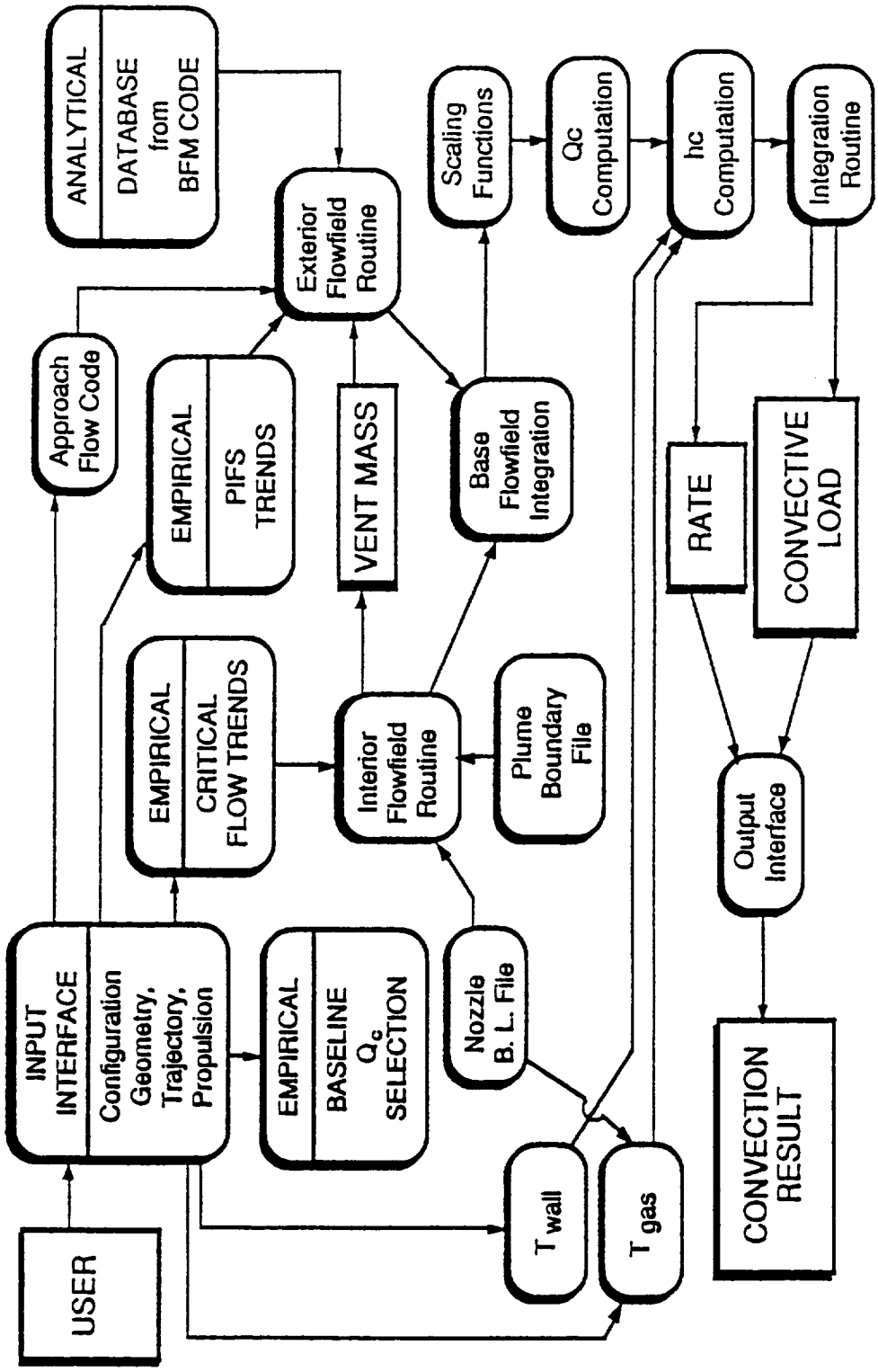


Figure 30: Computational Flow Processes for the Convective Subprogram

c. Analytical database

- Approach flow
- External flow/plume interaction
- Internal flow base recirculation
- Nozzle boundary layer

d. Trajectory trends derived from altitude effects and chamber pressure histories

2. **Convective Heat Transfer**

a. Baseline data for each propulsion system from empirical database
b. Scaled to new configuration
c. Reduced to heat transfer coefficient and gas temperature
d. Heating rate defined for varying wall temperature

Sources for the base region interior and exterior flowfields and limits in the empirical database are:

1. Nozzle boundary layer database developed by SECA, Inc.
2. Plume boundary database developed jointly by PST, Inc., and SECA, Inc.
3. Interior flowfield mass balance algorithm derived from BFM routine in SPF/3 code
4. Geometry effects and critical event algorithms derived from empirical database

a. 3 engine
b. 4 engine
c. 6 engine
d. Circle of engines around center engine
e. Core engines with opposed boosters

The heat transfer computations require data and scaling procedures derived as follows:

1. Base $Q_c$ (choked) from empirical database

a. $LO_2/LH_2$ systems
b. $LO_2$/RP-1 systems
c. SRM propellants with 16 percent and 19 percent Al

2. Chamber pressure scaling from empirical database
3. Nozzle area ratio scaling from empirical database
4. Base geometry/configuration adjustment factors from empirical database
5. Base gas recovery temperature from analytical database developed from nozzle boundary layer
6. Engine shutdown/throttling adjustments from empirical database

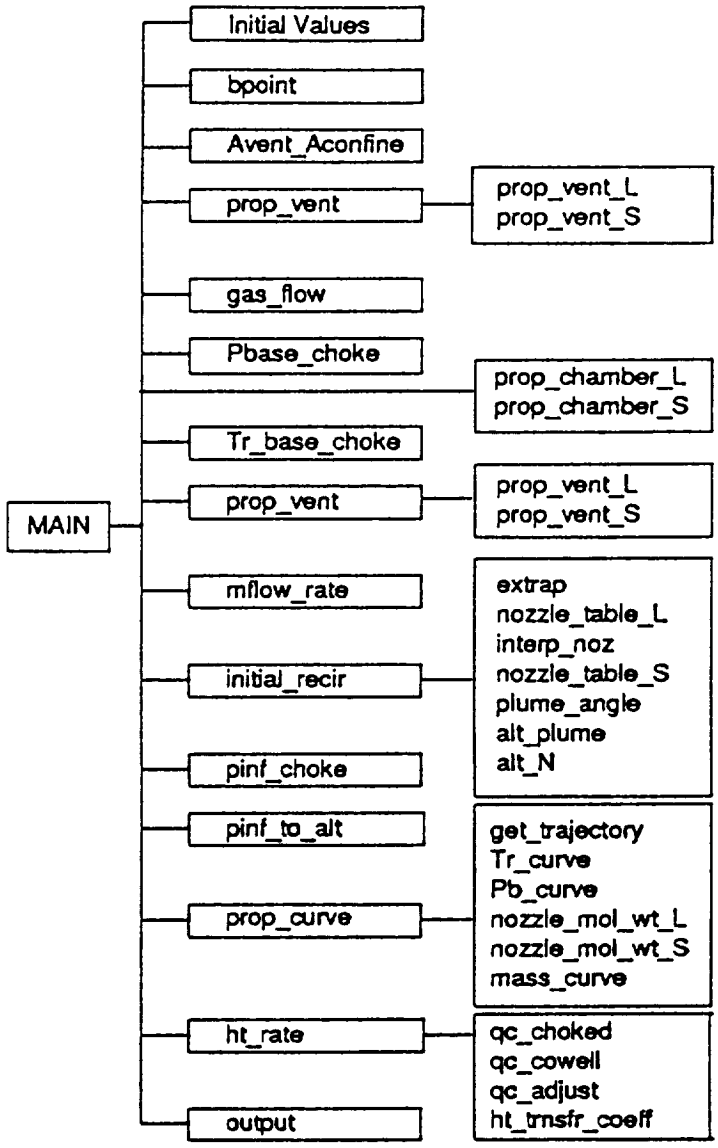


Figure 31: Subroutine Map for the Convective Subprogram

Subroutines in the convective subprogram are shown in Fig. 31. Typical output format is shown in Fig. 32. Details of the computational methodology are presented in Section 6.

## 5.4 Radiation Subprogram

The radiation portion of the prediction code consists of modules performing the following functions:

1. Interpretation of the user interface files to produce an input geometry which is common to both of the radiation codes used in the second module.

**Cold Wall Plume** NLS HLLV Plume Radiation Heating Trajectory
**Convection Rates for:** (EP55 (91-125) Sep 26 1991
**Booster:** SOLID O/F O/F = 0.19 2 150 dia Noz A/A* = 75
**Main Engine:** H2/O2 O/F = 6.0 4 87 dia Noz A/A* = 45

| Alt (kft) | Time (sec) | $T_{rec}$ (R) | Convective Rates [$T_{wall}$ = 520 R] (BTU/Ft$^2$-sec) for Points Shown HLLV-101 | HLLV-105 | HLLV-106 |
|---|---|---|---|---|---|
| 44.1 | 68.6 | 565 | 0.00 | 0.00 | 0.00 |
| 45.7 | 70.0 | 602 | 4.97 | 3.03 | 1.64 |
| 58.7 | 80.0 | 1533 | 45.42 | 27.65 | 15.01 |
| 73.3 | 90.0 | 2803 | 49.18 | 29.94 | 16.25 |
| 89.5 | 100.0 | 2986 | 44.60 | 27.15 | 14.74 |
| 106.9 | 110.0 | 2986 | 44.60 | 27.15 | 14.74 |
| 125.0 | 120.0 | 2986 | 44.60 | 27.15 | 14.74 |
| 143.7 | 130.0 | 2986 | 44.60 | 27.15 | 14.74 |
| 151.0 | 134.0 | 2986 | 44.60 | 27.15 | 14.74 |
| | | **Total Conv. Loads:** | **2731.10** | **1662.45** | **902.67** |

Convective load includes 68.6 to 134.0 sec
Separation at 140.26 sec; MECO at 432.61 sec

Figure 32: Typical Convective Subprogram Output

2. Selection of plume files, scaling of plume data, and execution of the appropriate radiation code. There are two distinct modules: one uses a viewfactor code for SRM and RP1/02 plumes and one uses a band-model code for $H_2/O_2$ plumes. These modules produce a sea-level rate and parameters specifying the necessary altitude adjustment functions.
3. Generation of radiation rates and loads using the trajectory data (time-altitude) specified by the user.

In development of the radiation code, emphasis was placed on providing modules which can be easily modified to expand the number of plumes and altitude functions as additional data are available from vehicle design experience or from studies made specifically to develop new models for the code. Initial data in the codes utilize methodology and flight experience developed for the Saturn S-IC, the original Space Shuttle, and the new Shuttle Advanced Solid Rocket Booster. The functions of the three modules are described below:

1. Control Function
   a. Prepares geometry associated with data structures

b. Based on booster propellant type:

- call VIEWFACTOR for $O_2$/RP1 or SOLID
- call BAND_MODEL for $O_2/H_2$

c. Based on main engine propellant type:

- call VIEWFACTOR for $O_2$/RP1 or SOLID
- call BAND_MODEL for $O_2/H_2$

d. Call RATES to assemble output rate files from environments provided by VIEWFACTOR and/or BAND_MODEL

2. Viewfactor Module

   a. Selects plume model and scales geometry
   b. Adjust emissive powers
   c. Compute sea-level rates
   d. Assign altitude adjustment functions

3. Band Model Module

   a. Selects plume type and applicable range of $P_c/p$
   b. Scales plume pressure, mole fraction and geometry
   c. Compute narrow band radiation to each body point at all $P_c/p$
   d. Scale narrow band radiation to estimate full spectra
   e. Define sea-level rate and altitude adjustment functions

The viewfactor module for solid propellant motors was developed as follows:

1. Based on 16 percent and 19 percent Al plume models developed for ASRM Cycle 1.5
2. Shape = 15 deg cone frustum, 10 Re long with 10 axial nodes
3. Emissive powers a function of propellant Al fraction:

   a. Emissive powers

| | | | | | | | | | | |
|---|---|---|---|---|---|---|---|---|---|---|
| 16% | 59 | 51 | 44 | 40 | 37 | 35 | 31 | 30 | 27 | 27 |
| 19% | 94 | 63 | 57 | 52 | 50 | 48 | 44 | 40 | 36 | 36 |

   b. Interpolate emissive power of each node based on Al fraction

$$E(x) = E(0.16) * \text{Scale Factor}$$

$$\text{Scale Factor} = \exp(E(0.19) - E(0.16)/0.03)(x - 0.16$$

Scale factor limited to the range 0.5 to 2.0

4. Adjustment functions

   a. Altitude adjustment is a function of $P_c/P_{c_{sl}}$
   b. Shutdown spike adjustment is a function of time from separation
   c. Functions selected for ALS correspond to the ET base center

*Used conservative assumptions based on S-IC flight data. Could improve later if O2/RP1 is seriously considered.*

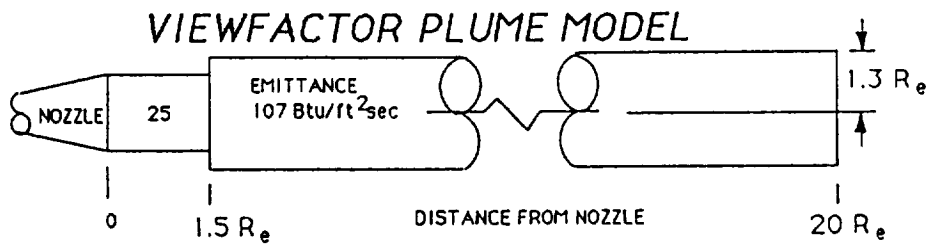


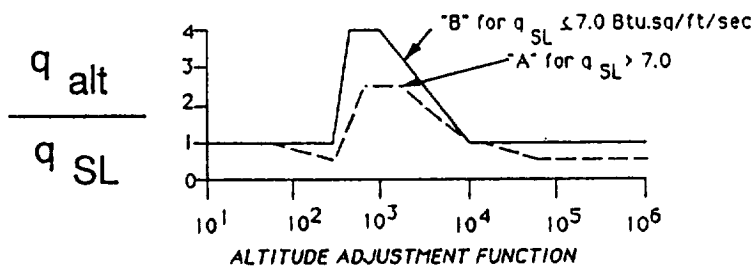


For $O_2$/RP1 engines, the viewfactor module will develop the plume model and altitude adjustment as described below:

1. Emittance and shape based on S-IC/F-1
2. Altitude adjustments:
   a. Aft facing points with high SL rates are less influenced by reversed gas
   b. Lateral surfaces of nozzles have lower sea-level rates, but have larger increase from reversed gas

The band model module performs the following steps in its computational process:

1. Select plumes
   a. Select plume with A/A* just larger than required (The larger A/A* gives more severe shock structure.)
   b. Select range of available $P_c/p_{alt}$ to represent design case from just below sea level to highest available altitude
2. Adjust plumes
   a. Scale plume pressures to represent required chamber pressure
   b. Adjust temperature and $H_2O$ mole fraction for O/F in non-afterburning regions
   c. Scale selected plumes to the required nozzle exit diameter
3. Perform radiation predictions
   a. Use narrow spectral band to improve response
   b. Scale results to represent entire spectra

| Plumes presently available for $O_2/H_2$ = 6: | | | | | | | |
|---|---|---|---|---|---|---|---|
| $P_c$ (psia) | Area Ratio | $P_c/P_{alt}$ | Alt (Kft) | $P_c$ (psia) | Area Ratio | $P_c/P_{alt}$ | Alt (Kft) |
| 3005 | 77 | 204 | 0 | 2250 | 60 | 153 | 0 |
| 3005 | 77 | 448 | 20 | 2250 | 60 | 824 | 20 |
| 3005 | 77 | 1073 | 40 | 2250 | 60 | 2145 | 60 |
| | | | | 2250 | 60 | 13128 | 100 |
| 1125 | 30 | 77 | 0 | 2250 | 60 | 98271 | 200 |
| 1688 | 30 | 115 | 0 | | | | |
| 1125 | 30 | 166 | 20 | 1688 | 45 | 138 | 5 |
| 1688 | 30 | 250 | 20 | 2250 | 45 | 153 | 0 |
| 2250 | 30 | 333 | 20 | 1688 | 45 | 167 | 10 |
| 1125 | 30 | 411 | 40 | 1688 | 45 | 250 | 20 |
| 1688 | 30 | 617 | 40 | 1688 | 45 | 617 | 40 |
| 2250 | 30 | 823 | 40 | 1688 | 45 | 1672 | 60 |
| 1125 | 30 | 1114 | 60 | 1688 | 45 | 10437 | 100 |

Figure 33: $O_2/H_2$ Plumes in Band Model Module

4. Prepare result file
   a. Interpolate in results to define sea-level rates
   b. Assign altitude adjustment based on results as a function of $P_c/p_{alt}$
   c. For input to the final output module, write sea-level rate and adjustment code to file `boost.rad` or `main_engine.rad`

Currently, the module contains $O_2/H_2$ plumes at four area ratios as shown in Fig. 33. Variations in engine chamber pressure will be accommodated by scaling the pressures in the database plume to provide equivalent plumes at the required pressure. For example, with the $A/A*$=45 plume, a $P_c$=1688 plume at 10 kft ($P/P_{sl}$ =0.688) could be used with a pressure scale factor of 1.33 to approximate the properties of a $P_c$ = 2250 plume at 2.4 kft ($P/P_{sl}$ =0.916). Typical plume structure for$A/A*$ = 60 plumes at $P_c$ = 2250 for various altitudes are displayed in Fig. 34.

Interaction between plumes is generally neglected for over-expanded plumes at low altitude, so axisymmetric plume property predictions are used. This has given good results on the Shuttle up to an altitude of 40 kft. As altitude increases, the shock regions between plumes become the predominant radiation source, but this source is relatively weak compared to the significant radiation at lower altitudes from Mach disk and afterburning. Once a stable base pressure is reached, the plume configuration affecting the base is essentially unchanged with altitude. This occurs just after staging on the Shuttle at about 160 kft. Because of the lack of 3–D prediction techniques at the time of the Shuttle design, approximations were developed using methods for axisymmetric

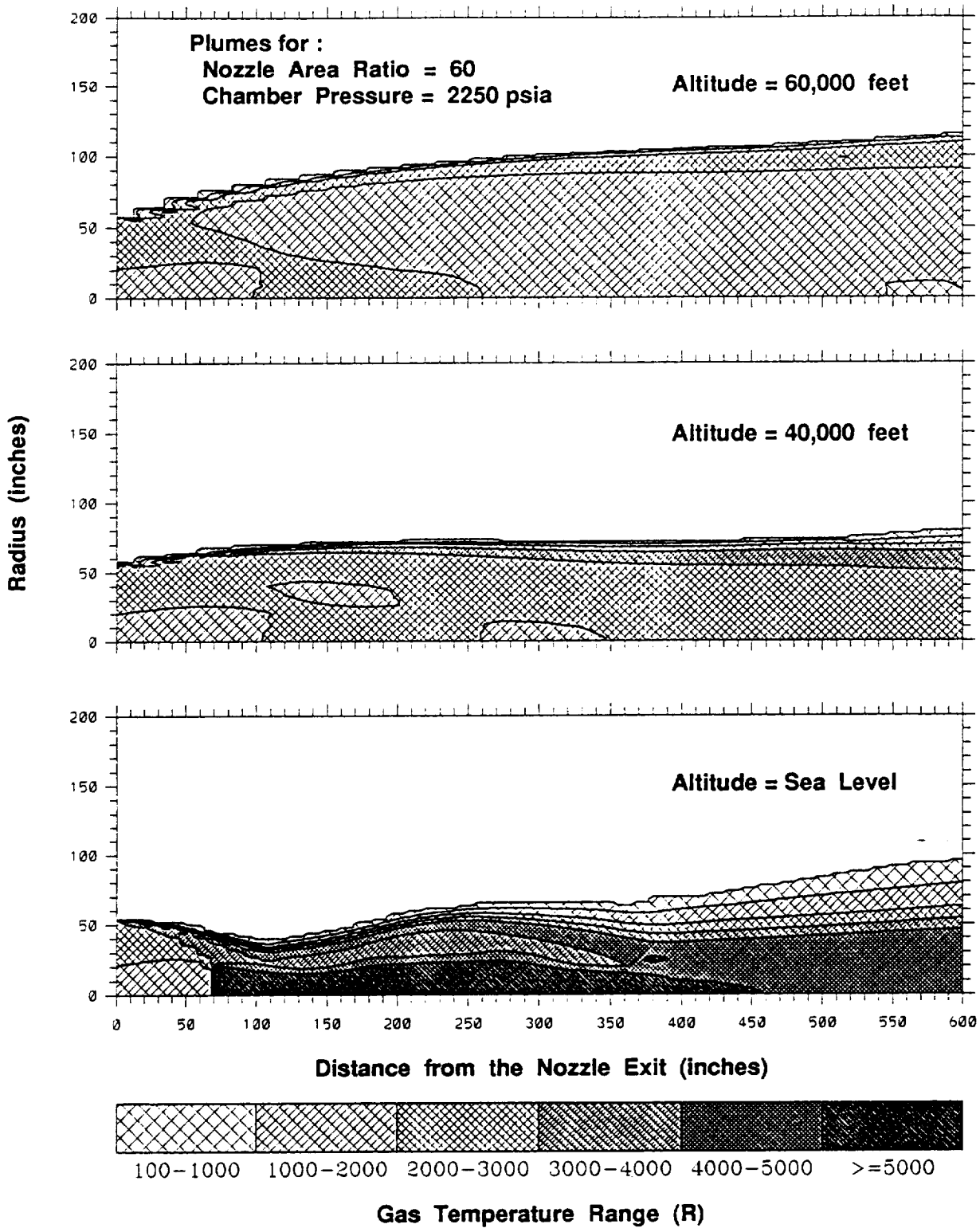


Figure 34: Plume Structure for $O_2/H_2$ Engines

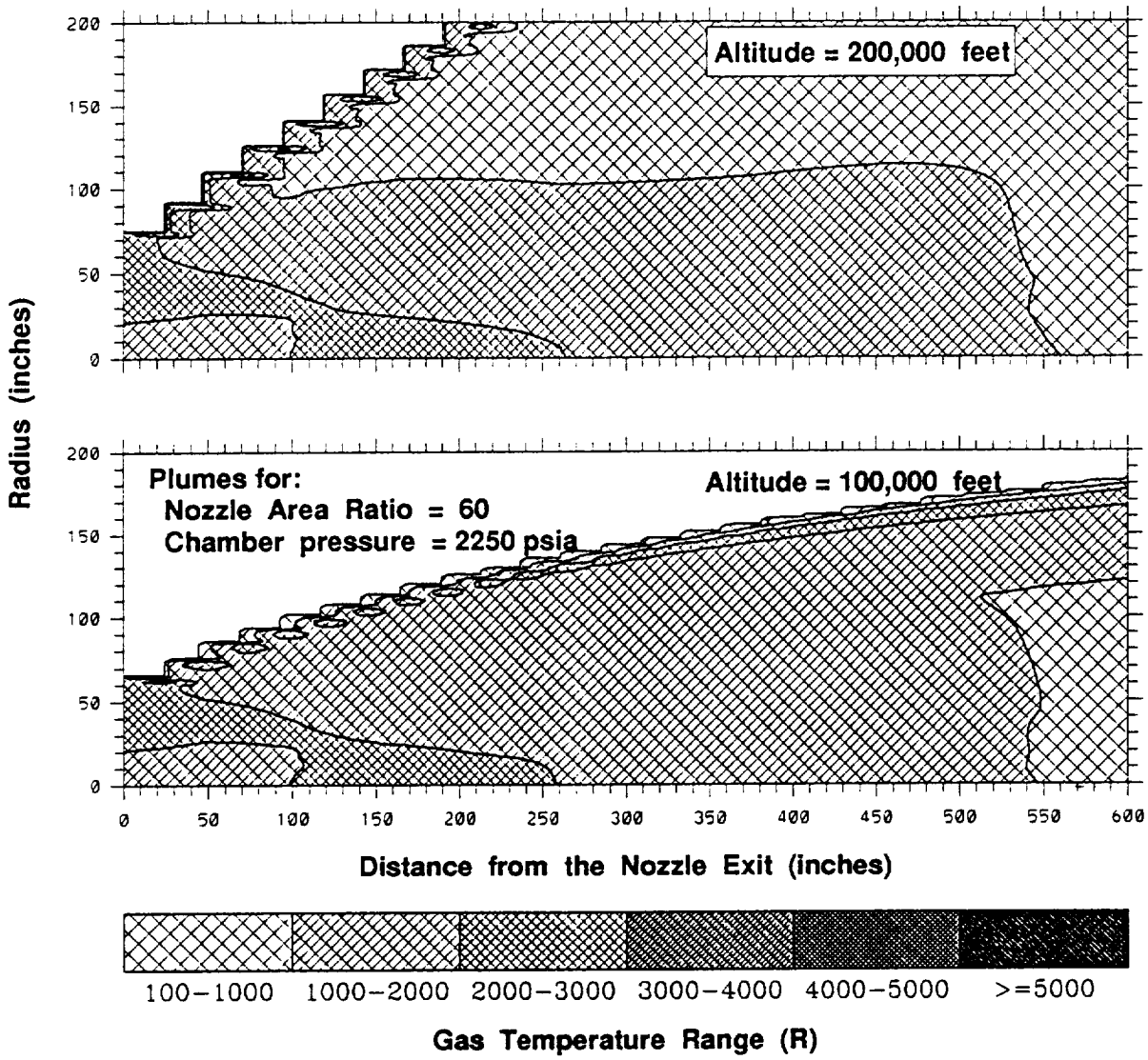


Figure 34: (concluded) Plume Structure for $O_2/H_2$ Engines

**Total Plume Rad for:** (SAFETY MARGINS: MAIN-ENGINE PLUME = 1.10 & BOOSTER = 1.25)
**Description File:** als.hllv
**Booster:** SOLID O/F = 0.19 2 149.64 dia Nozzles
**Main Engine:** H2/O2 O/F = 6.0 4 87.24 dia Nozzles
**Trajectory File:** HLLV.trj

| Alt (kft) | Time (sec) | Incident Radiation rates (BTU/Ft$^2$-sec) for Points Shown 101 | 105 | 106 |
|---|---|---|---|---|
| 0.0 | 0.0 | 30.60 | 29.60 | 25.76 |
| 0.8 | 10.0 | 32.76 | 31.68 | 27.52 |
| 3.6 | 20.0 | 37.38 | 36.15 | 31.22 |
| 337.6 | 350.0 | 0.36 | 0.35 | 0.33 |
| 349.5 | 400.0 | 0.36 | 0.35 | 0.33 |
| 361.5 | 432.6 | 0.36 | 0.35 | 0.33 |
| **Total Conv. Loads:** | | **2731.10** | **1662.45** | **902.67** |

Radiation load includes 0.0 to 432.61 sec
Separation at 140.26 sec; MECO at 432.61 sec

Figure 35: Typical Format for Radiation Heating Output

plumes and plume impingement to assemble a 3–D approximation of the plume and interaction regions.

Only axisymmetric plume predictions are used for the design code, because the complexity of preparing the 3–D plumes for the necessary range of possible configurations is well beyond the scope of the current task. The axisymmetric plumes will be used up to an altitude of about 80 kft, then the radiation will be defined to be constant above that altitude. Typical radiation subprogram output for a vehicle with solid rocket motor boosters and $O_2/H_2$ main engines is shown in Fig. 35.

## 5.5 Output

Design code output is prepared in seven separate files and individual files or combinations are selected by the user. A default option which provides tabular heating rates is also available. The output filenames are:

`stage` - stage description

| | |
|---|---|
| `body_points` | - body point data |
| `trajectory` | - trajectory data |
| `conv_hc` | - convective heat transfer coefficient |
| `conv_rates` | - convective cold wall rates |
| `rad_boost` | - radiation from booster plumes |
| `rad_main` | - radiation from main/sustainer plumes |

Typical convective and radiative output file data for an HLLV configuration were previously shown (with time truncated) in Figs. 32 and 35. Graphical output for one body point is shown in Fig. 36.

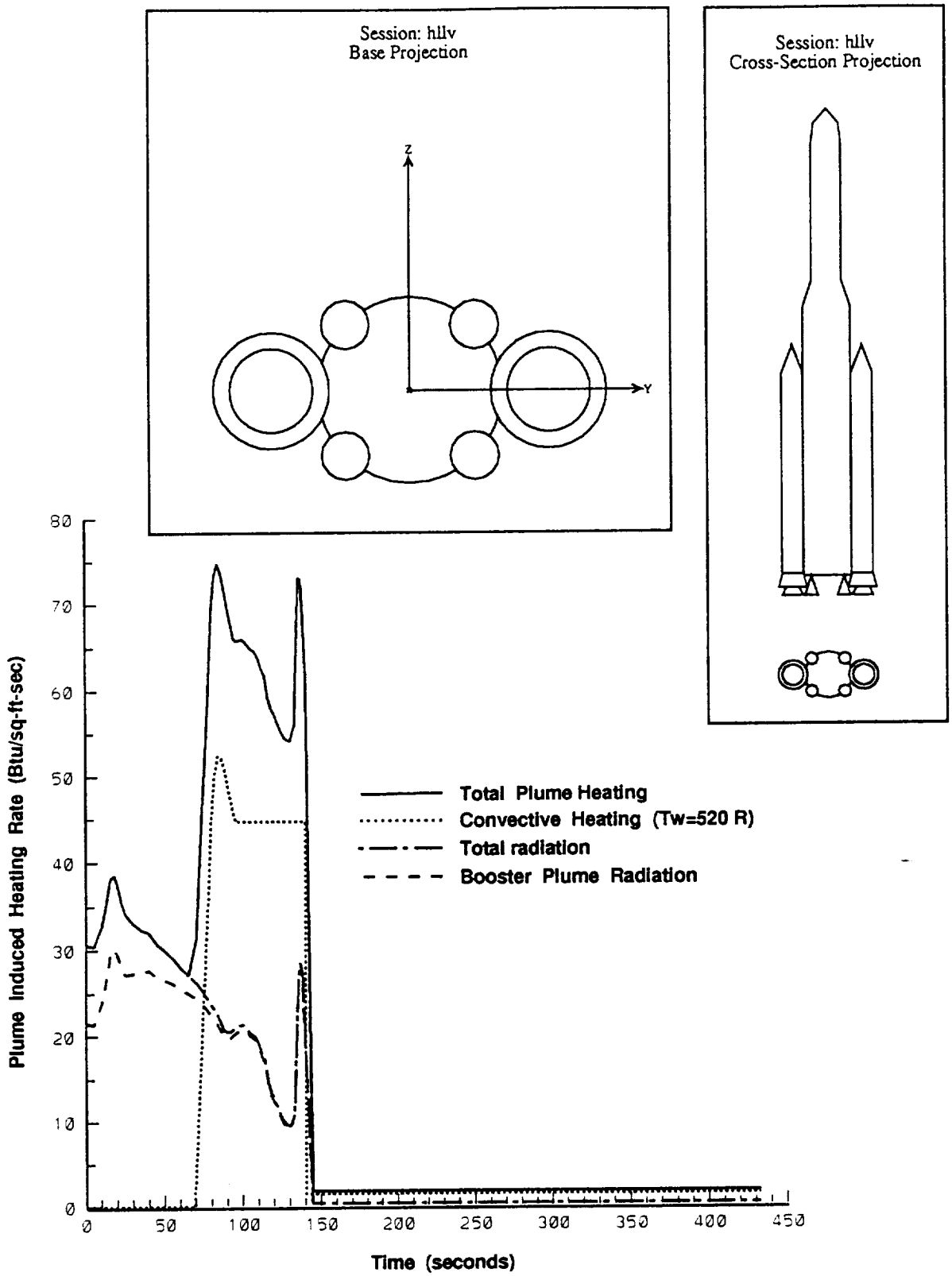


Figure 36: Typical Design Code Graphical Output

# Section 6
# CODE METHODOLOGY DEVELOPMENT

Specific objectives and limitations in both the radiation and convection subprograms were briefly described in Section 5. General steps in the overall computational flow processes were also listed in Section 5, but detailed explanations were not included. This section provides the specific methodology used in the code to generate environments for a set of common body points in the launch vehicle base region. It contains or explains the step-by-step processes which were followed to construct a plume radiation module or define a choked level of convective heating when a specific vehicle configuration and trajectory are chosen. In most cases, the methodology reflects and automates the judgmental decisions followed by REMTECH when providing base heating estimates to NASA over the past 20 years. The essence of the methodology is the utilization of condensed summaries of database trends, plume graphics, and simplified analytical approaches in combination to effect a quick and reasonably accurate base heating estimate.

Radiation and convective methodology were developed independently. In general, the radiation computation is more straightforward and computationally more difficult, but requires less judgement and scaling. Conversely, for convection, once the empirical trends were determined and programmed into look-up files, the final computation is fast and accurate. Coupling the various effects into a logical process which does not cancel or compound an individual effect was the biggest challenge in developing the convective methodology. As mentioned previously, the base flowfield is complex and highly three-dimensional. Eventually CFD solutions with coupled heating rate computation will provide more exact answers to the base heating questions. This design code bridges the technology between the existing empirically based estimates and the CFD time dependent solutions of the future. Details of the code methods are described in the following sections.

## 6.1 Plume Radiation

The prediction of plume radiation has been parameterized to allow estimations for three different propellant combinations using both viewfactor and band-model radiation prediction methods. The parameters and database provided for plume radiation estimates can be expanded in the future to include other propellants and a larger range of motor configuration parameters. However, because some approximations were required to prepared this general treatment, the results should be used to evaluate trends rather than directly for design.

The propellants considered in the initial code include RP1/$O_2$, solids (ammonium perchlorate and aluminum) and $H_2/O_2$ . The $RP_1/O_2$ and SRM plumes are modeled as opaque surfaces for viewfactor predictions while the $H_2/O_2$ plumes are modeled as tables of plume gas properties for band-model radiation predictions. The motors of each

stage, booster or main stage, must be of the same type and configuration, and they must be arranged within the configuration parameters available in the user interface in order to transfer the data to the radiation code. However, the radiation code does not contain assumptions which restrict the engine arrangement.

In the balance of this chapter, the approximations which have been made will be described along with the options available to modify the code and expand the database as other propellants and motor configurations are considered. The presentation is organized into sections describing configuration approximations and prediction methods for RP1/$O_2$, SRM and $H_2/O_2$ plumes.

### 6.1.1 Configuration Approximations

The radiation portion of the code uses configuration data entered by the user to prepare input records for the viewfactor and band-model codes portions of the code. The conical and cylindrical portions of the vehicle configuration are reproduced, and body points (receiver locations) are modeled as small disks (0.0001-inch radius). Nozzle shading surfaces are approximated using conical frustums which match the nozzle exit diameter.

All plumes are treated as axisymmetric, and overlap between plumes is ignored. In the viewfactor predictions, this assumption is automatically provided by using opaque plume surfaces, and in the band-model predictions, properties for each point in the integration is selected from the nearest plume. The axisymmetric assumption is usually reasonable at low altitude, but it ignores the interaction regions between plumes at higher altitudes. Radiation from the interaction regions are never explicitly handled for SRM and RP1 plumes because empirical approximations (to be described later) are used to estimate altitude behavior. In the case of $H_2/O_2$ plumes, the plume impingement regions are the significant radiation source at high altitudes, but the radiation from these sources for $H_2/O_2$ plumes is low, and conservative assumptions used in the code are expected to give appropriate trends.

Predictions of the booster and main-engine plumes are made separately since the motor configurations are likely to be different. This procedure ignores attenuation of the booster plume radiation by the main-engine plumes for many receiver locations. The resulting over prediction at some points cannot be avoided with the current methodology, but it should be considered by the user in evaluating the results.

Because the booster plume radiation is accounted for separately, radiation contribution from the boosters is only integrated to booster heating termination (separation time or end of the SRM shutdown spike). However, receiver locations located on the booster structure must be used with a trajectory file which has been modified to set the main-engine cut off (MECO) time equal to the booster separation time to provide the correct upper limit for main-engine radiation heat-load integration.

### 6.1.2 RP/$O_2$ Plumes

It is not possible to handle RP/$O_2$ plumes with band-model predictions because the

chemistry codes used for plume prediction do not model the soot production resulting from the combustion process. As a result, a viewfactor model (based on Ref. 6) is used for sea-level $RP/O_2$ plumes. These sea-level predictions are then used as a reference rate with adjustment functions based on trajectory variables to vary the radiation with altitude. The plume model is based on an approximation of experience on the Saturn S-IC stage, but the trends are difficult to model. The sea-level plume model, Fig. 37, is identical to the first portion of the Saturn S-IC model [37], but no data were available comparing predictions of this plume to flight experience. The trends with altitude shown in Ref. [37] illustrate the range of behavior noted as a function of location in the base. The radiation is high at sea-level, then is roughly constant with increasing altitude until reversal for the plume gases begin. This reversal begins a radiation "hump" caused by the proximity of hot highly-emitting gases in the base region. The increase is followed by a decrease as the base clears with increasing altitude. The ratio of the peak rate to sea-level rates depends upon base location. Generally, aft-facing points such as the heat shield, which have high sea-level rates have a smaller relative increase caused by the reversed gases than do lateral facing points which have low sea-level rates. This is modeled in the ALS code by using two altitude adjustment functions, Figure 38, with selection based on the sea-level rate being above or below 7 $Btu/ft^2$-sec. This is relatively arbitrary and the user should use judgment in evaluating the results.

No experience is available for varying the sea-level plume model with chamber pressure. The F-1 engine on the Saturn S-IC stage had a chamber pressure of 965 psia and a nozzle area ratio of 16. The turbopump exhaust gas was injected into the nozzle at an area ratio of 10 and formed a very sooty, low-energy, mantle of gas around the plume which significantly affects the characteristics of the radiation model used. This relatively cool gas produces lower radiation in the initial portion of the plume, but as it mixes with the balance of the plume and atmosphere to form an afterburning mantel, the radiation increases significantly. The plume radiation model used for the H-1 engine on the Saturn S-I stage [37] was not significantly different from the F-1 model. Both have a short initial section modeling the radiation before afterburning begins, then a long cylindrical section. The H-1 engine was smaller than the F-1 with a nozzle area ratio of 8 and chamber pressures of 580 to 690 in various versions. The turbopump exhaust was not dumped into the nozzle, but some outboard engines were fitted with "aspirators" around the nozzle which were used to dispose of the turbine exhaust. The H-1 plume radiation model without the aspirator had a slightly hotter initial section because of the lack of absorption by the cooler turbine exhaust, but after afterburning starts, the H-1 plume-model emission is similar to the F-1. The H-1 plume model had a cylindrical section 15-percent larger than the F-1 (relative to the exit) which may be attributed to a higher nozzle exit pressure.

### 6.1.3 SRM Plumes

Analytical methods are currently being developed [7,38] to treat scattering radiation from SRM plumes, but the plume models and computer codes are not yet suitable for this application. As a result, SRM radiation in the ALS code is modeled using opaque conical

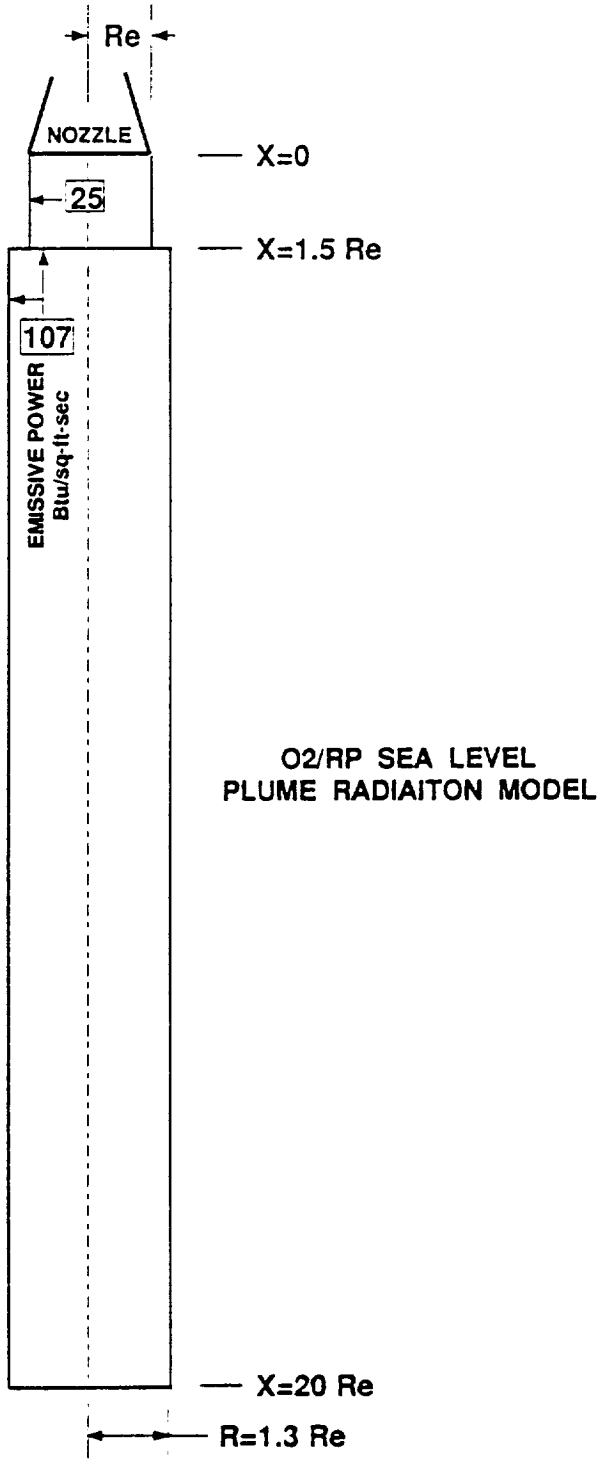


Figure 37: RP1/$O_2$ Sea-Level Plume Radiation Model

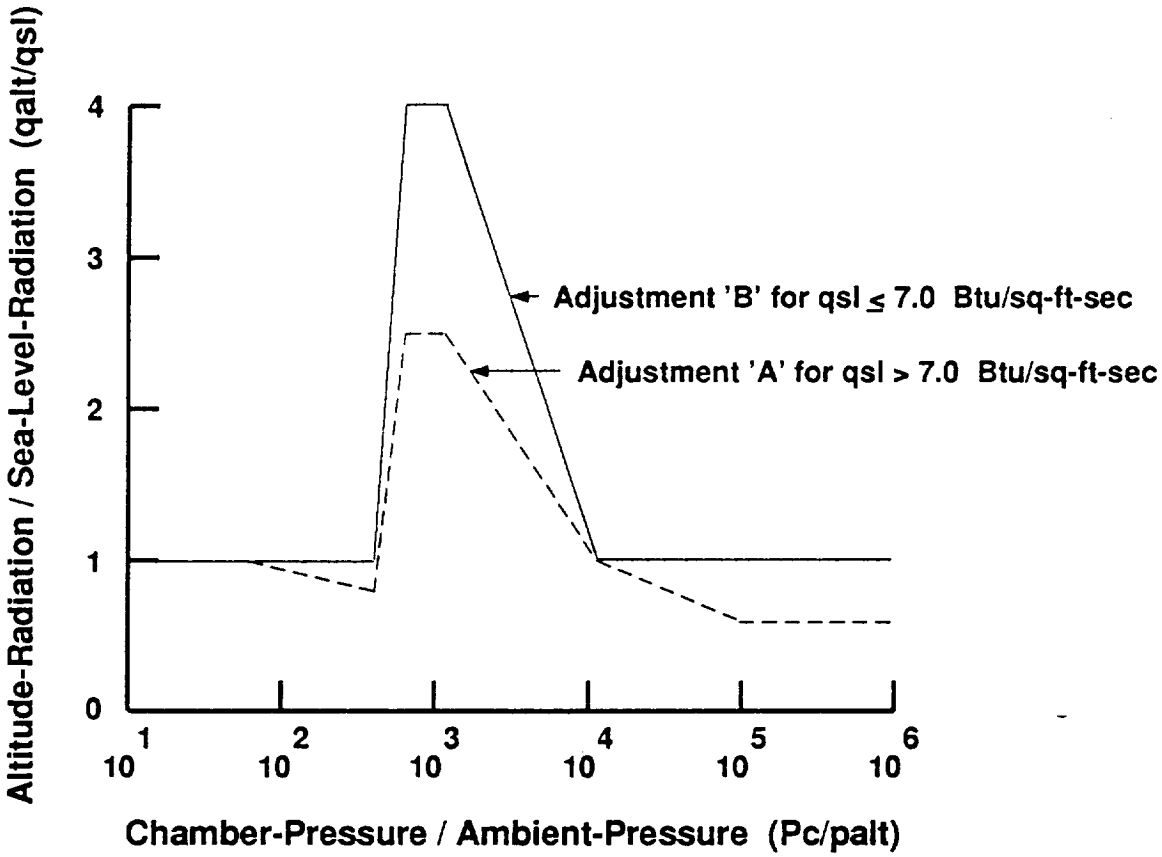


Figure 38: Altitude Adjustment Functions for RP1/$O_2$ Plume Radiation

frustum surfaces with assigned emissive powers for a sea-level model with empirically determined altitude adjustment functions. The model chosen for the code, Fig. 39, is a 15-degree conical frustum with 10 axial nodes, with each node being one nozzle exit radius long.

The emissive powers used for each node are a function of the propellant aluminum fraction. The functions were based on data used for the current Space Shuttle SRM [39] (69.7% AP, 16% Al and a PBAN binder) and estimates which have been made for the Space Shuttle Advanced Solid Rocket Motor (ASRM) [40] (68.9% AP, 19% Al and a HTPB binder). Extrapolation to 21% Aluminum content was attempted based on decreasing the binder fraction in the ASRM propellant. This extrapolation, with an extremely small binder fraction, was exaggerated, and attempts to make further predictions at 21% Al were extremely sensitive to assumptions made concerning the binder fraction. To prevent extrapolation far outside the range of Al fraction used in the model, the extrapolated values are limited to 0.5 to 2.0 times the 16% Al emissive powers. As a result, extreme variations in Al fractions may not produce the expected trends. The functions in Fig. 40 are defined in subroutine `srm_radiation`.

Functions to adjust for chamber pressure and nozzle area ratio were considered. Increasing chamber pressure tends to increase plume size, but the higher pressure ratio tends to reduce the plume temperature. Large changes in SRM booster chamber pressure are not expected from the Space Shuttle SRM range of 800 to 900 psia, so large changes in nozzle area ratio are also unlikely. Evaluation of ASRM (19% Al) predictions at chamber pressures of 750 and 870 psia indicated a mixed trend in plume emissive powers depending upon axial position. The average change was only −0.022 percent although individual node emissive powers varied from −3.8 to +8.1 percent. Because of the small and uncertain chamber pressure effects, no adjustment is made for chamber pressure. Therefore use of the code with extreme chamber pressures will not give correct trends. The effect of the ratio of chamber pressure to ambient pressure is included in the altitude adjustments described below.

Experience with the Space Shuttle indicates that the altitude and shutdown-spike adjustments for a SRM are dependent upon configuration and trajectory. Significant radiation can originates with reversed plume gases in separated regions in the base, and the shutdown spike, although brief, can produce peak radiation rates of twice the sea-level radiation. The gases which represent these secondary radiation sources do not have the same location and extent as the sea-level plume, so describing them as a function of the sea-level radiation is often a poor approximation. But it is essentially the only generic method available at this time. Future advances will allow more precise predictions with CFD codes supplying plume flowfield descriptions, including aerodynamic effects, which can be used with the Monte Carlo radiation codes currently under development [7] to more precisely model the problem.

The altitude and shutdown-spike adjustments in the initial version of the ALS code are shown in Fig 41 along with the Shuttle flight data. These data and the adjustment functions are those used for the Orbiter/External-Tank attach region for the Space Shuttle ASRM [41]. Both the low- and high-altitude adjustments use the ratio of plume radiation

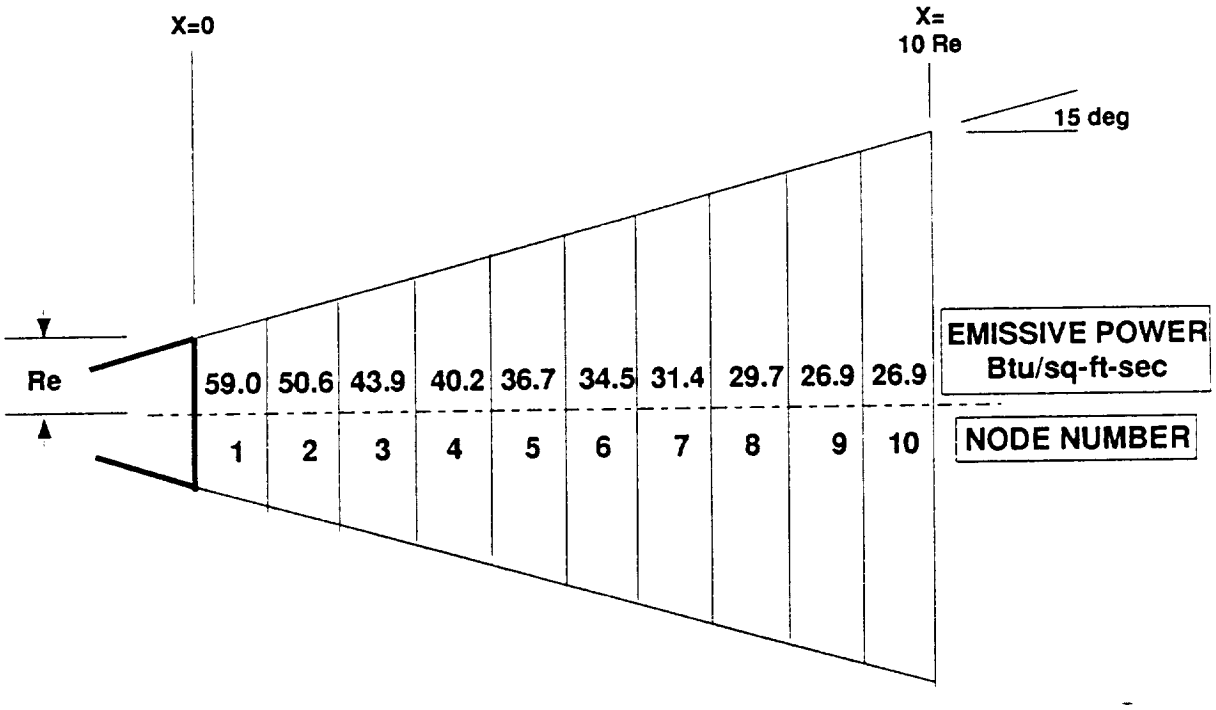


**REFERENCE SRM PLUME MODEL**
**WITH EMISSIVE POWERS FOR 16% ALUMINUM**

Figure 39: SRM Sea-Level Plume Model Geometry

Emissive powers are based on extrapolations using predictions at 16, 19 and 21 percent Aluminum. The reference powers shown for the plume model are those at 16 percent Aluminum. The extrapolated ratios to the reference values are limited to 0.5 to 2.0.

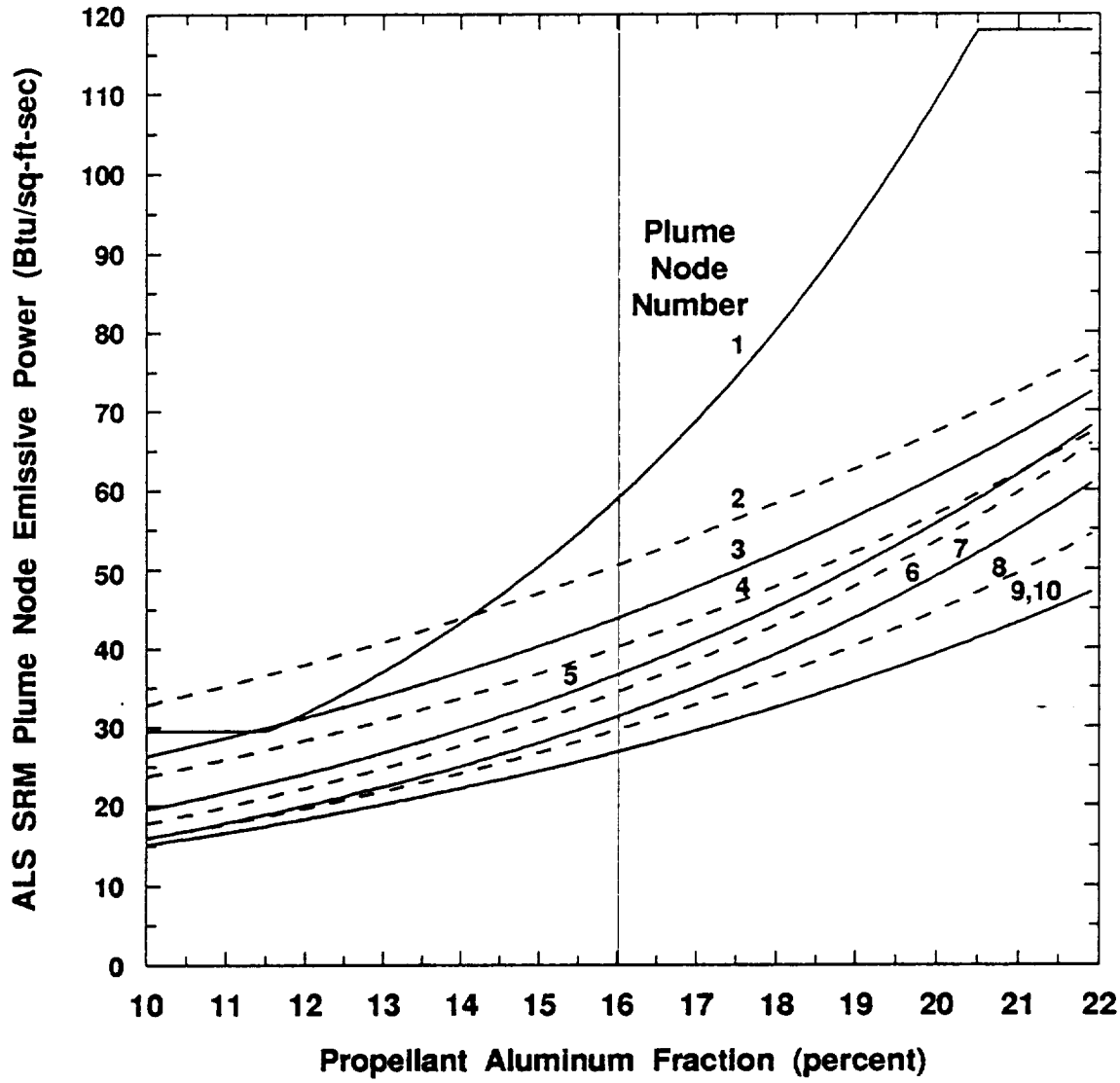


Figure 40: SRM Sea-Level Emissive Power as a Function of Plume Position and Aluminum Fraction

to the sea-level value ($q_{alt}/q_{sl}$) normalized by the ratio of chamber pressure ($P_c$) to the initial value at sea-level ($P_{c_{sl}}$). This is intended to recognize the effect of $P_c$ variation with time which is produced by the grain design. The altitude parameter in the low-altitude range is the ratio of $P_c$ to ambient pressure ($P_{alt}$) with each normalized by the initial values at sea level. This normalization by sea-level values is necessary to prevent variations in the sea-level rate as a function of initial chamber pressure.

Shuttle experience indicated that the SRM radiation increased with altitude to a maximum which is relatively constant between 10 and 30 kft. The transition between the low- and high-altitude adjustments is made in this plateau, and the sea-level normalization is removed from the altitude parameter for the high altitude function. The difficult part of the adjustment to generalize is the thrust tail-off. When the rate of decrease in $P_c$ exceeds the rate of decrease in ambient pressure, $P_c/P_{alt}$ increases and the high altitude function will not behave as intended. To avoid this on the Shuttle, a separate function is provided below $P_c$ = 400 psia which removes $P_c$ normalization functions and allows the radiation to decline until the shutdown spike rates exceed the altitude-adjusted rates. This Shuttle-specific function may need replacing to handle a larger range of SRMs.

The shutdown spike might be expected to be a function of $P_c$, but $P_c$ is difficult to define precisely during shutdown in preflight trajectories. As a result, the spike adjustment function is based on time relative to separation. If separation is delayed from the SRM thrust termination for any reason, the trajectory input file should be modified so that the separation time is closely associated with thrust termination. This will give the correct timing of the spike and the correct heating integration time for the booster. Because all of the SRM boosters expected to be evaluated are relatively large, no effect of scale has been included in sea-level or altitude parameters. If small plumes are considered, the emissive powers may tend to be lower because of the reduced optical depth, but the dynamics of the flow, which increase nonequilibrium between particles and gases, which will tend to increase particle temperatures at the same relative locations in the plume.

### 6.1.4 $H_2O_2$ Plumes

In order to provide the best implementation for $H_2/O_2$ and other future gaseous plumes, band-model radiation theory was used for the $H_2/O_2$ plumes. The plumes currently available for $H_2/O_2$ propellants are defined by the entries in the "plume_lib" file listed in Table 4. All plumes are for a mixture ratio ($O_2/H_2$) of 6 with a range-of-area ratios and chamber pressures: $A_e/A^*$ = 77 at $P_c$ = 3005 for the Space Shuttle Main Engine (SSME), $A_e/A^*$ = 60 at $P_c$ = 2250 from Advanced Launch System (ALS) studies, $A_e/A^*$ = 45 at $P_c$ = 2250 and 1688 from National Launch System (NLS) studies, and $A_e/A^*$ = 35 at $P_c$ = 2250, 1688, and 1125 which were prepared specifically to extend the range of the database. The user can add other files of plume property data as they become available, but they must be grouped by propellant type in descending order of nozzle area ratio ($A_e/A^*$) and chamber-to-ambient pressure ratio. Plumes that are added must fit the format assumed by the code to accommodate the coding of the property scaling. This requires definition of two mole fractions: $f_1$ = $H_2O$-fraction and $f_2$ = $N_2$-

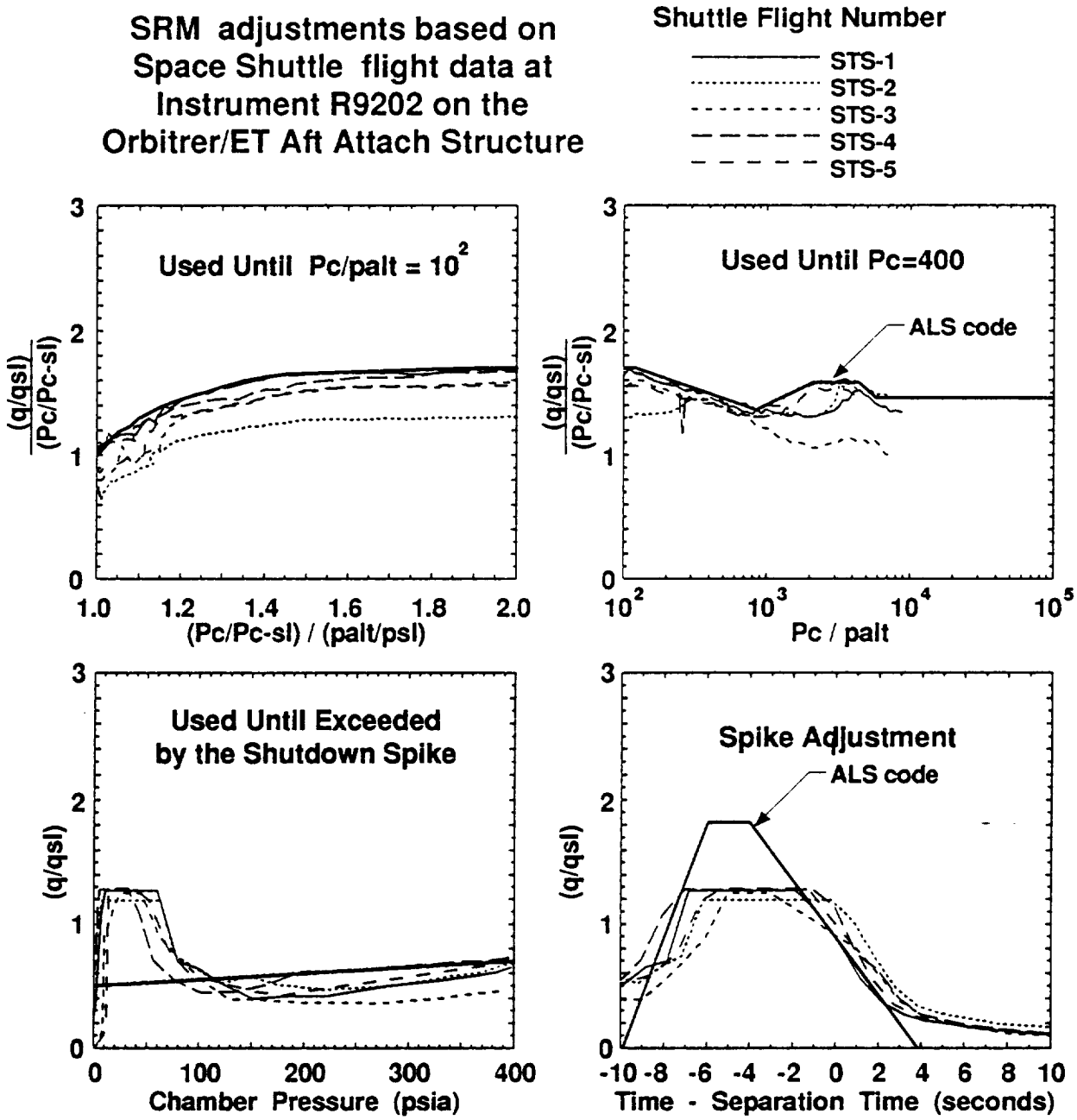


Figure 41: SRM Altitude and Shutdown-Spike Adjustments

Table 4: Current Plume Library for the Band Model Code

| Fuel/ Oxidizer | ----Nozzle--- Ae/A* | Re (inches) | O/F Ratio | Chamber Press. (psia) | Chamber/ Ambient Pressure | Filename |
|---|---|---|---|---|---|---|
| 'H2/O2' | 77. | 45.36 | 6. | 3005. | 204.4 | 'ssme1991_000.plu' |
| 'H2/O2' | 77 | 45.36 | 6. | 3005. | 448.4 | 'ssme1991_020.plu' |
| 'H2/O2' | 77. | 45.36 | 6. | 3005. | 1072.9 | 'ssme1991_040.plu' |
| 'H2/O2' | 60. | 52.44 | 6. | 2250. | 153.05 | 'als60_2250_000.plur' |
| 'H2/O2' | 60. | 52.44 | 6. | 2250. | 288.07 | 'als60_2250_040.plur' |
| 'H2/O2' | 60. | 52.44 | 6. | 2250. | 356.32 | 'als60_2250_060.plur' |
| 'H2/O2' | 60. | 52.44 | 6. | 2250. | 1015.99 | 'als60_2250_100.plur' |
| 'H2/O2' | 60. | 52.44 | 6. | 2250. | 17161.02 | 'als60_2250_200.plur' |
| 'H2/O2' | 45. | 43.62 | 6. | 1688. | 114.8 | 'stme45_1688_000.plulr' |
| 'H2/O2' | 45. | 43.62 | 6. | 1688. | 137.9 | 'stme45_1688_005.plulr' |
| 'H2/O2' | 45. | 43.62 | 6. | 2250. | 153.1 | 'stme45_2250_000.plulr' |
| 'H2/O2' | 45. | 43.62 | 6. | 1688. | 166.9 | 'stme45_1688_010.plulr' |
| 'H2/O2' | 45. | 43.62 | 6. | 1688. | 249.7 | 'stme45_1688_020.plulr' |
| 'H2/O2' | 45. | 43.62 | 6. | 1688. | 617.2 | 'stme45_1688_040.plulr' |
| 'H2/O2' | 45. | 43.62 | 6. | 1688. | 1671.7 | 'stme45_1688_060.plulr' |
| 'H2/O2' | 45. | 43.62 | 6. | 1688. | 10436.8 | 'stme45_1688_100.plulr' |
| 'H2/O2' | 30. | 35.60 | 6. | 1125. | 76.6 | 'stme30_1125_000.plur' |
| 'H2/O2' | 30. | 35.60 | 6. | 1688. | 114.9 | 'stme30_1688_000.plur' |
| 'H2/O2' | 30. | 35.60 | 6. | 1125. | 166.4 | 'stme30_1125_020.plur' |
| 'H2/O2' | 30. | 35.60 | 6. | 1688. | 249.7 | 'stme30_1688_020.plur' |
| 'H2/O2' | 30. | 35.60 | 6. | 2250. | 332.9 | 'stme30_2250_020.plur' |
| 'H2/O2' | 30. | 35.60 | 6. | 1125. | 412.1 | 'stme30_1125_040.plur' |
| 'H2/O2' | 30. | 35.60 | 6. | 1688. | 618.3 | 'stme30_1688_040.plur' |
| 'H2/O2' | 30. | 35.60 | 6. | 2250. | 824.2 | 'stme30_2250_040.plur' |
| 'H2/O2' | 30. | 35.60 | 6. | 1125. | 1072.7 | 'stme30_1125_060.plur' |
| 'H2/O2' | 30. | 35.60 | 6. | 1688. | 1609.5 | 'stme30_1688_060.plur' |
| 'H2/O2' | 30. | 35.60 | 6. | 2250. | 2145.3 | 'stme30_2250_060.plur' |
| 'H2/O2' | 30. | 35.60 | 6. | 1125. | 6961.1 | 'stme30_1125_100.plur' |
| 'H2/O2' | 30. | 35.60 | 6. | 1688. | 10444.7 | 'stme30_1688_100.plur' |
| 'H2/O2' | 30. | 35.60 | 6. | 2250. | 13922.1 | 'stme30_2250_100.plur' |

fraction. The plume units must be: length in inches, pressure in psfa and temperature in R. (These are converted to cm/atm/K before the band-model calculations.)

The current library plume selection and scaling routines only consider $H_2/O_2$ plumes with a mixture ratio of 6. This can be modified in the future as other propellants and mixture ratios are added. If the user specified nozzle area ratio is one which is not in the database, radiation predictions are prepared for two area ratios and the final result is obtained by linear interpolation on area ratio.

The code scales the plume to fit the nozzle of the user's application and contains approximations to scale the plume properties for variations in chamber pressure and mixture ratio. Each execution of the code uses a specific plume, so if effects of throttling or mixture ratio changes are necessary, they must be obtained by patching results from successive runs.

Chamber pressure scaling is performed by multiplying the pressure in the plume by the ratio of the application chamber pressure to the plume library chamber pressure. The plume is then used to represent the altitude corresponding to the chamber-to-ambient-pressure ratio specified for the plume in the library. This method involves unavoidable approximations in the plume/ambient mixing predictions. No adjustments can be made for changes in plume mixing caused by either differences between the user's trajectory and the velocity used for the prediction of the library plume, or the implied change in velocity caused by the correction to another altitude to match pressure ratio.

If the input mixture ratio is different from the value in the plume library, the plume $H_2O$ mole fraction and temperature are adjusted. These adjustments are only made in the portion of the plume where there has been no ambient mixing and afterburning (N2 mole fraction < 0.01). In these regions, the mole fraction is defined as

$H_2O$ mole fraction = (input O/F ratio) / 7.9365.

No adjustment is required for the $H_2$ mole fraction because $H_2$ is treated with all other foreign gases rather than being explicitly defined in the plume.

Temperature scaling uses a ratio which approximates changes in one-dimensional, equilibrium predictions for $H_2/O_2$. The temperature scale has been defined initially only for the initial plume library with reference to the O/F=6 as

T-scale = 1 + 0.2*(Input-O/F - 6.0).

When the O/F=6 plume temperature (T) increases behind shocks in the plume, this correction is too high, so when the plume temperature is above 3000 R, the adjustment is modified to

T-scale = 1 + 0.2(Input-O/F - 6.0)*(3000 / T)**2.

The scaled plume output files are available to the user to print or view with the system editor. These files appear with filenames of the form

`plu_aa_bb_cc_dd`

where the letters after "plu_" represent the following data rounded to integers:

aa = exit diameter in inches
bb = area ratio ($A_e/A^*$)
cc = mixture ratio (O/F)
dd = pressure ratio ($P_c/P_{amb}$)

The band-model radiation prediction is performed using a modification of the SEPRAD code [42] which was developed for predictions of Space Shuttle plume radiation. The code integrates over a hemisphere at each receiver point, and integration limits used for the calculation are set in the code (subroutine initialize) and can be modified by the user. The integration limit and increment for the radius of the hemisphere is a function of the nozzle exit radius (Re) with an upper limit of 20*Re and a increment of 0.05*Re.

Spectral integration is usually performed on the Space Shuttle using a range of 1000 to 9600 1/cm (1.04 to 10 microns) with an interval of 400 1/cm. Experience has shown that this interval gives satisfactory results for most plume heat transfer predictions because the atmosphere is neglected so there are no long cold-gas paths. Although this large interval results in significant time savings compared to smaller intervals (5 to 25 1/cm), the computation for the full spectrum was considered to be too slow for this application.

To further decrease computation time, a smaller spectral band was selected and the result is multiplied by a scaling factor to give results equivalent to the full-spectra integration. Several typical receiver locations were tested using a three-plume cluster of ALS nozzles with $A_e/A^*$=60, $P_c$ = 2250 psia at altitudes of 0, 40, 60 and 100 kft. The results in Table 5 show that the 2600-4600 1/cm band contains the most consistent fraction of the full band (1000-9600 1/cm) radiation over the range of altitudes. This band was chosen for integration in the code, and the predicted results are multiplied by 2.86 to obtain an approximation of the full-band result at sea level. This multiplier will cause over prediction above sea level, but this added conservatism will counterbalance possible under prediction at altitudes caused by the assumption of axisymmetric plumes and the uncertainties concerning the match of the plume-prediction vehicle velocity and the actual trajectory.

Table 5: Summary of Results for Evaluation of $H_2O$ Spectral Regions

| | | Spectral limits (1/cm) | | | | | |
|---|---|---|---|---|---|---|---|
| Lower | 1000 | 1000 | 2600 | 4600 | 6200 | 8200 | 2800 |
| Upper | 9600 | 2600 | 4600 | 6200 | 8200 | 9800 | 3600 |
| 00 kft | Predicted Flux (Btu/sq-ft-sec) and [ratio to 1000-9600] | | | | | | |
| BP 1 | 2.310 | 0.367 | 0.804 | 0.615 | 0.461 | 0.067 | 0.507 |
| | | [0.159] | [0.348] | [0.266] | [0.200] | [0.029] | [0.219] |
| BP 2 | 2.460 | 0.382 | 0.871 | 0.643 | 0.488 | 0.072 | 0.550 |
| | | [0.155] | [0.354] | [0.261] | [0.198] | [0.029] | [0.224] |
| BP 3 | 2.730 | 0.432 | 0.976 | 0.716 | 0.529 | 0.072 | 0.622 |
| | | [0.158] | [0.358] | [0.262] | [0.194] | [0.027] | [0.228] |
| BP 4 | 4.580 | 0.898 | 1.870 | 1.010 | 0.716 | 0.096 | 1.23 |
| | | [0.196] | [0.408] | [0.221] | [0.156] | [0.021] | [0.269] |
| BP 5 | 13.500 | 2.510 | 5.230 | 3.160 | 2.300 | 0.320 | 3.41 |
| | | [0.186] | [0.387] | [0.234] | [0.170] | [0.024] | [0.253] |
| 40 kft | Predicted Flux (Btu/sq-ft-sec) and [ratio to 1000-9600] | | | | | | |
| BP 1 | 0.338 | 0.116 | 0.149 | 0.046 | 0.025 | 0.001 | 0.107 |
| | | [0.343] | [0.441] | [0.137] | [0.075] | [0.004] | [0.317] |
| BP 2 | 0.264 | 0.093 | 0.116 | 0.035 | 0.019 | 0.001 | 0.084 |

Table 5: (Continued) Summary of Results for Evaluation of $H_2O$ Spectral Regions

| | | | | | | | |
|---|---|---|---|---|---|---|---|
| | | [0.353] | [0.439] | [0.133] | [0.072] | [0.004] | [0.318] |
| BP 3 | 0.305 | 0.105 | 0.135 | 0.042 | 0.022 | 0.001 | 0.097 |
| | | [0.344] | [0.443] | [0.137] | [0.071] | [0.004] | [0.318] |
| BP 4 | 0.476 | 0.204 | 0.224 | 0.035 | 0.014 | 0.000 | 0.165 |
| | | [0.429] | [0.471] | [0.074] | [0.029] | [0.001] | [0.347] |
| BP 5 | 1.370 | 0.558 | 0.632 | 0.125 | 0.057 | 0.002 | 0.464 |
| | | [0.407] | [0.461] | [0.091] | [0.042] | [0.002] | [0.339] |
| 60 kft | | Predicted Flux (Btu/sq-ft-sec) and [ratio to 1000-9600] | | | | | |
| BP 1 | 0.113 | 0.051 | 0.052 | 0.007 | 0.003 | 0.000 | 0.039 |
| | | [0.453] | [0.461] | [0.062] | [0.024] | [0.001] | [0.345] |
| BP 2 | 0.099 | 0.045 | 0.046 | 0.006 | 0.002 | 0.000 | 0.035 |
| | | [0.453] | [0.464] | [0.061] | [0.022] | [0.001] | [0.354] |
| BP 3 | 0.091 | 0.041 | 0.042 | 0.006 | 0.002 | 0.000 | 0.032 |
| | | [0.454] | [0.461] | [0.062] | [0.023] | [0.001] | [0.352] |
| BP 4 | 0.347 | 0.159 | 0.162 | 0.019 | 0.006 | 0.000 | 0.121 |
| | | [0.458] | [0.467] | [0.055] | [0.017] | [0.000] | [0.349] |
| BP 5 | 1.010 | 0.453 | 0.480 | 0.059 | 0.019 | 0.000 | 0.356 |
| | | [0.449] | [0.475] | [0.058] | [0.019] | [0.000] | [0.352] |
| 100 kft | | Predicted Flux (Btu/sq-ft-sec) and [ratio to 1000-9600] | | | | | |
| BP 1 | 0.072 | 0.035 | 0.033 | 0.003 | 0.001 | 0.000 | 0.025 |
| | | [0.481] | [0.460] | [0.044] | [0.012] | [0.000] | [0.347] |
| BP 2 | 0.066 | 0.032 | 0.030 | 0.003 | 0.001 | 0.000 | 0.023 |
| | | [0.486] | [0.459] | [0.043] | [0.012] | [0.000] | [0.348] |
| BP 3 | 0.047 | 0.023 | 0.021 | 0.002 | 0.000 | 0.000 | 0.016 |
| | | [0.498] | [0.451] | [0.039] | [0.011] | [0.000] | [0.340] |
| BP 4 | 0.299 | 0.142 | 0.139 | 0.014 | 0.004 | 0.000 | 0.103 |
| | | [0.475] | [0.465] | [0.047] | [0.013] | [0.000] | [0.344] |
| BP 5 | 0.897 | 0.413 | 0.425 | 0.045 | 0.013 | 0.000 | 0.315 |
| | | [0.460] | [0.474] | [0.051] | [0.014] | [0.000] | [0.351] |

The detailed radiation output files are available to the user to print or view with the system editor. These files appear with filenames of the form

`bmprad_out_ee_ff_gg_hh`

where the letters after "bmprad_out" represent the following data rounded to integers:

ee = area ratio ($A_e/A^*$)
ff = pressure ratio ($P_c/P_{amb}$) index, 01=lowest value
gg = stage_type, main or boost

After radiation predictions are completed, a sea-level rate is obtained by interpolation between the two $P_c/p_{alt}$ pressure ratios bracketing the sea-level pressure ratio. The rates at higher pressure rates are then divided by the sea-level rate to produce an altitude adjustment function. If two nozzle area ratios were required for the solution, the sea-level rates and two sets of altitude ratios are interpolated linearly on area ratio to obtain the final sea-level reference rate and altitude adjustment ratios which are passed to the output routines for the stage being processed, boost or main.

### 6.1.5 Output Format

Output of the code which is available through the user interface consists of tables of incident radiation rate as a function of time and integrated radiation load for the booster-engine plumes, the main-engine plumes and the total of the two. Integration of the load is terminated at separation (end of the shutdown spike for SRMs) for the booster-engine plumes and at MECO for the main-engine plumes. In order to obtain proper integration of radiation load for receiver locations on the booster structure, the trajectory input file must be modified to set MECO to the appropriate time to terminate main-engine radiation to the booster.

In the process of preparing the results, explicit safety margins are applied to the main-engine and booster plume radiation rates. These margins printed in the output table headers, and can be modified by changing the code. They have been initially set at 1.10 for the main engines and 1.25 for the booster by data statements in subroutine `rad_rates.f`.

## 6.2 Convection

The convection environment in the launch vehicle base region during ascent can be either a heating or cooling environment depending upon the base gas temperature relative to surface temperatures of base region components. For component wall temperatures of approximately 80°F or 540°R, the general trend in convection is for cooling to occur as cool free-stream air is drawn through the base at low altitudes and for heating to prevail when hot plume gases are recirculated into the base at higher altitudes. Distinctly different methods are employed to determine the cooling and heating environments. Therefore, the significant first step in the overall computational methodology was to develop a criteria for the code to determine when transition from cooling to heating occurs. The code then proceeds through the cooling and heating environment determinations, which ultimately are merged to form one time-dependent environment.

Significant parameters which are determined by the code are the base gas recovery temperature, $T_r$, and convective heat transfer coefficient, $hc$. These parameters along with wall temperature define the convective environment according to the following relationship:

$$q_c = h_c(T_r - T_w)$$

For this code, values of cold wall $q_c$ are extracted from the database, then adjusted and scaled to the conditions being investigated. Recovery temperature is either derived from the database or determined directly as a fraction of engine chamber conditions. Heat transfer coefficient is not computed directly from the base flow conditions, but rather is deduced form the heating rate, recovery temperature, and wall temperature conditions previously determined. It is then used directly in the output to generate a variety of heating rates for a range of constant wall temperatures.

Subroutine `conv_main` controls the computational flow. It reads in values of input parameters from the X Windows input interface. The following general input data are needed to begin the convective calculations:

- Engine or booster operating conditions
- Base geometry/engine arrangement
- Nozzle description
- External flow/trajectory conditions

From the user input, the problem is defined into one of these categories:

- Core stage only with a symmetrical arrangement (circle of three to six engines)
- Core stage only with either one or two center engines inside the outer ring of symmetrical engines
- Core stage with either two or four symmetrically positioned solid rocket boosters

When the choice of vehicles has been made, subroutine `initial_values` initializes the various parameters and ratios required in later subroutines to interpolate data trends. For example, an important ratio to determine when plume interactions occur is the ratio of engine spacing to engine nozzle diameter, S/De. If S/De is small, the engines are relatively close together and plume interactions occur at low altitudes. Conversely, when S/De is large, the engines are wide apart and plume recirculation due to strong plume interactions is delayed. Once the necessary parameters are initialized, the determination of convection can begin.

### 6.2.1 Utilization of the Flight and Model Databases

Extensive use was made of the flight and model databases summarized in Section 2. Over many years and prior to this contract, these data had been organized and analyzed extensively to assist in the hand calculated convective environments. General objectives in these previous analyses included:

1. Arranging the model data to show:
   a. Effects of number of engines
   b. Effects of engine arrangement
   c. Effect of different propellants
   d. Effect of chamber pressure
   e. Effect of nozzle area ratio
   f. Effect of heat shield location
   g. Effect of vehicle afterbody geometry (skirts)

h. Effect of altitude (ambient pressure)

2. Arranging the flight data to show:

   a. Trends for altitude of peak heating
   b. Altitude of choked base pressure
   c. Effects of forebody geometry
   d. Effects of throttling
   e. Effects of gimbaling
   f. Effects of adding boosters
   g. General trajectory trends

The general trends were reevaluated under this contract for applicability to the code. Specific new data trend curves were also developed to help define:

1. Choked base pressure in the center of an engine cluster as a function of chamber and ambient pressure.
2. Initial altitude of recirculation for multinozzle vehicles with different engine spacing and chamber pressures.
3. Heating rate trends as recirculated flow progresses forward from nozzle exit toward the base heat shield located near the nozzle throat.
4. Heating rate trends across heat shield as flow is vented outboard between engines
5. Heating rate trends when the base and nozzles are enshrouded with a base region "skirt."

The data trend curves and working paper curves are too extensive for inclusion in this report. However, the user can review the table look-up data developed from the original data by listing the files contained in the various subroutines. For example, subroutine **pbase_choke** contains equations fitted to choked base pressure data taken from the classic Goethert Base Flow Characteristics Report [34]. The data are listed in tabular form versus different base region variables in comments at the beginning of the subroutine.

Another example of the use of experimental data to develop table look-up information is the use of 1/25th scale $LO_2/LH_2$ J-2 engine short-duration model data from the Saturn Base Heating Handbook [37]. The data were organized to illustrate heating variation across the base heat shield as a function of altitude, Fig. 42; combustion chamber pressure, Fig. 43; and vent area, Fig. 44. On these figures, base location is ratioed to the distance from the center of the vehicle to the centerline of the outboard engines. Heating rate is also dimensionless, having been ratioed to the heating rate at the sensor closest to the base center. Distribution data of this type were used to develop heating rates at locations other than the vent plane in Section I of subroutine **qc_adjust**.

### 6.2.2 Initial Recirculation Altitude

Recirculation of plume exhaust gases into the base region is initiated when plume-free-stream flow interactions or plume-to-plume interactions create local pressures (at the plume intersection) which are greater than the interior base region pressure. In the

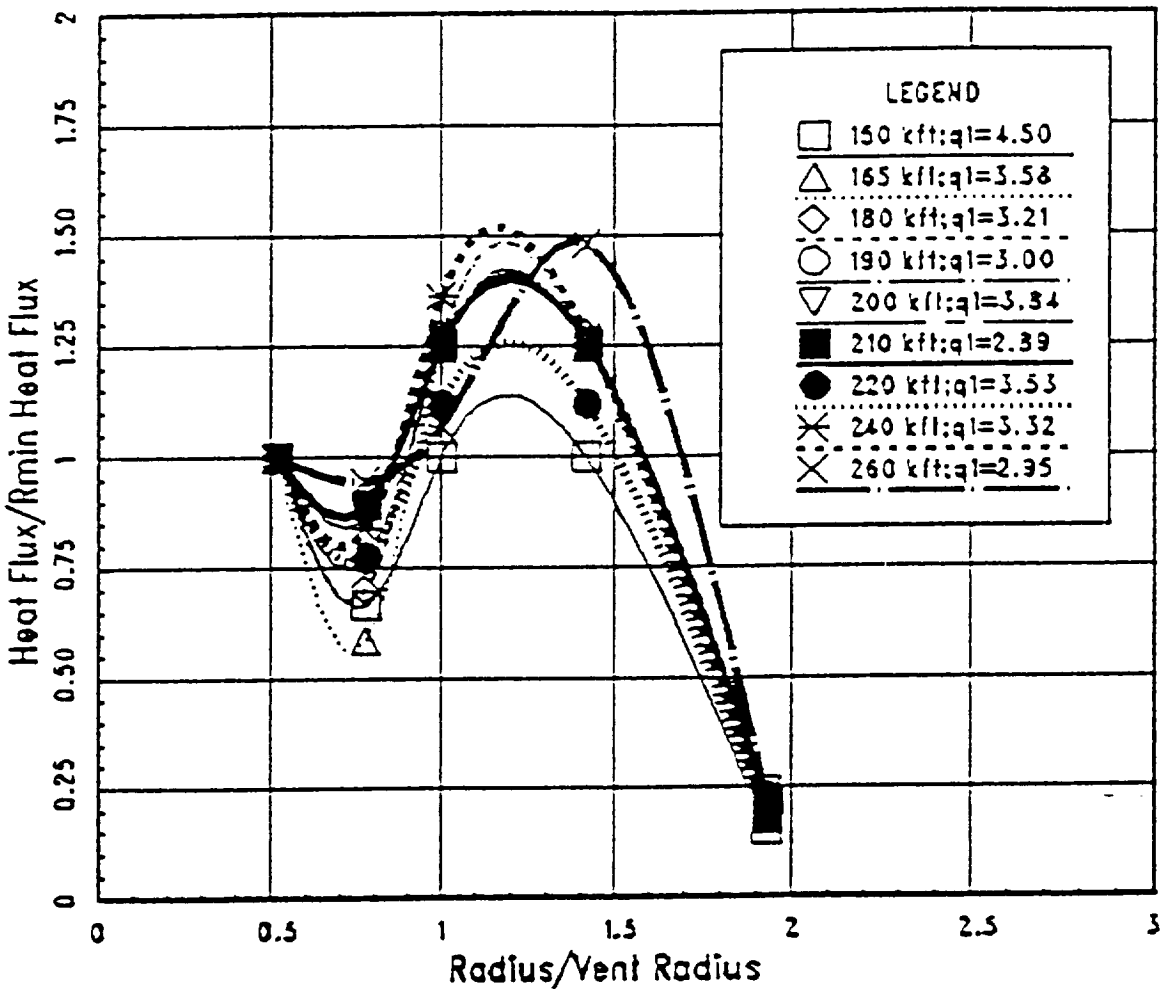


Figure 42: Heat Shield Convective Heating As a Function of Altitude

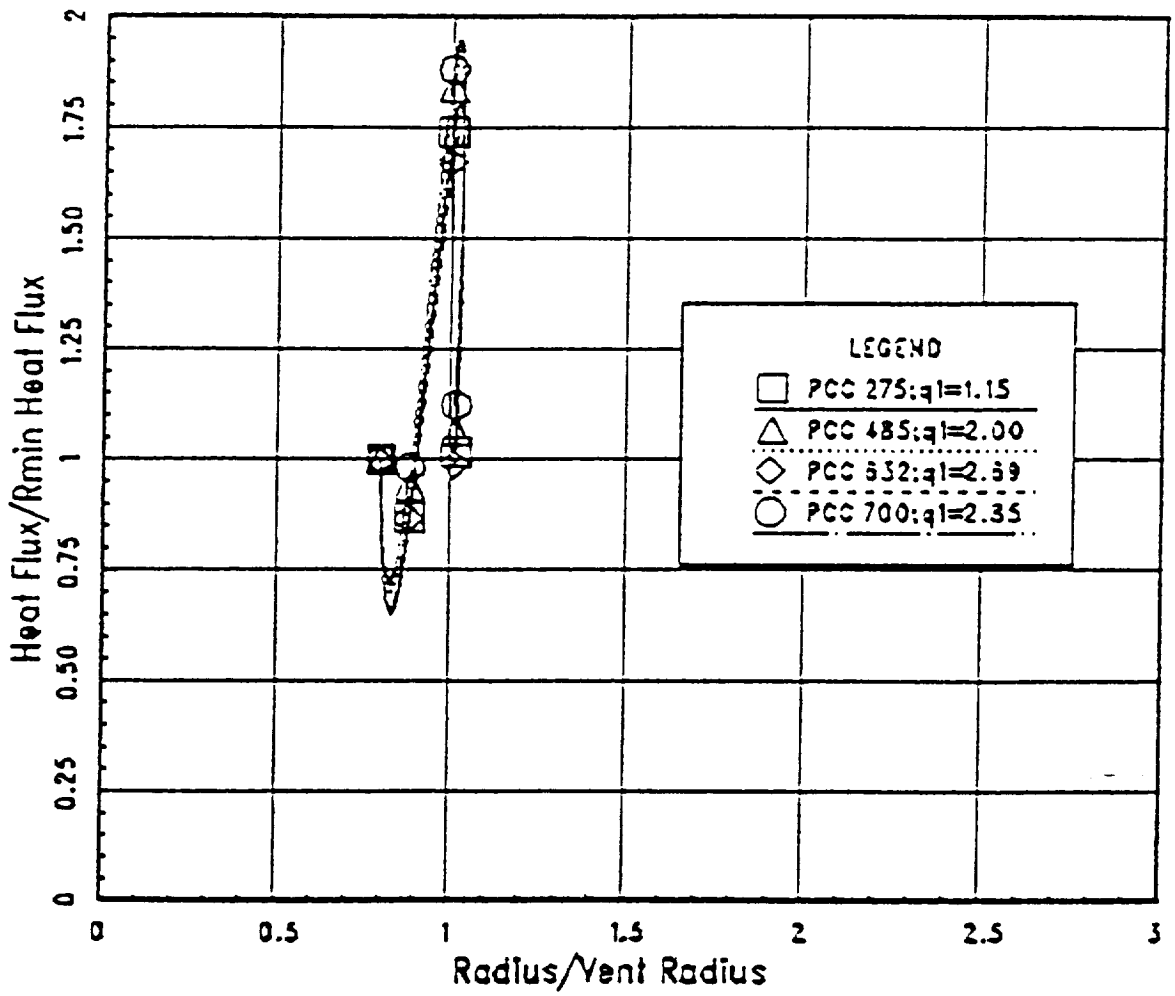


Figure 43: Heat Shield Convective Heating As a Function of Chamber Pressure

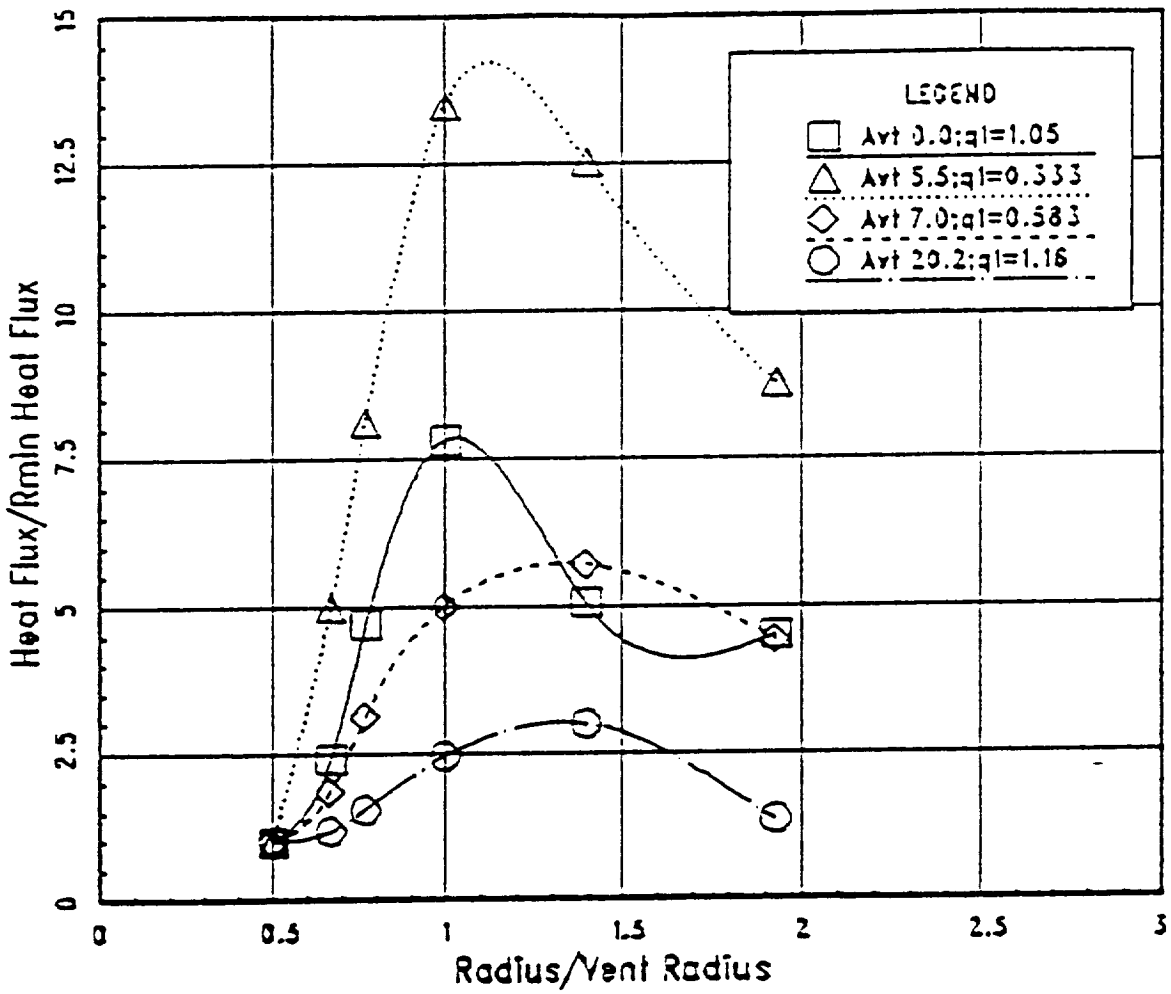


Figure 44: Heat Shield Convective Heating As a Function of Nozzle Vent Area

general flight and model databases, the plume-to-free-stream interaction region is usually strongest along the outboard plume boundary, and the recirculation which does occur is confined along the aft outboard portion of the nozzle. Plume-to-plume interactions dictate the flow reversal which feeds hot plume gases into the base interior region between the engines and forward to the heat shield. Therefore, as a simplification to the code, it was decided to base the determination of initial recirculation solely on criteria developed from plume-to-plume interactions.

Over many years and from a variety of multiengine flight vehicle datasets, the onset of convective heating has been correlated versus flight altitude. Although many variables affect the beginning of recirculation, the most important correlating parameter is the engine spacing. The data have shown that for very closely spaced engines, recirculation can occur at altitudes below 30,000 feet, but typical engine spacing which allows for gimbaling would create recirculation conditions at 60,000 to 70,000 feet. Under some extreme, widely spaced engine conditions, recirculation was delayed to approximately 100,000 feet.

Typical launch vehicles have overexpanded nozzles for first stage ascent to increase overall performance. These nozzles would typically overexpand to approximately 6 psia at the nozzle lip. For this typical case, the plumes do not balance until about 20,000 feet when ambient pressure equals the nozzle lip pressure. Only above that altitude does the plume expand and have the possibility of interacting with an adjacent plume. Therefore, 25,000 to 30,000 feet represent a likely lower limit for recirculation from plume-to-plume interactions.

Additional correlations with base pressure and convective heating data have shown that when base pressure equal ambient (it is below ambient during aspiration) incipient heating is evident. Therefore, the criteria selected for the code and implemented in subroutine `initial_recir` was a determination of the altitude when base pressure first equals ambient pressure, correlated to plume expansion angle. The baseline criteria for known plume angles was developed from five sets of model and flight data as listed below:

- Three Engine Configurations

  IH-39 Base Heating Test Data Analysis (SSME engines), REMTECH TR, 1978.
  J-2 Nozzle Test Data, Hayes International Corp., Engineering Report 1551, Nov. 1968.

- Four Engine Configurations

  Goethert, B. H., *Aerospace Engineering*, 1961
  Musial, N. T. and Ward, J. T., NASA TN D-1093, 1961

- Five Engine Configuration

  Saturn Base Heating Handbook (F1 engines) Boeing NASA CR, 1971

- Six Engine Configuration

  Saturn Base Heating Handbook (H1 engines) Boeing NASA CR, 1971

For each set of model or flight data where initial recirculation could be determined, a plume expansion parameter was needed which could be related to other plumes. During our analysis, SECA, Inc., provided plume boundaries for a variety of engines. These boundaries were overlaid to graphically determine the plume-to-plume intersection angle at which first recirculation was observed for different engine spacing. Since a computation of specific plume boundaries was not part of our code capability, a correlating parameter which was relatively easy to compute and which reflects the degree of plume expansion was needed.

After examining many possibilities, the simplest procedure and one which met our overall accuracy requirement was to relate plume expansion to initial recirculation by comparing the Prandtl-Meyer expansion angle at the nozzle lip. From the known database, the Prandtl-Meyer angle and altitude of initial recirculation were correlated with $P_{base} - P_{inf}$ equal to zero. For a new configuration or new engine, the code calculates the Prandtl-Meyer angle at different ambient pressures, then interpolates in the database for initial recirculation altitude, as a function of nozzle-to-nozzle spacing.

To accomplish the determination of Prandtl-Meyer angle in subroutine `initial_recir`, the ideal gas equations for isentropic flow of continuum gases were utilized. Based upon the choice of propellants, chamber conditions, nozzle area ratio, and nozzle half-angle, the code computes the nozzle exit Mach number and Prandtl-Meyer expansion angle. Interpolation in the tables gives the altitude of initial recirculation and sets $P_{base}$ equal to $P_{inf}$ at that altitude. Within the interpolation routines, adjustments are made for different gamma gases and number of symmetrically spaced nozzles.

A series of runs with variations in number of engines and engine spacing were made to illustrate the code determination of initial recirculation altitude. Two types of propellants were considered. The results are shown in Fig. 45.

### 6.2.3 Convective Environment at Choking Conditions

The base interior flowfield is solved by the code to define the maximum convective heating levels. The base volume of interest is that bounded by the heat shield, three or more nozzles, and the interior plume boundaries. At higher altitudes when the plumes strongly interact, the reversed flow fills the interior volume creating a base pressure sufficiently high to prohibit flow of external air into the interior. At certain altitudes, the flow exiting the base interior becomes choked in the vent regions between engines when the base pressure to exterior (ambient) pressure reaches the critical ratio. This choked condition is characterized by Mach 1.0 flow in the vent region.

The source of the reversed flow is the nozzle boundary layer flow which mixes with base gas present at the nozzle lip to form the plume interior boundary shear layer. The reversed gas is that portion of all interacting plume shear layer with insufficient pressure to pass the shock created by the interaction of the plumes. The interior flow is the circulating flow of reversed shear layer gases which is uniformly subsonic, but whose velocity is high as it is reversed, slows as it stagnates in the center heat shield region, then accelerates either out of the base or back along the nozzle toward the plume. This

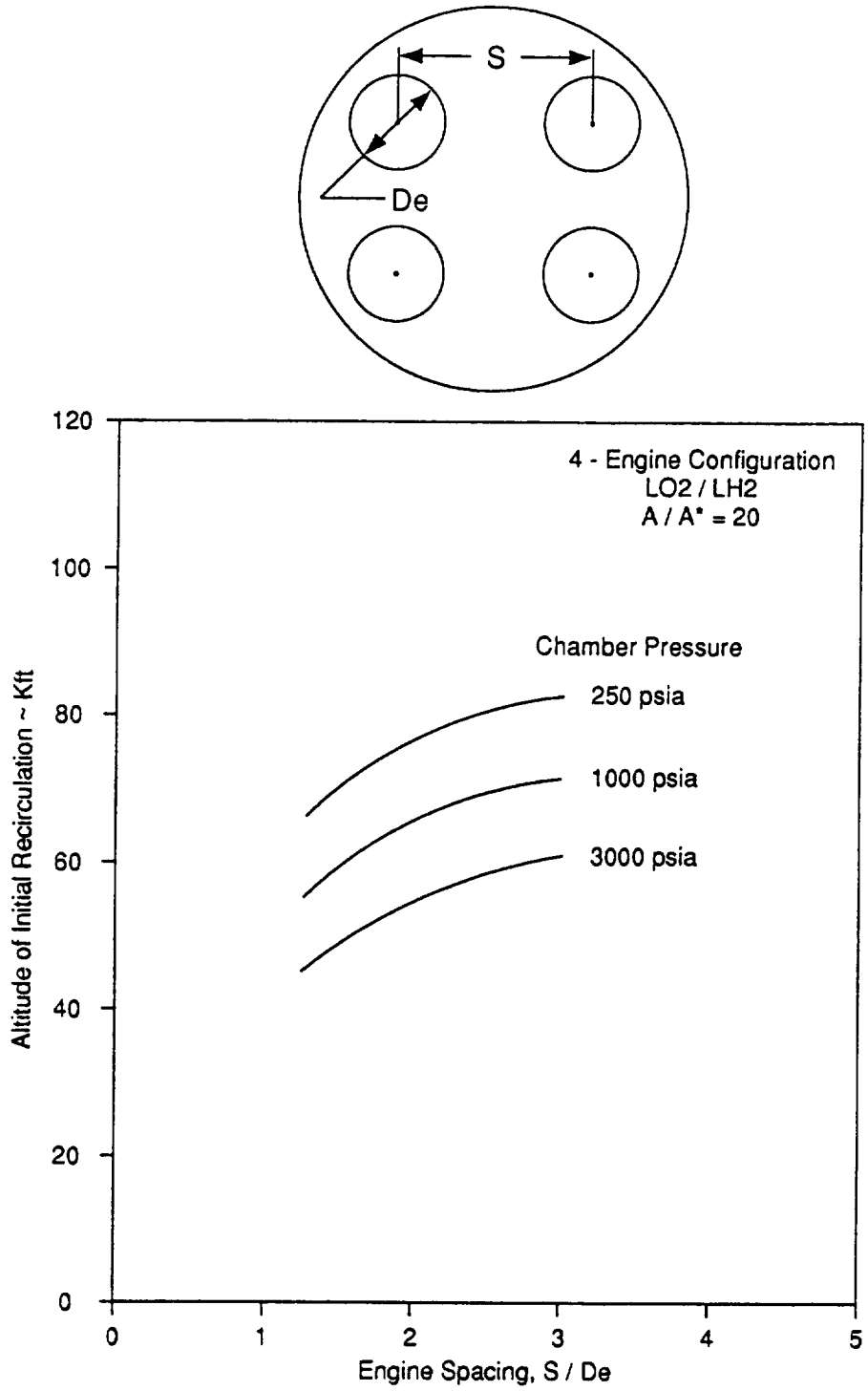


Figure 45: Altitude of Initial Recirculation

flowfield is modeled in the code to provide properties necessary to calculate convective heat transfer.

Our approach to model this interior flowfield is contained in subroutine **pbase_choke**. It is an extension of the mass balance algorithm developed by Brewer [32], and includes an exterior base pressure estimate from the flow module developed by PST, Inc. The mass balance approach assumed that for a given set of geometric conditions (base arrangement) the base pressure in the geometric center of an engine cluster is a constant percentage of the engine chamber pressure. Using the previously mentioned empirical data, such as that provided by Goethert, Fig. 46, an algorithm equating choked base pressure to chamber pressure was developed for a range of engines, chamber conditions, and nozzle spacing. When the base pressure to external pressure ratio from the dataset indicates choked flow, mass flow out of the base for all vent areas is calculated assuming a temperature value of 45 percent of engine chamber temperature to determine base gas density. This total mass flow is assumed to originate from the nozzle boundary mass over the circumferential zone of each nozzle bounded by the interior base vent planes. Utilizing nozzle boundary layer solutions for each selected nozzle to provide boundary layer temperature profiles, an average value of gas temperature recirculated into the base is determined. This value is incorporated into the vent mass computation, and iterated with the boundary mass averaged temperature profile until a steady state solution is reached. The mass balance analysis will provide the gas composition gamma for the base gas as well as the stagnation point properties and vent plane properties.

Subroutine **pbase_choke** determines the value of choked base pressure and the altitude at which it occurs based upon the closest spacing between engines in the cluster. It also defines base gas temperature corresponding to the choked base pressure. It does not define convective heating rate at the choked condition. This determination is developed in subroutine **qc_choked**. The algorithm in this subroutine does not compute heating rate directly based upon local, interior base flow properties because that proved to be difficult and required assumptions in the Reynolds number. Instead of a direct analytical calculation, the procedure which evolved after extensive analysis was to scale model data with appropriate corrections for chamber pressure and geometry.

Four separate heating rate calculations schemes are contained in subroutine **qc_choked**. The schemes address four different configurations possibilities:

1. Single ring of liquid propellant engines
2. Two concentric rings of liquid propellant engines or a ring around a center engine.
3. Two SRMs around a single or double ring of liquid propellant care engines
4. Four SRMs around a single or double ring of liquid propellant core engines.

For all cases, two types of propellants are considered for the core engines: $LO_2/LH_2$ and $LO_2$/RP-1. When calculations are made for the solid propellant motors, the baseline data are developed from typical SRM exhaust products with aluminum content of 16 percent.

All heating rate calculations at choking conditions were based upon the following procedure. A nominal heating rate was selected from the experimental database for each configuration and propellant type. Heating rate data from each database were normalized by chamber pressure and plotted versus chamber pressure to define the exponent for the Reynolds number in the heat transfer calculation. The scaling factor

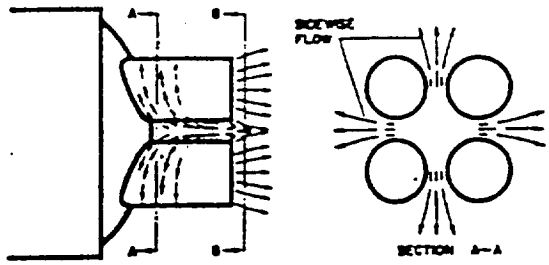


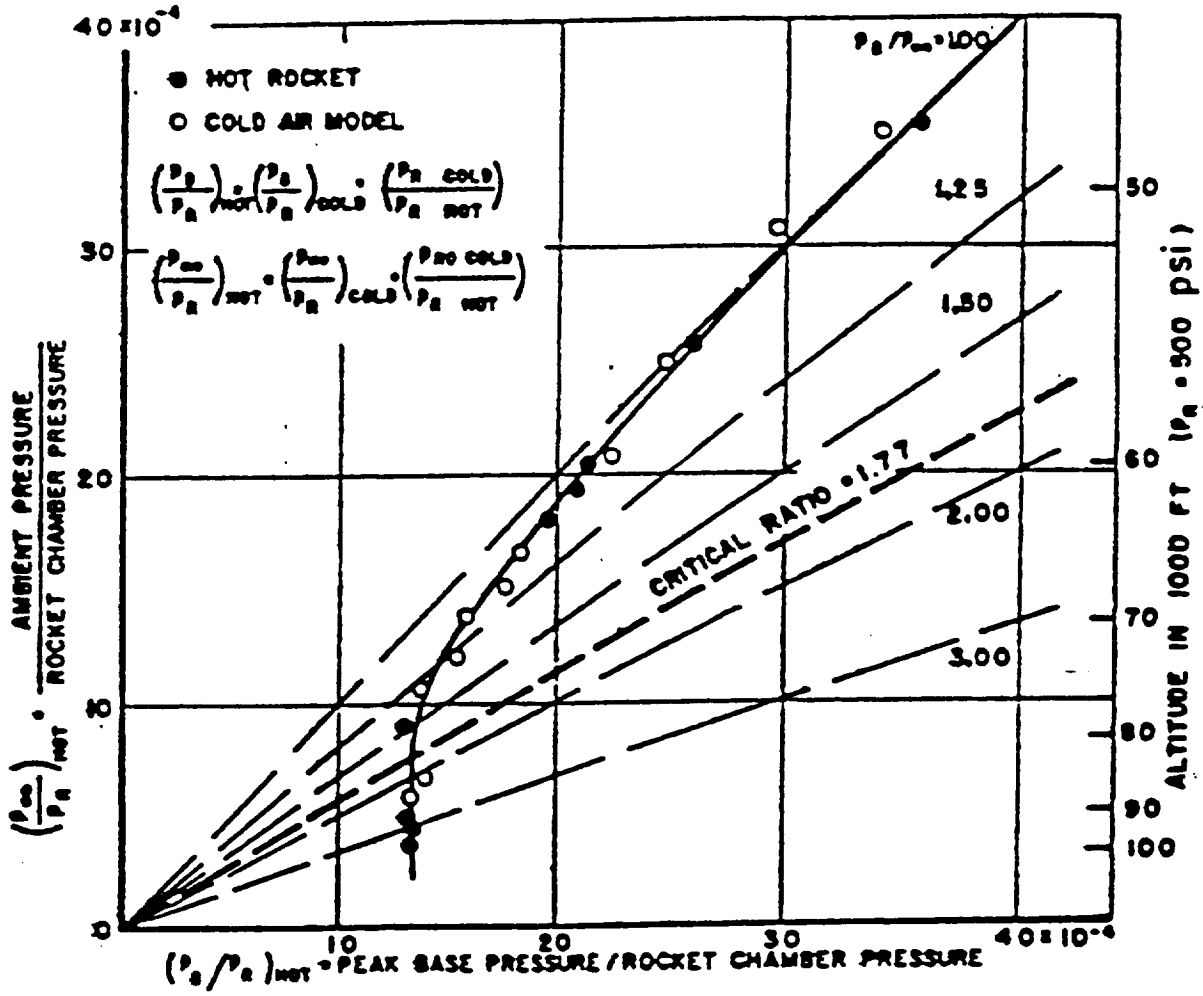


Ref: "Base Flow Characteristics of Missiles with Cluster-Rocket Exhausts," B.H. Goethert, Aerospace Engineering, March 1961.

Figure 46: Choked Base Flow Experimental Data

was simplified to treat the two largest factors: the density term in the Reynolds number and the physical size difference between the nominal configuration and the vehicle under consideration. Ultimately, an explicit heating rate equation can be developed for any vehicle from the general relationship:

$$qc = qc_{nominal} \times C_1 \times (P_{b_{choked}})^a (De)^{-0.2}$$

where

| | | |
|---|---|---|
| $C_1$ | = | constant based upon configuration and thermodynamic properties |
| $a$ | = | Reynolds number exponent from database |
| De | = | exit diameter of nozzle |

The database source, nominal dataset, and explicit computational algorithm for each configuration contained in **qc_choke** are listed below

1. For a single ring of engines:

   The $LO_2/LH_2$ data are based upon CAL tests of four RL-10 engines as documented in the Saturn Base Heating Handbook, NASA CR-61390, May 1972:

| | | |
|---|---|---|
| $P_{chamber}$ | = | 350 psia |
| O/F | = | 5.0 |
| $A/A*$ | = | 40 |
| $L_{De}$ | = | 0.608 |
| $Lskirt_{De}$ | = | 0.0 |
| De | = | 3.78 inches |
| $r_{rvent}$ | = | 0.0 |
| $q_{conv}$ | = | $81.1435 \times (P_{b_{choke}}^{0.8} \times (De)^{-0.2})$ |

   The $LO_2/RP\text{-}1$ data is based upon LEWIS tests of four bell-shaped nozzles as documented in NASA TN D-1093, Dec. 1961.

| | | |
|---|---|---|
| $P_{chamber}$ | = | 600 psia |
| O/F | = | 2.2 |
| $A/A*$ | = | 12 |
| $L_{De}$ | = | 0.0425 |
| $Lskirt_{De}$ | = | 0.0 |
| De | = | 2.94 inches |
| $r_{rvent}$ | = | 0.0 |
| $q_{conv}$ | = | $93.655 \times (P_{b_{choke}}^{0.656} \times (De)^{-0.2})$ |

2. For two rings of engines (four outside engines + one inside engine):

   The $LO_2/LH_2$ data are based upon tests of five J2 engines as documented in the Saturn Base Heating Handbook, NASA CR-61390, May 1972:

   $P_{chamber}$ = 632 psia
   O/F = 5.0
   A/A* = 27.7
   $L_{De}$ = 0.551
   $Lskirt_{De}$ = 0.0
   De = 76.8 inches
   $r_{rvent}$ = 0.775
   For $LO_2/LH_2$:
   $q_{conv} = 213.0 \times (P_{b_{choke}}^{1.02} \times (De)^{-0.2})$
   For $LO_2$/RP-1:
   $q_{conv} = 213.0 \times (P_{b_{choke}}^{1.02} \times (De)^{-0.2})$

3. Solid propellant (with single or double ring engine core)

   Two SRM strap-on engines from Titan III — From: SLV-4 and SLV-8 Flight Test Report, The Martin Company, Nov. 1965.

   SRM Solid Propellant
   De = 5.85 inches
   A/A* = 8
   theta = 15 deg
   $P_{chamber}$ = 480 psia
   $q(nominal)$ = 3.6 BTU/ft$^2$-sec
   $P_{b_{choke}}(nominal)$ = 0.20 psia
   $q_{conv} = 44.0 \times (P_{b_{choke}}^{0.638} \times (De)^{-0.2})$

4. Four J-2 outside engines + one J-2 inside engine + four SRM strap-on engines

   From: Etemad and Korkan, *J. of Astronautical Sciences*, Vol. 15, No. 1, Jan.-Feb. 1968, pp. 5–13.

   SRM Solid Propellant
   A/A* = 10
   theta = 15 deg
   $P_{chamber}$ = 480 psia
   $q(nominal)$ = 12.0 BTU/ft$^2$-sec
   $P_{b_{choke}}(nominal)$ = 0.09 psia

$$q_{conv} = 168.2 \times \left(P_{b_{choke}}^{1.02} \times (De)^{-0.2}\right)$$
$$q_{conv} = 236.14 \times \left(P_{b_{choke}}^{1.02} \times (De)^{-0.2}\right)$$

### 6.2.4 Convective Heating Adjustments for Altitude and Geometry Distributions

Previous sections have described the program procedures for determining when initial recirculation and choking occur, and also have described the computation of heating rate and base pressure at choking conditions. Two major subroutines, **prop_curve** and **qc_adjust** determine the base region properties and resulting environments between those two known altitudes and also adjust the heating for differences in base geometry and axial location along the heat shield. Several internal subroutines within **prop_curve** are required to spline fit properties for recovery temperature, base pressure, and molecular weight of the base gas between the known values at the initial recirculation altitude and at choking altitude. These known values are listed below:

1. Recovery temperature —

   at initial recirculation:
   equal to the free-stream stagnation temperature
   at choking:
   equal to the base recovery temperature at choked conditions

2. Base pressure —

   at initial recirculation:
   equal to the free-stream pressure (aspirated flow)
   at choking:
   equal to the base pressure at choked conditions

3. Molecular weight —

   at initial recirculation:
   equal to mass of 100 percent air
   at choking:
   equal to mass of 100 percent plume gas (from CEC nozzle runs)

When the properties have been defined between the known altitudes and assuming that heating and pressure remain constant above the choking altitude, the code proceeds through subroutine **qc_adjust** to define the time (or altitude) dependent environments. Subroutine **qc_adjust** contains several internal subroutines which perform the following function:

- Corrects the choked heating rate for L_De, Lskirt_De (normalized skirt length or interstage length) and r_rvent (normalized radial distance from the base center)

  a. a single cluster of engines
  b. a double cluster of engines

c. solid strap-ons to a single or double ring of core engines

- Adjusts the choked heating rate throughout the flight trajectory as a function of Reynolds number and nozzle wall temperature
- Adjusts the heating rate for the axial location, or the distance forward from the nozzle exit plane.

Specific methodology for the choked heating rate corrections for base heat shield location is presented in subroutine `q_lde` and is based upon four engine model data. The skirt length correction is made in subroutine `q_skirt` and the correction for changes in vent area are contained in subroutine `rvnt`. Heating correction for the radial location from the center of the base is computed in subroutine `q_rvent`. All of these corrections essentially ratio the geometry from the problem being investigated to that for the standard choked flow analysis times a factor derived from the database analyses.

In subroutine `q_alt_892` (revised in August 1992), the convective heating rate at choking altitude is adjusted throughout the flight altitude range by a Reynolds number factor normalized with choked heating rate as follows:

$$\frac{q}{q_chok} = \frac{hc}{hc_chok} \times \frac{T_{recovery} - T_{wall}}{T_{chok} - T_{wall}} = \left[\frac{Re}{Re_chok}\right]^M \times \frac{T_{recovery} - T_{wall}}{T_{chok} - T_{wall}}$$

where $hc$ is the convective heat transfer coefficient , $T_{chok}$ is the base recovery temperature at choking, $T_{wall}$ is the wall temperature (540°R default) and the Reynolds number, $Re$, is determined as

$$Re = \frac{\rho V L}{\mu}$$

Using the equation of state

$$p_base = \frac{\rho_base\, R\, T_{recovery}}{W\,(molecular\ \ weight)}$$

the heat transfer factor becomes

$$\frac{q}{q_{chok}} = \frac{(W\,p)^m}{(T_{recovery})^n} \times \frac{(0.45\,T_{chamber})^n}{(W_plume\ Pb_chok)^m} \times \frac{(T_{recovery} - T_{wall})}{(T_{chok} - T_{wall})}$$

where $T_{recovery}$, $W$ and $p$ are obtained from spline fitting as described previously.

At turbulent base conditions,

The velocity, $V$, is proportional to $(T^{0.5}_{recovery})$
The viscosity, $\mu$, is proportional to $(T^{0.5}_{recovery})$
Therefore, $n = ((0.8 + 0.5) \times 0.8/0.8) \times m$

The increase of $T_{recovery}$ with altitude and the decrease of $P_{base}$ and $W$ (or $\rho$) with altitude leads to a maximum heating factor. This results in an increase of heating from the lowest altitude, up to the altitude where the heating rate peaks, and then a decrease to the choked heating value.

Exponent values $m$ and $n$:

1. $LO_2/LH_2$ — $m = 0.500$; $n = 0.650$, based upon J2 data from the Saturn Base Heating Handbook SSME data from IH-5 test
2. $RP\text{-}1/LH_2$ — $m = 0.580$, $n = 0.754$, based upon F1 data from the Saturn Base Heating Handbook
3. Solids
   a. Two boosters — $m = 0.620$, $n = 0.806$
   b. Four boosters — $m = 0.640$, $n = 0.832$

The convective heating rate convection for axial location is performed in subroutine `q_axial`. The corrections were derived by curve fitting data from these sources:

- Brewer's report [32]
- ALS heat shield predictions [43]
- Shuttle flight data along the SSME
- S-II stage thrust cone data [37]

This subsection is valid for engines located symmetrically in the base region with approximately the same S/De values, and is not appropriate for strap-on motors.

### 6.2.5 Convection During Early Flight (Aspirating Flow)

Methods for defining recovery temperature and convective heating rate from the altitude of initial recirculation to main engine shutdown have been described in previous sections. To complete the environment definition, procedures for defining recovery temperature and heat transfer coefficient from engine start-up (liftoff) to initial recirculation were needed. Recovery temperature during this portion of flight is determined in Section I of subroutine `Tr_curve`. The coefficient is determined in subroutine `ht_trnsfr_coeff`. For typical large launch vehicles, the aspirating flow convective environment predominates through the first 50 to 70 sec of flight.

The trend in ambient temperature for altitudes from sea level to about 50,000 feet is a steady drop from 520°R to approximately 390°R at 35,000 feet, followed by a gradual rise to 460°R. As the vehicle velocity increases, the free-stream total temperature begins a gradual and then more dramatic increase. Base pressure correlations with convective cooling flight data coupled with gas probe data have shown that the air temperature in the base region is approximately equal to the free-stream total temperature. Therefore, for the code computation, subroutine `tr_curve` extracts ambient temperature from a table look-up versus altitude, then computes free-stream total temperature based upon the input trajectory table of vehicle velocity or Mach number. Because all of the velocity is not converted to temperature increase in the gas as it stagnates (or slows dramatically) in the base, a computation of recovery factor was needed. This is accomplished in real function `Tr_function` contained within subroutine `Tr_curve`. Typical values of recovery temperature in the base region during aspiration range from about 520°R at liftoff to as high as 750°R before recirculation begins.

Convective heat transfer coefficient during aspirating flow is extremely difficult to determine from the databases because of the difficulty in deducing convection from the total calorimeter and radiometer data, and because the temperature difference between the air and gage surfaces is small. Over the years of flight data analyses, a range of coefficients at various subsonic vehicle velocities has been defined. From this range, a discrete history of coefficients has been refined which has shown consistent agreement with flight trends. This coefficient has been tabulated versus altitude in the code assuming a nominal base region running length of the flow of 15 ft. Within subroutine `ht_trnsfr_coeff` when altitudes up to initial recirculation are being considered, a table lookup of the nominal coefficient is accomplished followed by an adjustment to the coefficient based upon half the base diameter ratioed to the nominal base diameter to the 0.8 power.

### 6.2.6 Wall Temperature Effects

In subroutine `ht_trnsfr_coeff`, the computation of convective heat transfer coefficient assumes a value of wall temperature which is constant throughout the base region and constant with time. The choice of wall temperature is left to the user; however, the following potential error can result from improper choice of the wall temperature. As mentioned previously in Section 6.2.4, cold wall convective heating rate is adjusted throughout the flight altitude range by a Reynolds number factor which contains a wall temperature correction. The default value of this wall temperature is 540°R which is approximately correct for typical flight and model calorimeter sensor surface temperatures. For the heat transfer coefficient to be accurate, reduction of the cold wall heating rate must be made initially at approximately the 540°R temperature value.

If the code user desires a computation of convective heating rate at other wall temperature values, it can be computed in subroutine `ht_trnsfr_coeff` at the desired value utilizing the coefficient previously determined at 540°R. The choice of wall temperature can be very important to the computation of integrated convective heating load. If, for example, a value of wall temperature of 400°R were chosen, convective heating will occur throughout flight. Conversely, choosing a wall temperature of 1000°R will result in significant convective cooling initially in flight which may offset the heating experienced later and result in a net heating load of approximately zero.

Normal convective output of coefficient and recovery temperature versus time is useful to the thermal analyst in his computation of actual wall temperature. In the usual procedure, as the thermal analysis proceeds in time, the computation of local surface heating for each time increment is based upon the temperature difference between recovery temperature and actual wall temperature at the beginning of the time increment.

# Section 7
# SUBCONTRACT OUTPUTS

In order to expedite specific tasks in the plume modeling and base flowfield efforts, REMTECH initially issued two subcontracts. The first subcontract provides for development of an external flow computational model which would define flow which influences the periphery of the ALS/NLS base region. This contract was awarded to Propulsion Science and Technology, Inc. of Princeton, NJ, on October 2, 1989, and provides for support over a 17–month period.

Additional specific expertise was needed to generate nozzle internal flowfields and startline information which ultimately was utilized to refine plume radiosity models and base interior flowfields. To obtain this expertise and expedite this facet of the plume modeling tasks, a contract was awarded to SECA, Inc. of Huntsville, AL, on October 2, 1989. This contract provided for a continuous low level of support throughout the main contract performance period.

As the ALS program transitioned to the NLS program, NASA modified the contract to include preliminary definition of base heating and plume induced environments to NLS configurations. REMTECH received the contract change order on September 18, 1991, and immediately modified the subcontract to SECA to provide for specific remaining plume induced environments for two NLS concepts to support the NLS Cycle 1 and Cycle 2 assessments. Specific tasks addressed by SECA included plume impingement environments to the mobile launch platform and to the spent ASRBs on the HLLV concept and on the stage 1 core engines on the 1.5 stage concept following separation.

## 7.1 Forebody Flowfield Module (PST, Inc.)

The forebody flowfield module was developed by Propulsion Science and Technology, Inc. This code computes the axisymmetric, launch vehicle external flowfield from body to shock, as shown in Fig. 47, and provides upstream conditions for the base region exterior flowfield calculation. In addition, a model to compute the base flowfield and free stream-plume interaction region in the peripheral base region of a typical NLS multinozzle configuration was implemented. Preliminary calculations of exterior base properties, using a variant of the base/separation region flowfield module (BSRM) of SPF/3, with mass addition were presented.

The forebody flowfield module was developed from methodology contained within the standardized plume flowfield model (SPF/3). The inviscid forebody flowfield is comp0uter from body to fitted vehicle shock via an inviscid/shock capturing component (SCIPPY). An overlaid boundary layer is provided by the turbulent mixing component (SPLITP). The code is designed to treat bodies with sharp or spherical noses for supersonic flight Mach numbers ($M_\infty$ greater than about 1.7). The subsonic region upstream of a spherical nose is treated by the NSWC NOSTIP code, a time marching flow solver, which produces a supersonic startline for SCIPPY as shown in Fig.48.

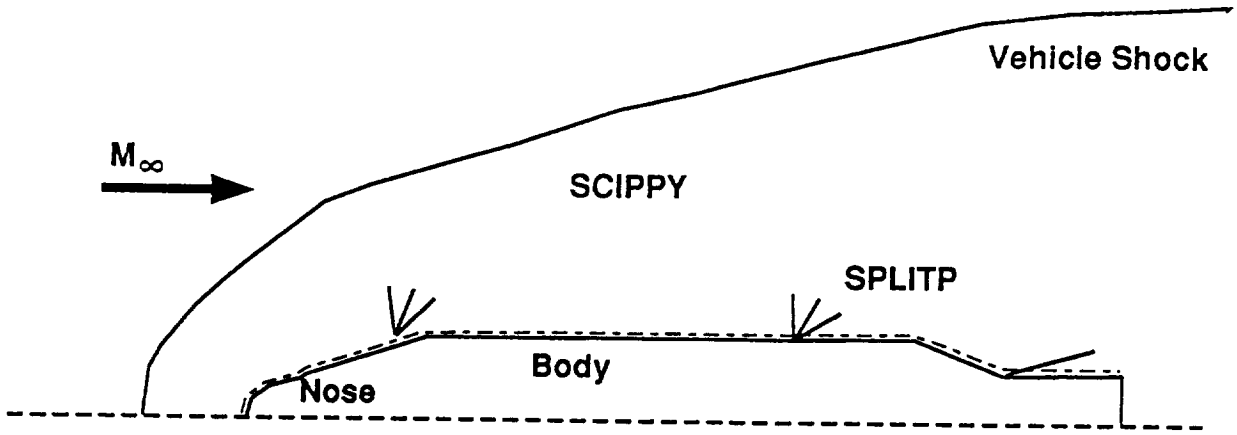


Figure 47: Afterbody Code Methodology

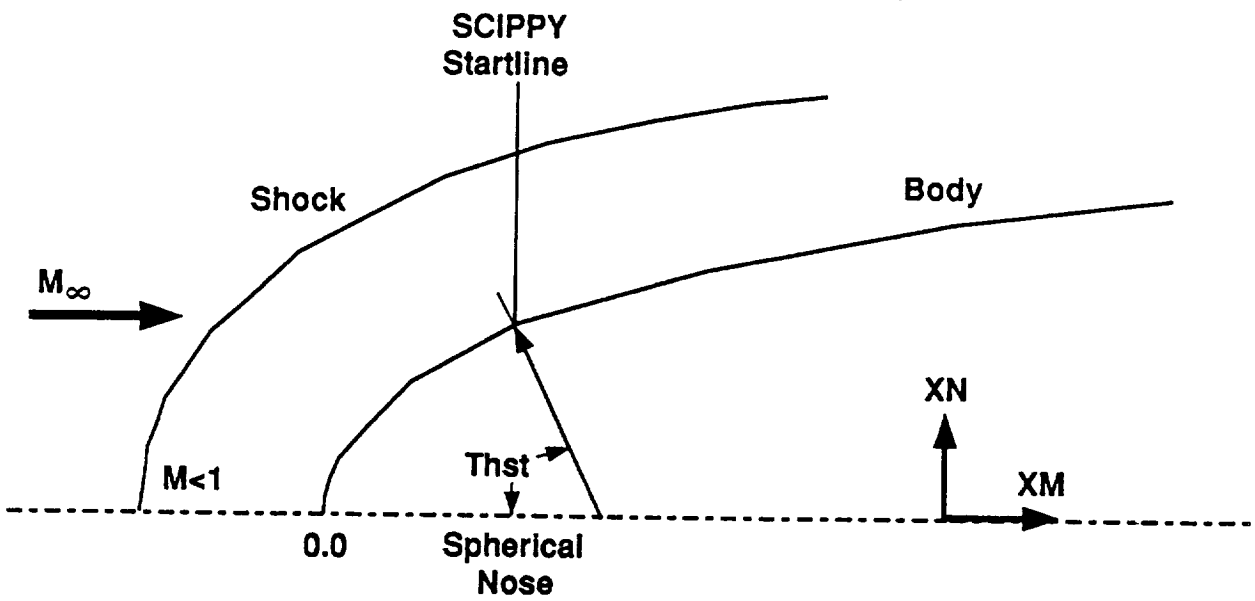


Figure 48: Spherical Nose Initialization

At this stage of code development, on a limited number of test cases have been run. We have made many successful runs with the SCIPPY algorithm (no boundary layer) and found it to be very reliable. However, we have found that the overlaid boundary layer computation in SPLITP is sensitive to pressure gradients generated by junctures in the body geometry. We have made a number of successful runs. However, further development work is necessary to provide a more reliable boundary layer computation in these regions.

Various input/output options are available in the code which can be tailored to the specific needs of the user. A defaulted input option provides the user with a simple interface to the code, whereby only vehicle body shape and flight trajectory information are necessary code inputs. All other run parameters are defaulted internally in the code. A full input option is also available which allows the user to vary run parameters as



C 2

necessary for more generalized code usage.

Excerpts from the PST final report are included in the following discussion. Computational procedures within the code are described along with instructions for making the code operational on a UNIX system. Import instructions and typical output are described and a test case is presented. Results from a preliminary exterior base prediction are also reviewed.

**Computational Methodology**

**Nose Initialization** — For blunt nosetips, the NSWC NOSTIP code has been added as a subroutine to generate a starting plane profile for a spherically capped body in supersonic flight. The NSWC NOSTIP code performs a time-dependent, perfect gas Euler calculation. (Note that for flight Mach numbers above about 8–9 the accuracy of this calculation starts to diminish due to real gas effects downstream of the detached vehicle shock.) As shown in Fig. 48, the nosetip initialization provides a startline for SCIPPY, which must be supersonic in the axial direction. If the angle THST is not large enough, the calculation must be repeated using a larger value of THST (smaller tangency angle).

For sharp nosed bodies (conical or ogive) an initial supersonic profile is established from properties calculated downstream of the attached nose shock using standard shock fitting procedures. The SCIPPY calculation is then initiated a small distance downstream of the nose (~0.1 ft.).

**Body Geometry** — The body geometry is specified by a series of polynomials, as shown in Fig. 49. (An option is available to read in body X, R coordinates, but should only be used on a smoothly varying body with no sharp discontinuities in slope). The code automatically checks the consistency between the geometry computed by the NOSTIP code (obtained from $R_{nose}$, THST) and the first polynomial. The code also checks for consistency in radial location from one polynomial to the next. The hardcopy output files contain messages to alert the user when inconsistencies in body geometry are present.

**SCIPPY Algorithm** — The inviscid forebody flowfield is calculated by the SCIPPY algorithm, which employs the same shock-capturing methodology that is contained in SPF/3. The flowfield equations are cast in conservative form and are integrated in mapped coordinates evenly distributed between the body and the shock. The explicit,

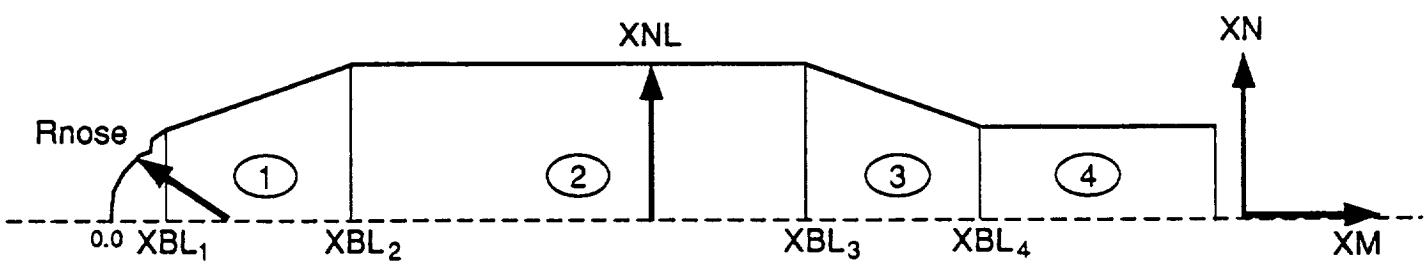


$$XNL = ABL_i*(XM - XBL_i)^2 + BBL_i*(XN - XBL_i) + CBL$$

Figure 49: Definition of Body Geometry

predictor/corrector, shock-capturing algorithm of MacCormack is used. Boundary points are solved employing a two-step characteristic procedure in conjunction with a statement of the boundary conditions.

A shock condition is used as the upper boundary in the forebody analysis. The shock point location is determined from the shock angle; the gas properties are iteratively determined by varying the shock angle until the pressure and flow angle given by the shock jump relations satisfy the uprunning characteristic compatibility relation. A geometric boundary condition is used as a lower boundary such that the flow angle associated with the downrunning characteristic compatibility relation matches the slope of the local body geometry.

**SPLITP Algorithm** — An overlaid boundary layer is calculated using the SPLITP algorithm, written in body-normal coordinates. SPLITP utilizes a fully implicit algorithm for solving the parabolic boundary layer equations. A two equation turbulence model ($K\epsilon$) is utilized in conjunction with a modified Van Driest mixing length model in the near wall region.

The equations are solved in a mapped coordinate system using a fixed number of grid points, distributed in a stretched fashion as shown in Fig. 50. This allows adequate resolution near the body surface while limiting the total number of radial grid points.

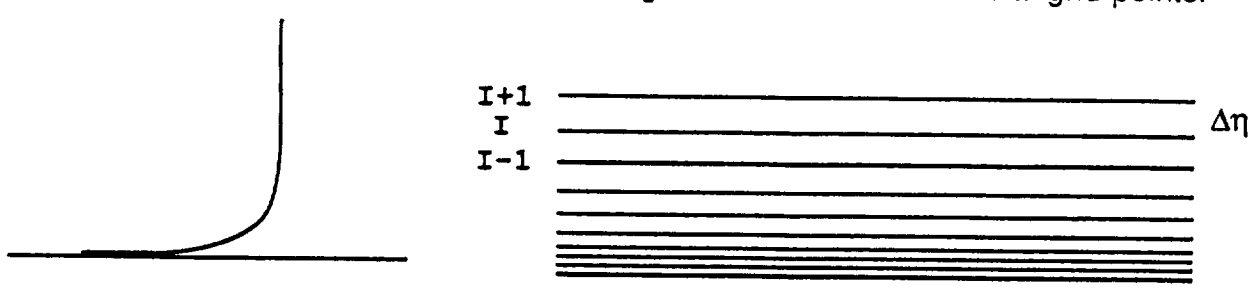


Figure 50: SPLITP Mapped Grid

A no-slip wall boundary condition is enforced, with either constant wall temperature, $m$, adiabatic wall or a convective wall thermal boundary condition. The outer boundary conditions and pressure field are obtained from a inviscid flowfield calculated by SCIPPY. The outer computational boundary is diffusion boundary whose growth is controlled by local gradients.

The boundary layer calculation is initialized using a laminar, Blasius profile just downstream of the SCIPPY startline plane. In the default version this profile is allowed to transition to turbulent flow over a transition length of 0.5 feet, so that the profile will be fully turbulent 1.5 feet from initialization. The user can also input the start of transition and the transition length.

**Exterior Base Flowfield Predictions** — The Base Separated Region Module (BSRM) of SPF/3 was used as a computational model to calculate the base flowfield and free-stream-plume interaction region in the peripheral base region. A summary of the methodology utilized in the BSRM is included in Appendix A. The BSRM was modified to account for mass transfer into or out of the periphery of the base simply by redefining

the mass flux parameter $M^o$ such that:

$$M^o = \frac{\Psi_i}{M_j + M_o + M_{vent}}$$

where $\Psi_j$ is the jet mass flow, $M_j$ is the mass entrained into the jet side base shear layer, $M_o$ is the mass entrained into the external side base shear layer and $M_{vent}$ is mass addition from the interior base. The recompression processes at the base shear layer and $M_{vent}$ is mass addition from the interior base. The recompression processes at the base triple point are assumed to be unaffected by the additional vent mass.

A sample exterior base calculation was performed for a typical NLS configuration. A summary of the case is provided in Fig. 51.

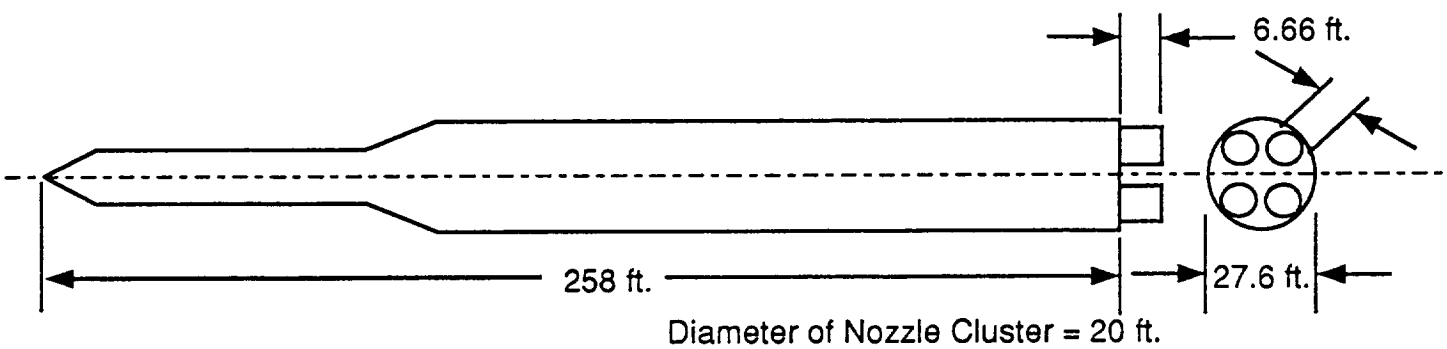


| FLIGHT CONDITIONS: | NOZZLE: Exit Conditions Provided by REMTECH | |
|---|---|---|
| Altitude = 40 km | Pc = 2250 psi | LOX/H2 |
| Mach # = 4.5 | Tc - 3583 R | O/F = 6 |
| Pinf = 2.97 (-3) atm | | |

**GAS COMPOSITION**

| *SPECIES* | *JET* | *EXTERNAL* |
|---|---|---|
| H | 8.91 (-6) | 0.0 |
| H2 | 2.44 (-1) | 0.0 |
| H2O | 7.56 (-1) | 0.0 |
| N2 | 0.0 | 7.0 (-1) |
| O | 0.0 | 0.0 |
| OH | 8.48 (-7) | 0.0 |
| O2 | 0.0 | 2.1 (-1) |

Figure 51: Run Summary

Results from the exterior base calculations are summarized below. Two cases were considered (Fig. 52); Case 1 has a jet radius of 6.66 feet which represents the single equivalent nozzle size, Case 2 has a jet radius of 10.0 feet (which equals the four nozzle cluster radius). The body radius was the same for both cases.

The effect of the vent mass tended to decrease the base pressure by about 25 percent from the baseline case where no venting was assumed. It should be noted

that the vent mass was on the same order as the total mass entrained into the base shear layers ($M_j + M_e$). The base pressures for Case 1 ($R_b/R_j$ = 2.07) were about a factor of 2 lower than for Case 2 ($R_b/R_j$ = 1.38).

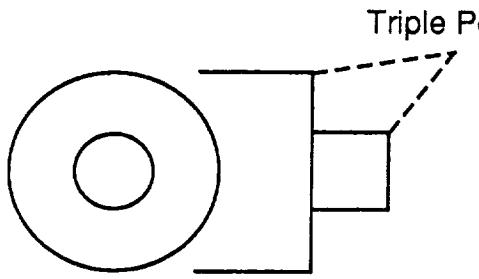


**Case 1**

$R_b$ = 13.79 ft
$R_j$ = 6.66 ft. (Equivalent)
$R_b/R_j$ =2.07
Distance from heat shield to nozzle exit plane = 6.66 ft.

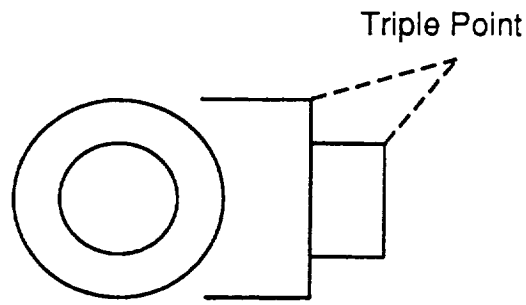


**Case 2**

$R_b$ = 13.79 ft
$R_j$ = 10.0 ft (Cluster Radius)
$R_b/R_j$ =1.38
Distance from heat shield to nozzle exit plane = 6.66 ft.

| | Pbase (atm) | Tbase (deg K) | Φbase | .Mbase (lbs/s) | $X_{tp}$ (ft) | $Y_{tp}$ (ft) |
|---|---|---|---|---|---|---|
| Case 1 | 1.88 (-3) | 1965 | .109 | 0.0 | 4.91 | 13.07 |
| Case 1a | 1.44 (-3) | 1958 | .107 | 19.75 | 4.25 | 12.67 |
| Case 2 | 3.22 (-3) | 1854 | .090 | 0.0 | 3.4 | 14.04- |
| Case 2a | 2.34 (-3) | 1846 | .089 | 19.75 | 2.77 | 13.55 |

Figure 52: Exterior Base Calculation

## 7.2 ALS/NLS Plume Descriptions (SECA, Inc.)

The purpose of the SECA subcontract was to supply REMTECH with plume flowfields to provide the inputs for the base heating design code for the Advanced Launch System (ALS) and to provide plume characteristics and plume impingement environments to support design studies for the National Launch system (NLS) class of vehicles.

Early trade studies for the ALS vehicle investigated a range of liquid engines that utilized nozzles that had area ratios from 30 to 60:1 and primarily focused on a hydrogen/oxygen engine producing 580K pounds of thrust. The first tasks performed were to characterize the 30 and 60:1 exhaust plumes form sea level to shutdown to provide the data necessary to produce the radiation and convective base heating environments

for the ALS base heating design code. These analyses are described in Appendix IV. Typical results are shown in Figs. 53 and 54.

During the course of the study, the ALS class of vehicles was dropped in favor of the NLS class of vehicles. The NLS vehicles consisted of a 1.5 stage and a heavy lift vehicle. The 1.5 stage vehicle consisted of six 583K thrust Space Transportation Main Engines (STMEs). The STMEs utilize hydrogen/oxygen as propellants and have 45:1 contoured nozzles. The four outboard engines comprise the propulsion module that is jettisoned at 240K feet and the remaining two sustainer engines continue to fire until shutdown. The heavy lift vehicle used four STEM engines in the core vehicle and two Advanced Solid Rocket Motors (ASRMs) that were staged anywhere from 150–200K feet.

To support the base heating design studies the STME exhaust plumes were characterized from sea level to shutdown. The 45:1 exhaust plumes were also used as part of the ALS base heating design code database. Typical temperature contours for the STME at 10,000 feet are displayed in Fig. 55.

The NLS class of vehicles requires significant modifications to the launch stand at Kennedy Space Center. As part of this study, pressure and heating environments due to the 1.5 and HLLV were calculated to a candidate launch stand. Heating rate predictions for B. P. 7 on the MLT are shown in Fig. 56.

In addition to the two center sustainer engines the 1.5 stage NLS vehicle uses four outboard engines called the propulsion module (PM). During the staging maneuver the PM flies through the two sustainer engine exhaust plumes which will produce high forces, moments and heating rates. To support the separation studies, it was necessary to calculate the plume impingement forces and moments. Typical results are presented in Fig. 57.

During the staging of the ASRBs from the heavy lift launch vehicle, the ASRBs fly through the four core STME exhaust plumes. Since the ASRBs are recoverable and to ensure no recontact of the ASRBs with the core vehicle, the STME induced pressure, heating force and moments to the ASRBs are necessary. Section 2.5 of Appendix IV discusses the analysis that was performed to provide the separation environments to the ASRBs. Impingement forces and moments versus time from separation resulting from this analysis are shown in Fig. 58.

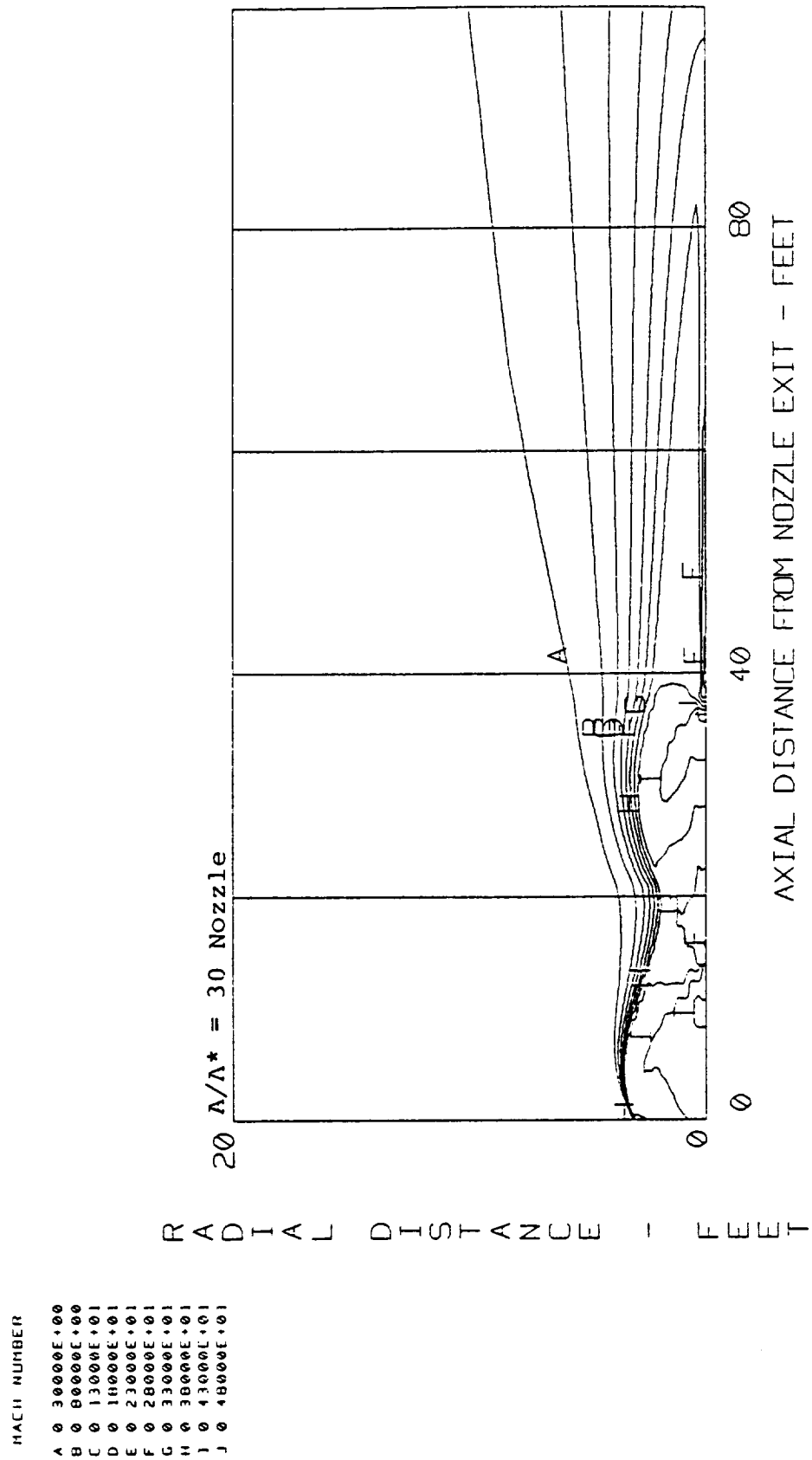


Figure 53: Mach Number Contours for 30:1 Engine Plume at 20,000 Feet

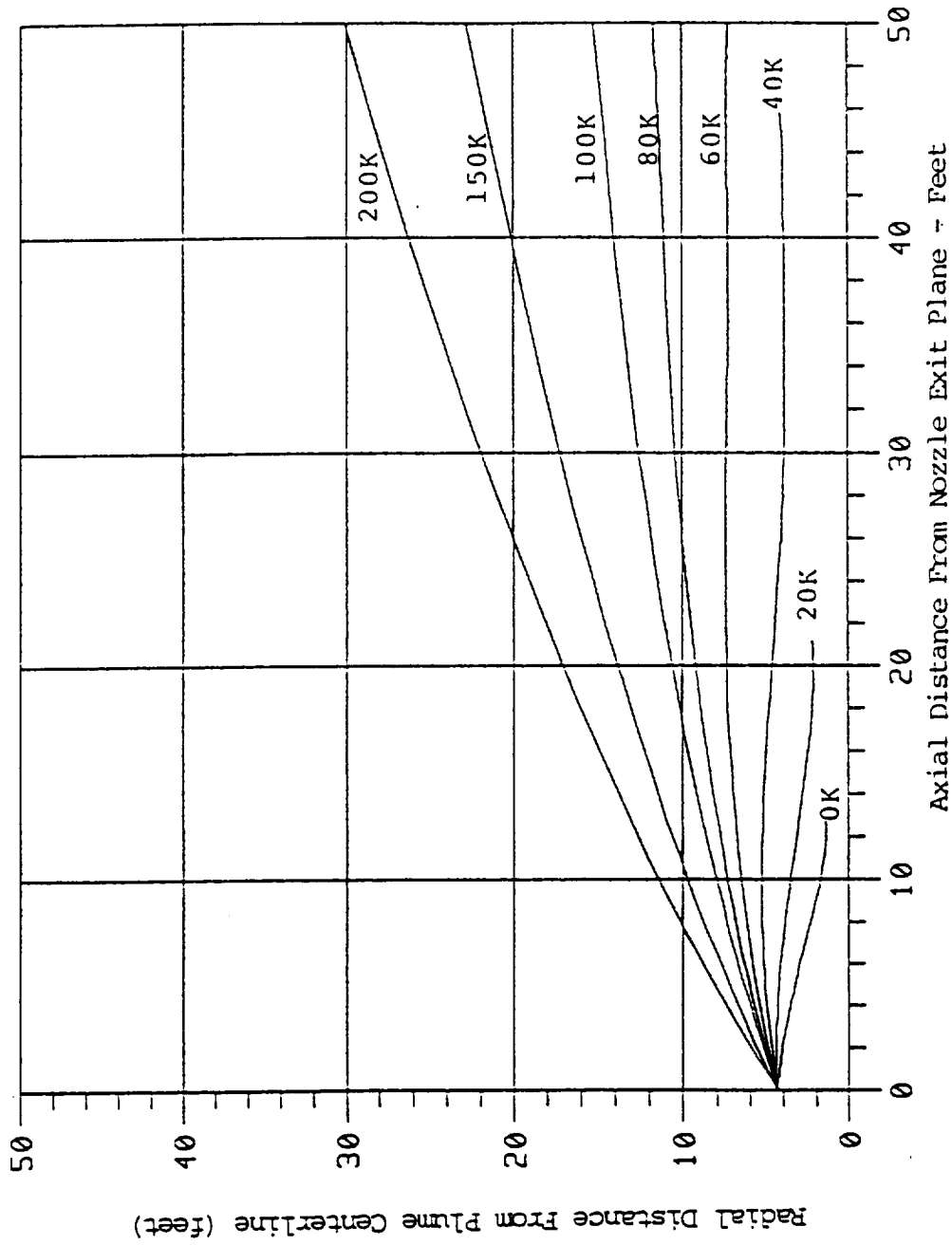


Figure 54: Inviscid Plume Boundaries for 60:1 Engine Including Free-Stream Effects

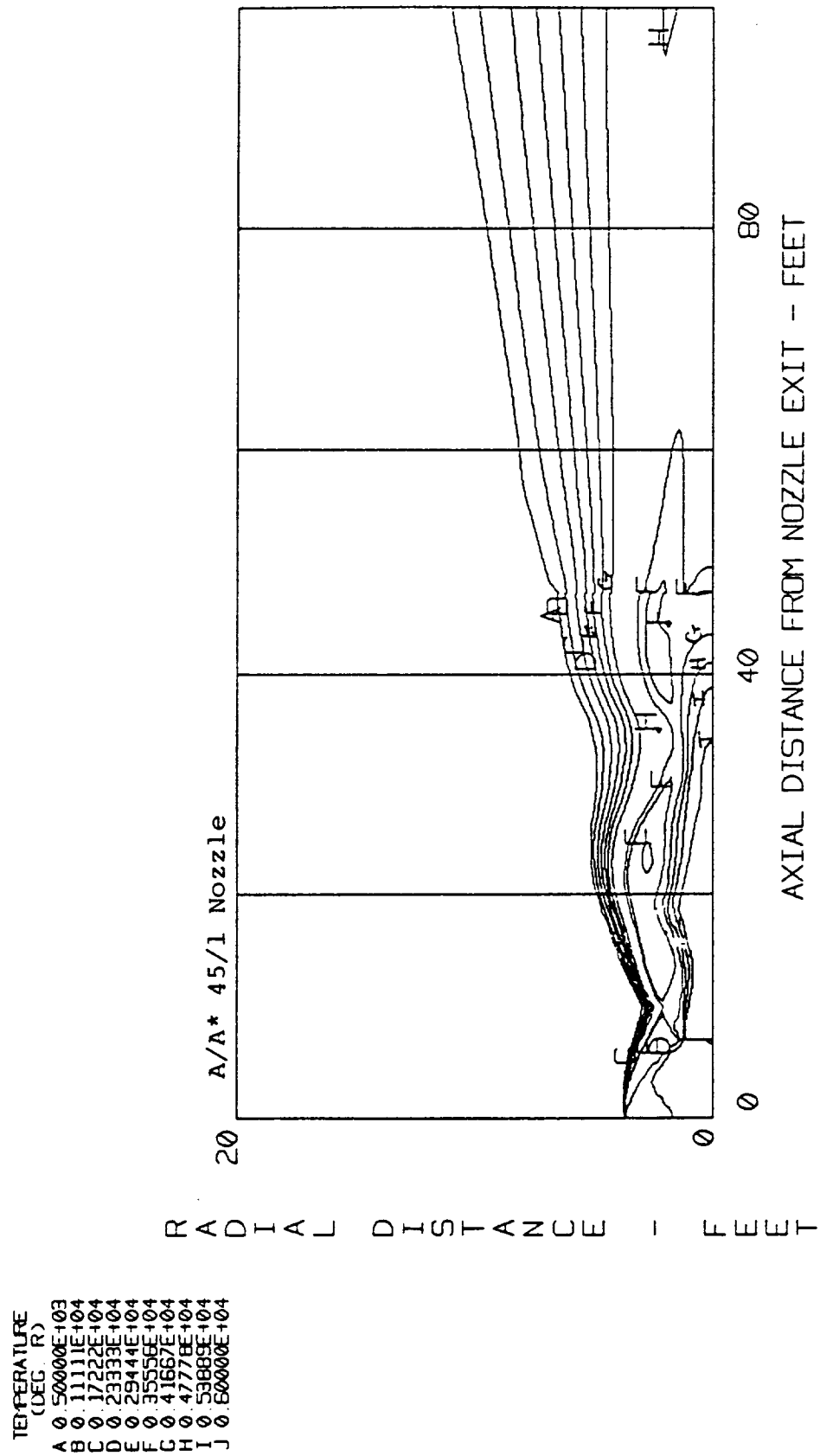


Figure 55: Temperature Contours for STME Plume (75 Percent Thrust) at 10,000 Feet

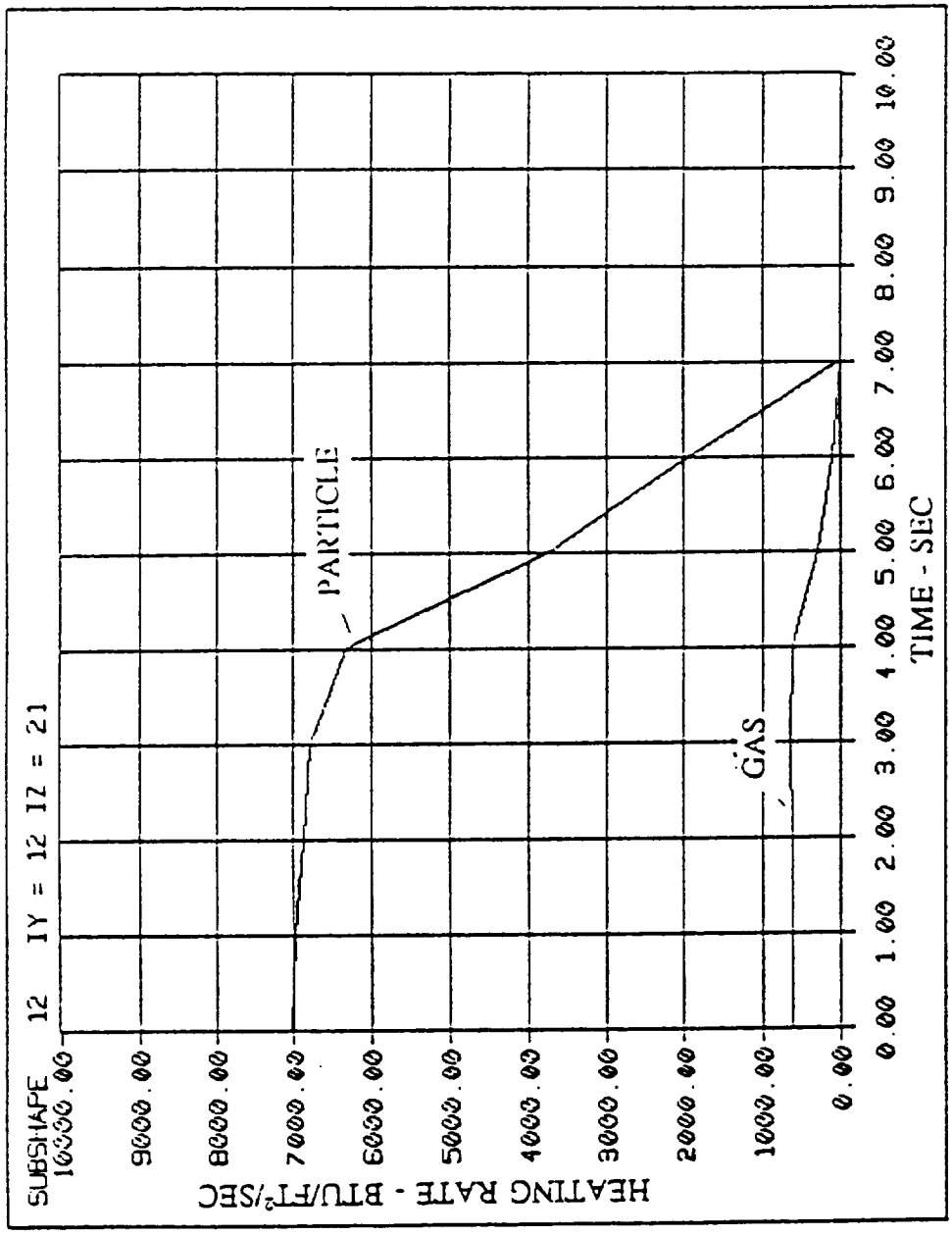


Figure 56: Heating Rate vs. Time for Body Point 7 on MLT

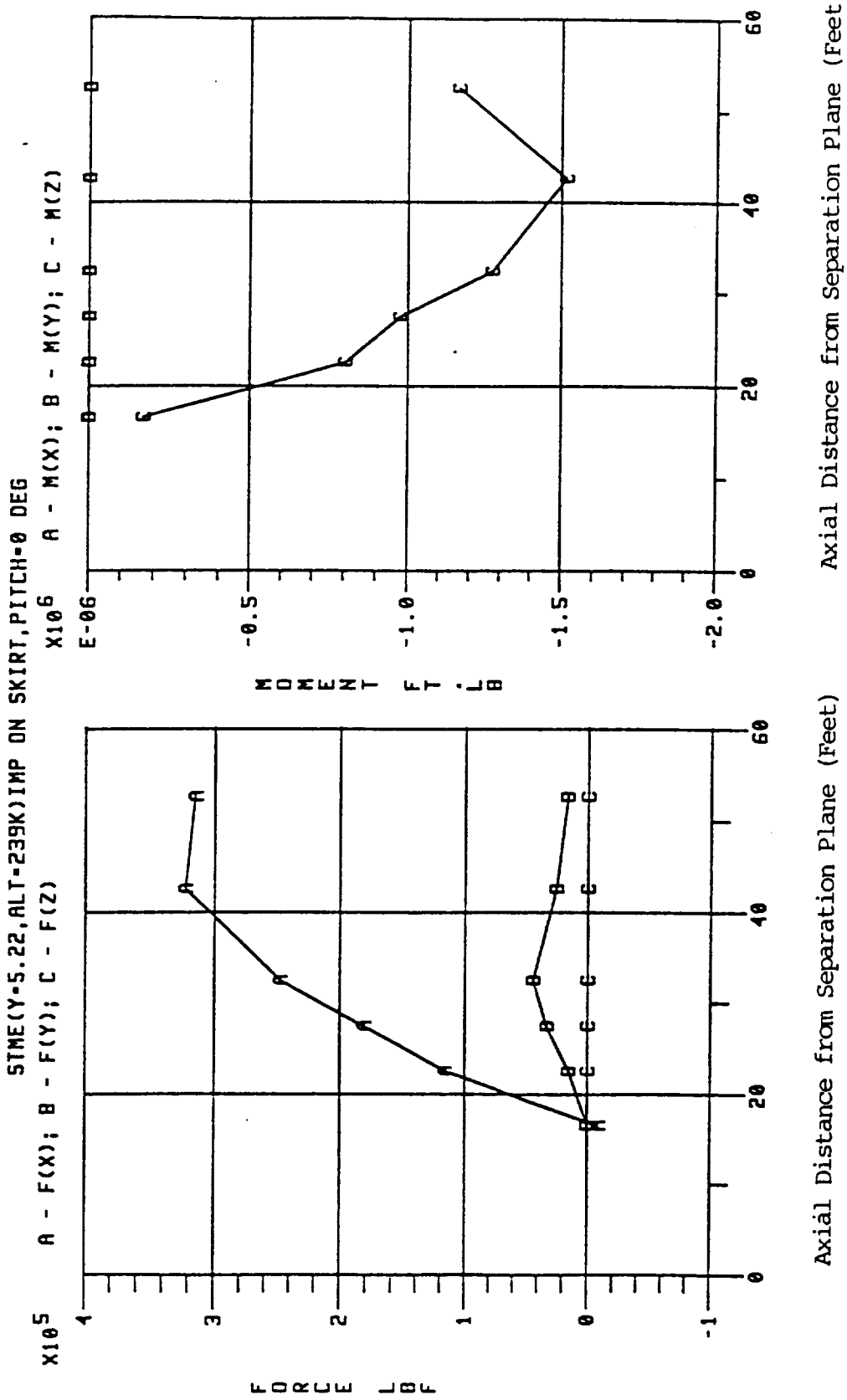


Figure 57: Upper STME Sustainer Engine (No Gimbal) Plume Impingement Forces and Moments on the Propulsion Module as a Function of Distance from the Separation Plane

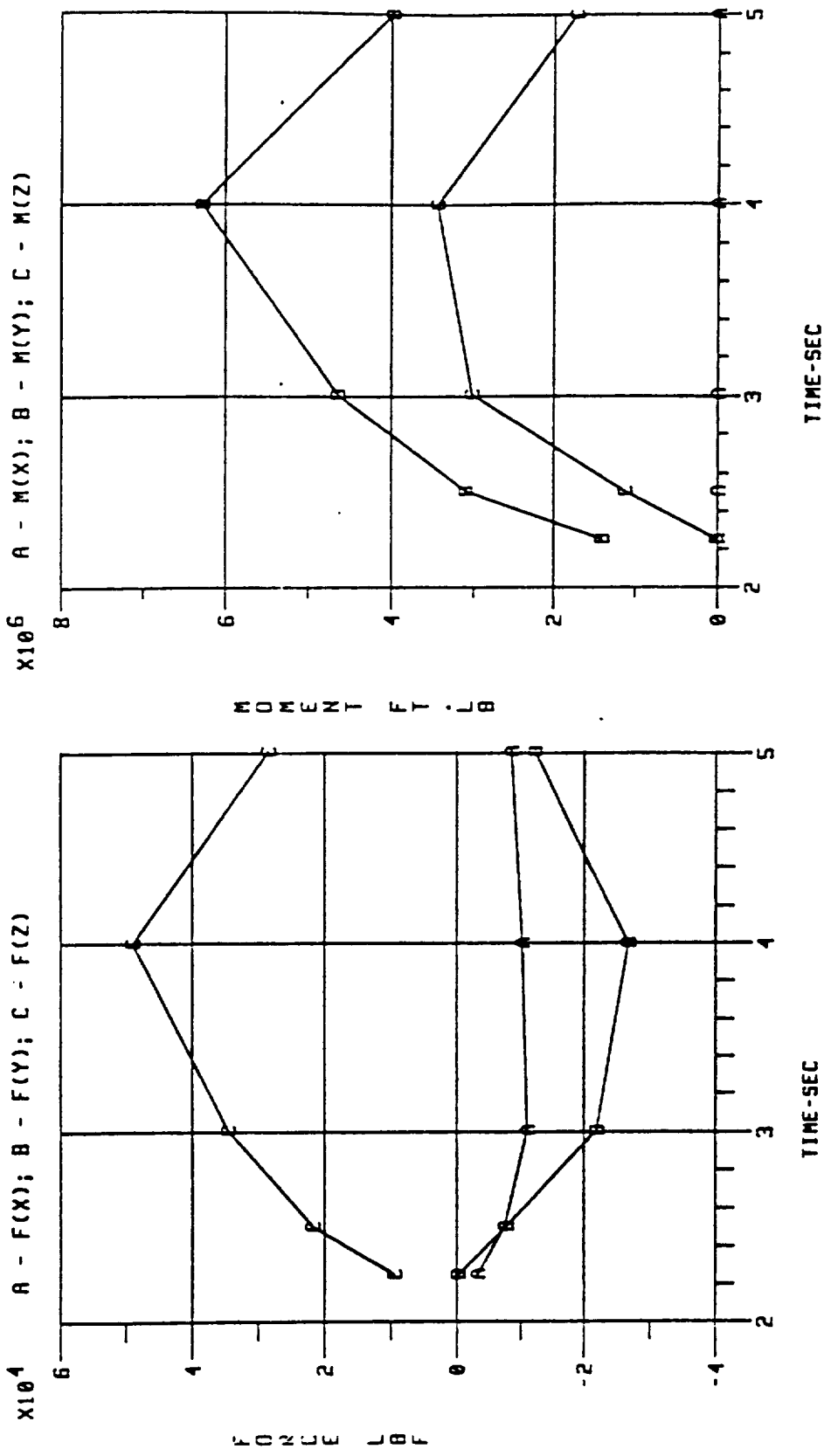


Figure 58: STME Plume Impingement Forces and Moments vs. Time from Separation on the HLLV ASRBs

# Section 8
# RECOMMENDED IMPROVEMENTS

As discussed in Section 4, the current code was developed with reasonable limits on the vehicle configurations which could be analyzed, as well as limitations on the choice of propulsion systems. It was also developed as a generalization of first principles in the prediction methods and does not attempt to provide the specific, point-by-point flowfield and environment data possible with CFD techniques. It is a design tool which enables design trades to be assessed (from a base heating standpoint) quickly and with reasonable accuracy.

During the process of code development and checkout, current code limitations have been assessed against two criteria:

1. The complexity and resource requirement to implement a change, improvement, or extension to the current capability to eliminate or work around the limitation.
2. Does the improvement significantly impact run time, accuracy, or computer friendliness of the code?

With these criteria as guidelines, a list of improvements has been prepared which REMTECH believes will enhance the code, and are reasonably easy to accomplish. These improvements are listed below:

- Enable result plotting capability.
- Enhance staging capabilities
    1. Provide change in configuration at staging for convection code.
    2. Provide identification of booster body points so heat load integration can be terminated at staging.
    3. Provide 1.5 stage configuration in addition to strap-ons
    4. Modify code to handle series staging in addition to the parallel staging capability
- Expand propulsion database
    1. Increase $P_c$ and area ratios in the $O_2/H_2$ plume library
    2. Devise/improve methods of extending empirical radiation models for $O_2$/RP and solid propellants to a larger range of $P_c$ and area ratios
    3. Add other propellants of interest
- Expand geometry

    Allow axial off-set in nozzle exit planes

Many of these improvements could be accomplished quickly; however, the prudent course of action and that recommended by REMTECH will be to distribute preliminary versions to potential users and collect and assess user comment before implementation of changes. A longer term objective is to convert the code to other operating systems so that the code is usable with other computer hardware.

# Section 9
# REFERENCES


[1] Aerothermodynamics Task 4202, "Advanced Launch System, Advanced Development Program Plan," Revision C, Volume I, Program Summary, May 1989.

[2] Anderson, L. W. and Morse, H. L., "Boundary Layer Integral Matrix Procedure (BLIMP)," AFWL-TR-69–114, Vol. 1 (Supp.), Air Force Weapons Laboratory, NM, Oct. 1971.

[3] Gordon, S. and McBride, B. J., "Computer Program for Calculation of Complex Chemical Equilibrium Compositions, Rocket Performance, Incident and Reflected Shocks, and Chapman-Jouguet Detonations," NASA SP-273, NASA/Lewis Research Center, 1971.

[4] Smith, D. D., "High Altitude Supersonic Flow of Chemically Reacting Gas-Particle Mixtures: Vol. I — RAMP2, A Theoretical Analysis and Development of the Numerical Solution," LMSC-HREC TR D867400–I, Lockheed Missiles & Space Co., Huntsville, AL, Oct. 1984.

[5] Reardon, J. E. and Lee, Y. C., "A Computer Program for Thermal Radiation from Gaseous Rocket Exhaust Plumes (GASRAD)," REMTECH RTR 014–9, Dec. 1979.

[6] Lovin, J. K. and Lubkowitz, A. W., "User's Manual for RAVFAC — A Radiation View Factor Digital Computer Program," Lockheed Missiles and Space Company, NASA CR-61321, Nov. 1969.

[7] Everson, J. and Nelson, H. F., "Development and Application of a Reverse Monte Carlo Radiative Transfer Code for Rocket Plume Base Heating," To Be Presented at the AIAA 31st Aerospace Sciences Meeting in Reno, NV, Jan. 1993.

[8] Olson, D., "624A Phase IV Base Heating and Recirculation Wind Tunnel Test Post-Test Report," Martin-Marietta Report SSD-CR-64-85, June 1964.

[9] Tang, H. H., Gardiner, C. P., Anderson, W. A., and Navickas, J., "Space Shuttle Booster Multi-Engine Base Flow Analysis," NASA Technical Memorandum TM X-2507, p. 519, Feb. 1972.

[10] Hong, Y. S., "Base Flow Analysis of Multiple-Engine Boosters," Aerospace Corporation Report AD-768 967, July 1973.

[11] Allen, J. L., "Base-Flow Aerodynamics of a Saturn-Type Booster Stage at Mach Numbers 0.1 to 2.0," NASA Technical Note TN D-593, March 1962.

[12] Sadunas, J. A., French, E. P., Sexton, H., "S-II Stage 1/25 Scale Model Base Region Thermal Environment Test," NASA Contractor's Report CR-129009, May 1, 1973.

[13] Dearing, D. L., "The Saturn S-IV Stage Base Thermal Environment Flight and Scale Model Data Comparison," AIAA Paper No. 66-45, Jan. 1966.

[14] Marion, E. D., Daniels, D. J., Herstine, G. L., and Burge, G. W., "Exhaust Reversal from Cluster Nozzles: A New Flow Model," Douglas Aircraft Company Engineering Paper No. 1374, Nov. 1962.

[15] Brewer, E. B., "Results of the Saturn S-IV Cold Flow Base Recirculation Tests Conducted at AEDC," NASA Technical Memorandum M-AERO-A-13-62, 6 March 1962.

[16] Hendershot K. C., "Some Observations on Exhaust Recirculation from Clustered Rocket Nozzles," Cornell Aeronautical Laboratory, Inc. Report, 1966.

[17] Hand, A. E., McKay, G. B., and Fuller, C. E., "Short Duration Base Pressure and Heat Transfer Test of 1/25 Scale, 3 Engine, J-2 Nozzle Model," Hayes International Corp. Report 1551, Nov. 1968.

[18] "Space Shuttle STS-1 Final Flight Evaluation Report - Volume II - Base Heating VI," July 22, 1981.

[19] Greenwood, T. F., "STS-2 Flight Evaluation Report - Base Heating," NASA/MSFC Memorandum ED33-82-3, Jan. 15, 1982.

[20] Greenwood, T. F., "STS-3 Flight Evaluation Report - Base Heating," NASA/MSFC Memorandum ED33-82-25, April 25, 1982.

[21] Greenwood, T. F., "STS-4 Flight Evaluation Report - Base Heating," NASA/MSFC Memorandum ED33-82-46, Aug. 10, 1982.

[22] Greenwood, T. F., "STS-5 Flight Evaluation Report - Base Heating," NASA/MSFC Memorandum ED33-82-65, Dec. 2, 1982.

[23] Mueller, T. J., Sule, W. P., and Hall, C. R., Jr., "Characteristics of Separated Flow Regions within Altitude Compensating Nozzles," University of Notre Dame Report UNDAS TN-029-FR-9, Jan. 1971.

[24] Rhodes, R. P., "Analysis of Gas Dynamic Parameters Affecting Modeling of Rocket Plume Radiance," AEDC Report AEDC-TR-77-85 and Air Force Report AFRPL-TR-77-66, March 1978.

[25] Charczenko, N. and Hayes, C., "Jet Effects at Supersonic Speeds on Base and Afterbody Pressures of a Missile Model Having Single and Multiple Jets," NASA Technical Note TN D-2046, Nov. 1963.

[26] Musial, N. T. and Ward, J. J., "Base Flow Characteristics for Several Four- Clustered Rocket Configurations at Mach Numbers from 2.0 to 3.5," NASA Technical Note TN D-1093, Dec. 1961.

[27] Chiccine, B. G., Valerino, A. S., and Shinn, A. M., "Experimental Investigation of Base Heating and Rocket Hinge Moments for a Simulated Missile through a Mach Number Range of 0.8 to 2.0," NASA Technical Memorandum TM X-82, Oct. 1959.

[28] Wasko, R. A., "Effects of Boattailed Afterbodies on Base Heating and Motor Aerodynamic Hinge Moments of a Rocket Missile," NASA Technical Memorandum TM X-386, Sep. 1960.

[29] Beheim, M. A., Klann, J. L., and Yeager, R. A., "Jet Effects on Annular Base Pressure and Temperature in a Supersonic Stream," NASA Technical Report R-125, 1962.

[30] Samanich, N. E., Lovell, J. C., Barnett, D. O., "Some Observations of Base Heating at Mach 3.0 on a Simulated Missile with a JP-4 - Liquid-Oxygen Rocket," NASA Technical Memorandum TM X-411, Nov. 1960.

[31] Cubbage, J. M., "Investigation of Exhaust Backflow from a Simulated Cluster of Three Wide-Spaced Rocket Nozzles in a Near-Space Environment," NASA Technical Note TN D-3016, Sep.1965.

[32] Brewer, E. B. and Craven, C. E., "Experimental Investigation of Base Flowfield at High Altitude for a Four-Engine Clustered Nozzle Configuration," NASA TN D-5164, May 1969.

[33] Wasko, R. A. and Cover, T. L., "Experimental Investigation of Base Flow Field at High Altitudes for Configurations of Four and Five Clustered Nozzles," NASA Technical Memorandum TM X-1371, May 1967.

[34] Goethert, B. H., "Base Flow Characteristics of Missiles with Cluster-Rocket Exhaust," *Aerospace Engineering*, March 1961, pp. 29, 108–117.

[35] Lilienthal, P. F., II, Brink, D. F., Addy, A. L., "An Investigation of Factors Influencing the Annular Base Drag of Bodies of Revolution with Jet Flow in Transonic and Supersonic Streams," University of Illinois at Urbana- Champaign, Department of Mechanical and Industrial Engineering, July 1970.

[36] Bridwell, Porter, "National Launch System Overview and Status," MSFC Presentation to Admiral Truly, Feb. 8, 1992.

[37] Mullen, C. R., et al., "SATURN Base Heating Handbook," The Boeing Company, NASA CR-61390, May 1, 1972.

[38] Reardon, J. E., Everson, J., and Smith, S. D. (SECA, Inc.), "Analytical Methodology for the Cycle 1.5 ASRB Plume Radiation Predictions," REMTECH RTN 250-1-02, Oct. 30, 1991.

[39] Greenwood, T. F., "Orbiter/SSME Operational Base Heating Environments," MSFC Memo ED33-84-32 to L. K. Zoller, July 3, 1984.

[40] Reardon, J. E. and Everson, John, "ASRM Cycle 1 Plume Radiation Methodology," REMTECH RTN 213-09, Feb. 28, 1991.

[41] Reardon, J. E. and Fulton, M. S., "Development of Cycle 1.5 ASRB Plume Radiation Altitude and Shutdown-Spike Adjustment Functions," REMTECH RTN 250-1-06, March 16, 1992.

[42] Reardon, J. E., "A Computer Program for Thermal Radiation from Shuttle Exhaust Plumes (SEPRAD)," REMTECH RTR 109-01, July 1987.

[43] Bender, R. L. and Reardon, J. E., "Preliminary Base Heating Environments for a Generalized ALS $LO_2LH_2$ Launch Vehicle," REMTECH RTN 218–01, Oct. 1989.